INVESTIGATIONS ON ROBUST MOTION CONTROL DESIGNS FOR MOBILE MANIPULATORS

Ph.D. Thesis

By

SWATI MISHRA

DISCIPLINE OF METALLURGY ENGINEERING & MATERIAL SCIENCE

INDIAN INSTITUTE OF TECHNOLOGY INDORE

AUGUST 2019

INVESTIGATIONS ON ROBUST MOTION CONTROL DESIGNS FOR MOBILE MANIPULATORS

A THESIS

Submitted in partial fulfilment of the

requirement for the award of the degree

of

DOCTOR OF PHILOSOPHY

by

SWATI MISHRA

DISCIPLINE OF METALLURGY ENGINEERING & MATERIAL SCIENCE

INDIAN INSTITUTE OF TECHNOLOGY INDORE

AUGUST 2019

INDIAN INSTITUTE OF TECHNOLOGY INDORE

CANDIDATE'S DECLARATION

I hereby certify that the work which is being presented in the thesis entitled **" Investigations on Robust Motion Control Designs for Mobile Manipulators"** in the partial fulfilment of the requirements for the award of the degree of **DOCTOR OF PHILOSOPHY** and submitted in the **DISCIPLINE OF METALLURGY ENGINEERING & MATERIAL SCIENCE, Indian Institute of Technology Indore**, is an authentic record of my own work carried out during the time period from July 2015 to August 2019 under the supervision of **Dr. Santosh Kumar Vishvakarma, Associate Professor, Discipline of Electrical Engineering** and **Dr. Santhakumar Mohan, Associate Professor, Discipline of Mechanical Engineering, IIT Palakkad .**

The matter presented in this thesis has not been submitted by me for the award of any other degree of this or any other institute.

Swati 09/08/2019

Signature of the student with date

(SWATI MISHRA)

This is to certify that the above statement made by the candidate is correct to the best of my/our knowledge.

Signature of Thesis Supervisor#1 with date	Signature of Thesis Supervisor#2 with date
(Dr. SANTOSH KUMAR VISHVAKARMA)	**(Dr. SANTHAKUMAR MOHAN)**

Signature of Chairperson (OEB) Date:	Signature of External Examiner Date:	Signature(s) of Thesis Supervisor(s) Date:
Signature of PSPC Member #1 Date:	Signature of PSPC Member #2 Date:	Signature of PSPC Member #3 Date:
Signature of Convener, DPGC Date:	Signature of Head of Discipline Date:	

DEDICATED TO MY DAUGHTER

ACKNOWLEDGEMENTS

First and everlasting, all praise to GOD to give me strength, intelligence and patience to carry out this work in a good manner. I would like to express my gratitude to all those people who helped me in accomplishment of this Ph.D. thesis.

I would like to express my deepest awe and veneration to my thesis supervisors **Dr. Santhakumar Mohan and Dr. Santosh Kumar Vishvakarma**, for their splendid, assistance, guidance, support, patience and encouragement for these several years and I wish to have their valuable support in future as well I am grateful for their dedicated supervision and without them the work reported in this thesis would not have been possible. I spend about four years with them in which I learned to appreciate their persistence in research. I appreciate the time they spent with me realizing this work both theoretically and especially experimentally with real-time prototype developed in our research laboratory.

I express my thanks to **Prof. Pradeep Mathur**, Director IIT Indore, Dean of Academic Affairs (DOAA), Dean of Research and Development (DORD), Dean of Student Affairs (DOSA) for providing their kind support and facilities.

I would like to thank my PSPC committee members, **Dr. Shaikh Mobin**, **Dr. I. A Palani** and **Dr. Dhirendra Kumar Rai** for their valuable suggestion right from the beginning of my research work.

I express my sincere thanks to **Dr. Parasharam Shirage**, present head of Discipline of Mechanical Engineering for provide opportunity, facilities and necessary infrastructure to carry out my research work.
I am indebted to Centre for Robotics and Control, Kinematics and Dynamics of Machines Laboratory, Central Workshop of IIT Indore for their valuable support in developing my research prototypes.

I extend my hearty thanks to all the staff members Discipline of Metallurgy Engineering and Material Science, Central Library, Academic Section, Account Section, Purchase Section and all Disciplines of IIT Indore for their kind cooperation.

I would like to thank to my senior research scholar **Dr. Yogesh Singh**, **Dr. Jayant Kumar Mohanta** and my colleagues, **Mr. Jagadeesh Kadiyam** for their support and encouragement.

I specially thank**, Mr. Vasanthakumar, Mr. Hemant Raghuwanshi, Mr. A G Sai Kiran, Mr. Hitesh Badabagni, Mr. Barre Alex Epenetus** of IIT Indore for their continuous support, encouragement and willingness to help me in my graduate career.

My research was partially supported by the Department of Higher Education, Ministry of Human Resource Development (MHRD), India, Research Grant #1-36/2016-PN-II Research and I gratefully acknowledged its support.

At last, my most special gratitude to my spouse, daughter, mother in-law and my parents for trusting me and their valuable support and encouragement all these years.

SWATI MISHRA

LIST OF PUBLICATIONS

1**. Mishra S.,** Londhe P.**S.,** Mohan S., Vishvakarma S.K., Patre B.M. (2018) Task space motion control of a mobile manipulator using a nonlinear PID control along with an uncertainty estimator, Computers and Electrical Engineering 67, 729-740. (IF = 2.189)

2**. Mishra, S.,** Sharma, M., & Mohan, S. (2019). Behavioural fault tolerant control of an omni directional mobile robot with four mecanum wheels**.** Defence Science Journal **,** 69(4), 353-360**.** (IF = 0.589)

3. **Mishra S.,** Mohan S., Vishvakarma S.K**.** (2019) A simplified motion control of a vehicle manipulator for the coordinated mobile manipulation. Defence Science Journal 70(1), 72-81. (IF= 0.589)

CONFERENCE PAPERS

1. Mishra S., Mohan S., Vishvakarma S.K**.** (2016) Task space motion control of a mobile manipulator using a nonlinear PID control along with an uncertainty estimator, International Conference on Advancements in Automation Robotics & Sensing ICAARS June, 2016

2**. Mishra S.,** Epenetus B.A., Mohan S. (2018) Double-loop robust motion control of a ground-based vehicle-manipulator system. International Conference on Advancements in Automation Robotics & Sensing ICAARS December, 2018

ABSTRACT

Keywords: Mobile manipulator; kinematic redundancy; nonlinear proportional-integral-derivative control; adaptive control; backstepping control design; operational-space motion control; disturbance observer; resolved motion control; computed velocity control; omni-directional mobile robot; mecanum wheel-drive; differential-drive; fault-tolerant-control; line-of-sight; kinematic control; double-loop control; robust control;

This thesis proposes various robust and adaptive motion control schemes such as a simplified operational-space control, an adaptive motion control, an improved backstepping control design, a double-loop motion control or dual loop control and an actuator fault tolerant control schemes for mobile manipulators. Mobile manipulator comprises of a manipulator arm mounted on a mobile platform. A mobile manipulation system offers a dual advantage of mobility offered by a mobile platform and dexterity offered by the manipulator.

The thesis work is folded in three parts, the dynamic model formulation of a generalized mobile manipulator based on the recursive Newton-Euler method is discussed and the dynamic model developed for a real-time mobile manipulator namely JR2 consists of a four mecanum wheeled mobile base and a six degrees of freedom serial chain manipulator arm. Further, a robust nonlinear control method with an uncertainty estimator is proposed and applied to the mobile manipulator for its position tracking in its operational-space (Cartesian space). The proposed robust motion control method incorporates a feed-forward control term to reinforce the control action with extravagance from the desired acceleration vector; an uncertainty estimator to reimburse for the unknown effects such as

parametric uncertainties, unknown external disturbances, unmodeled dynamics and a decentralized PID (proportional-integral-derivative) controller as a feedback loop to strengthen the stability of the system. It is observed that the main strengths of the proposed scheme are its high robustness against parameter uncertainties and external disturbances, simplicity in design and ease of implementation. The effectiveness, feasibility, and robustness of the proposed method are illustrated using the computer-based simulations based on the derived dynamic model of the JR2 with and without uncertainty estimator.

An extension of the previous control, an improved backstepping control technique is proposed for the entire operational-space, i.e., the end-effector pose tracking of the mobile manipulator. As mentioned earlier, the mathematical model used for the computer-based simulations is derived based on a real-time mobile manipulator and the derived model is further verified with an inbuilt gazebo model in a robot operating system (ROS) environment. In addition, the proposed scheme is also verified on an in-house fabricated mobile manipulator system. Further, the recommended controller performance is compared with the conventional backstepping control design in both computer-based simulations and in real-time experiments.

Further, the thesis work considers a simplified resolved kinematic motion control approach for controlling a spatial serial manipulator arm that is mounted on a vehicle (mobile) base. The end-effector’s motion of the manipulator is controlled by a new kinematic control scheme, and the performance is compared with the well-known operational-space kinematic control scheme. The proposed control scheme aims to track the given operational-space (end-effector) motion trajectory with the help of resolved configuration-space motion without using the Jacobian matrix inverse or pseudo inverse. The experimental testing results show that the suggested control scheme is as close to the conventional operational-space kinematic control scheme.

Further, to fulfil the motion requirement which can handle variability in payload and unknown model parameters, the simplified resolved kinematic control is extended as a robust motion control scheme with the help of double-loop control. The effectiveness and usefulness of the proposed manipulator is shown with the implementation of the motion controller through the computer based numerical simulations. The controller robustness is further analysed at different working conditions. In comparison to the conventional controllers, the proposed control scheme possesses few advantages namely better robustness, less chattering, high precision and can work in the presence of parameter uncertainties. Afterwards, the proposed motion control scheme is also validated on an in-house fabricated prototype and a commercial mobile manipulator through the motion control experiments.

In order to strengthen the field robotics, the thesis work is extended for an actuator fault tolerant as well. In this direction, as a first step, the four-mecanum wheeled drive mobile robot is considered for the actuator fault tolerant control. A behavioural fault tolerant control scheme is proposed and verified with faulty wheels' configurations that will give near desired performance with one fault and two faults for both set-point control and trajectory-tracking (circular profile). For one fault the system remains in its full actuation capabilities and gives the desired performance with the same control scheme. In case of the two-fault wheel all combinations of faulty wheels have been considered and the same control scheme has been used upon whereby some configuration gave desired performance within the tolerance limit defined while some does not even use pseudo inverse since using the system becomes under-actuated and their wheel alignment and configurations greatly influenced the performance.

.

TABLE OF CONTENTS

CHAPTER 4 MOTION CONTROLLER DESIGN

CHAPTER 5 RESULTS AND DISC\USSIONS

LIST OF FIGURES

LIST OF TABLES

NOMENCLATURE

Symbols

B	Actuator configuration matrix
$F(q,\dot{q})\dot{q}$	Manipulator joint frictional effects
F_{dis}	Lumped disturbance vector
A	Actuator input matrix
A_w^+	Weighted pseudo inverse matrix
K_c and K_o	Controller and estimator gain matrices
W	Weighted matrix
J	Jacobian matrix
S	Set of all points
$\in$	Small positive real value
$M(q)\ddot{q}$	Vector of inertial forces and moments of the manipulator
$C(q,\dot{q})\dot{q}$	Vector of Coriolis and centripetal effects of the manipulator
G(q)	Vector of gravity effects of the manipulator
q	Vector of configuration (joint) position variables
ζ	Vector of mobile base positions
ξ	Vector of manipulator joint positions
x, y , and ψ	Mobile base translation positions and yaw angular displacement
d_1 , θ_2 , θ_3 , and θ_4	Manipulator joint displacement and angles of the corresponding Mobile Manipulator
f_{edis}	Vector of external disturbances acting on the MM
f_{idis}	Vector of internal disturbances acting on the MM
$\Delta M(q)\ddot{q}$, $\Delta C(q,\dot{q})\dot{q}$, *and* $\Delta g(q)$	Parameter uncertainties
$\mathbf{n}(\mathbf{q},\dot{\mathbf{q}})$	Dissipative and non-conservative forces vector

$\hat{\mathbf{M}}(\mathbf{q})$, $\hat{\mathbf{n}}(\mathbf{q},\dot{\mathbf{q}})$ and $\hat{\mathbf{g}}(\mathbf{q})$	Known (inaccurate) model equations of the mobile manipulator
$\mathbf{F}(\mathbf{q},\dot{\mathbf{q}})$	Frictional effect vector consists of static, coulomb and viscous frictional effects.
$\mathbf{K}_1, \mathbf{K}_2, \mathbf{K}_3$	Controller gain matrix and observer gain matrix
$\mathbf{K}_s$	Sliding control gain
$\mathbf{x}_2^{vc}$	Virtual control input vector
$\mathbf{x}_{1d}$	Desired operational space position vector
x_1, x_2	State variables
$\dot{\mathbf{e}}_1, \dot{\mathbf{e}}_2$ and $\dot{\mathbf{e}}_3$	Error derivatives
$\mathbf{J}^+$	pseudo inverse of the Jacobian matrix
x_V, y_V and θ_V	Mobile base or vehicle positions and the heading (yaw) angle
$\mathbf{J}(\boldsymbol{\eta}) \in \Re^{6\times 9}$	Jacobian matrix which maps the end-effector (operational-space) velocities to the vehicle-fixed frame (configuration-space) velocities.
$\mathbf{W}$	Actuator configuration matrix
$\mathbf{W}^+$	Weighted pseudo matrix inverse
k	Controller parameter
$R_{\min}$	Minimum safe radial distance between the vehicle frame and the end-effector frame
$\mathbf{B}^+ = \mathbf{B}^{\mathrm{T}}\left(\mathbf{B}\mathbf{B}^{\mathrm{T}}\right)^{-1}$	Moore-Penrose Pseudo Inverse
$\mathbf{H}$	Health performance matrix
$(\mathbf{BH})^+$	Weighted pseudo inverse
$\mathbf{K}_p$	Controller gain matrix
$\dot{q}_1, \dot{q}_2, \dot{q}_3, \dot{q}_4$	Angular wheel velocities
$\mathbf{M}(\boldsymbol{\eta})\dot{\xi}$	Vector of inertial forces and moments of the vehicle-manipulator
$\mathbf{n}(\boldsymbol{\eta},\xi)$	Dissipative and non-conservative forces vector which includes frictional, Coriolis and centripetal effects of the vehicle-manipulator

Greek Symbols

η_{ct}	Computed torque control term
η_{PID}	PID controller
η_{est}	Disturbance estimator
Γ	A positive diagonal matrix
χ	Control input vector
$\ddot{\mu}r$	Vector of reference acceleration
μd , $\dot{\mu}d$, and $\ddot{\mu}d$	Given desired task space position, velocity and acceleration vectors
γ	Positive fractional coefficient
$\hat{\nu}$	Estimated vector of nonlinear terms
δ	Estimated uncertainty and disturbance vector
τ_m	Vector of input torques used to control a serial manipulator
τ_b	Vector of input torques used to control a mobile base
τ	Actuator input allocations or vector of control input torques
η	Vector of actuator inputs or vector of configuration (joint) space position variables
$\boldsymbol{\eta}_v$	Vector of vehicle base positions and orientation
$\boldsymbol{\eta}_m$	Vector of manipulator rotary joint angles
ν	Vector of nonlinear terms
$\boldsymbol{\tau}_{edis}$	External disturbances vector
$\boldsymbol{\tau}_{idis}$	Internal disturbances vector due to frictional effects ,parameters and system uncertainties, disturbances occurred due to process noises and measurement
$\boldsymbol{\kappa} \in \Re^{7x1}$	Actuator inputs vector
$\hat{\boldsymbol{\tau}}_{dis}$	Estimated disturbance vector
$\tilde{\boldsymbol{\mu}}$	Operational-space pose errors vector

$\boldsymbol{\mu}$	Operational-space positionvector
$\dot{\boldsymbol{\mu}}$	Operational-space velocities
$\boldsymbol{\mu}_d$	Desired operational-space trajectory
$\boldsymbol{\xi}_v$	Vector of velocity inputs of the mobile base (vehicle)
$\boldsymbol{\xi}_m$	Vector of input joint torques of the serial manipulator
$\boldsymbol{\rho}$	operation-space pose vector
$\boldsymbol{\xi}$	Vector of control inputs in body-fixed coordinate frame or command velocities
$\dot{\boldsymbol{\rho}}_{\mathbf{d}}$	Vector of desired operational-space velocities
$\tilde{\boldsymbol{\rho}}$.	Vector of operational-space pose errors
$\mathbf{J_1}(\boldsymbol{\eta})^{\mathrm{T}} = \mathbf{J_1}(\boldsymbol{\eta})^{\mathbf{-1}}$	Inverse of the vehicle Jacobian matrix
$\boldsymbol{\rho}_{\mathbf{d}}$	Desired operational space pose vector
$\dot{\boldsymbol{\eta}}_{\mathrm{d}}$	Vector of desired inertial frame (earth-fixed) configuration-space velocities which is obtained from the desired operational-space velocities
$\tilde{\boldsymbol{\eta}} = \boldsymbol{\eta}_d - \boldsymbol{\eta}$ . .	Vector of configuration-space pose errors
$\boldsymbol{\eta}_{\mathbf{d}}$	Desired configuration-space pose vector which is resolved from the operational-space pose vector
$\boldsymbol{\Lambda}$	Controller gain matrix
$\boldsymbol{\eta}_{dv}$	Vector of desired positions and orientation of the vehicle.
$\boldsymbol{\eta}_{md}$	of desired joint angles of the spatial manipulator arm
ω	Controller parameter
Λ	Controller gain
$\boldsymbol{\sigma}$.	Control inputs vector
$\boldsymbol{\sigma}_v$	Inputs of the mobile base vector

$\boldsymbol{\sigma}_m$	Input torques vector of the serial manipulator attached on a mobile base
$\dot{\boldsymbol{\xi}}_{dis}$	Disturbance vector
$\dot{\boldsymbol{\sigma}}_{dis} \approx 0$	Lumped disturbance vector

ACRONYMS

DC	Direct Current
MM	Mobile Manipulator
dof	degree of freedom
ms	Milliseconds
PC	Personal Computer
PD	Proportional-Derivative
PID	Proportional-Integral-Derivative
PRRR	Prismatic-revolute-revolute-revolute
PPR	Prismatic- prismatic -revolute
PWM	Pulse width modulation
USB	Universal Serial Bus

Chapter 1

Introduction

1.1 Introduction

Mobile manipulator comprises of a manipulator arm mounted on a mobile platform. A mobile manipulation system offers a dual advantage of mobility offered by a mobile platform and dexterity offered by the manipulator. It has provided a new concept and direction in robot application and a hot research topic in recent years. It has lot of functional capabilities with several advantages such as large flexibility, singularity avoidance, and easy obstacle avoidance. It can be used in the areas such as material transportation [1], building constructions, and safety and rescue operations. In general, a minimum of 6 dof are needed to fully describe the pose of an object in space: 3 dof are needed to specify the Cartesian position of the object and 3 dof are needed to present the object orientation. Therefore, at least 6 dof, or six joints, are needed in a robotic system to have full manipulation capability of an object in space. Redundancy happens when the number of controllable inputs is higher than the system responses, this can happen based on kinematic arrangement or actuator arrangement, if the number of actuated robotic system joints exceeds the number of system response, it is called kinematic redundancy, that is, the redundancy is due to the kinematic arrangement of bodies. Whereas, just the number of actuators is higher than the system response, then the system simply called over actuated system or actuator redundant system. A kinematically redundant mobile manipulator has more dof than required to execute its task. In such a case, the inverse kinematics problem provides an infinite number of solutions. From these redundant solutions, mobile manipulator configurations, as well as a motion trajectory, can be chosen to best satisfy the desired secondary objectives, such as avoiding joint limits, singularities and obstacles. Kinematic redundancy in a mobile manipulator can be exploited to enhance the dexterous and manipulability capability, avoid obstacles, avoid kinematic singularities, and minimize energy consumption. To enlarge the workspace manipulators are placed on mobile platforms. Mobile manipulation requires integrating perception, control, motion planning, grasping, navigation and learning in a cohesive manner to act effectively in large unstructured environments. But when a robot is redundant infinite solutions exist, the robot has self-motions, i.e. internal motions in the joint space which do not affect the task variables. So here arises a problem of selecting a solution of the inverse kinematic problem. The problem is usually addressed by different methods such as at a velocity level, null space motion, finding a solution, pseudo inverse, weighted pseudo inverse, possible objective functions, cyclicity, extended Jacobian, solution at the acceleration level, kinematic control, etc.

Robots are divided according to the environment used like grounded robots, aerial robots, and underwater robots. There are various types of robots used which comes under ground robots such as service robots, military robots, medical robots, domestic robots, space robots etc. which performs different jobs according to the requirement. Figure 1.1 shows all types of robots used in the environment.

This research work proposes robust motion control designs for kinematic redundant mobile manipulators. The motion control designs have become a wide topic of research nowadays. Mobile manipulators are used in several areas where human cannot even reach. There are some examples of mobile manipulators shown in Figure 1.2. There are various industrial mobile manipulators companies such as KUKA, neobotix, robotnik which designs and manufactures according to the requirement. Mobile platforms designs can differ accordingly such as, differential drive, omni-wheel drive, mecanum wheel mobile base.

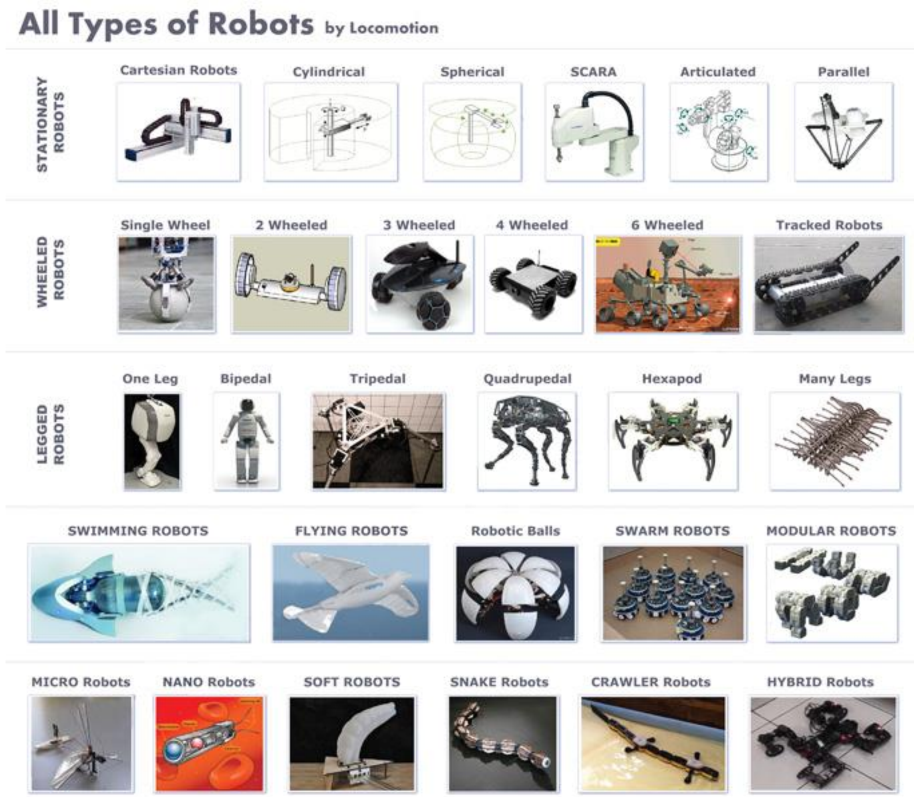

Figure 1.1 Types of Robots [11]

While performing tasks, mobile manipulator must follow the trajectory by overcoming obstacles. When mobile platform and manipulator arm combines there occurs redundancy. In [10], an unified approach has been defined to exploit the kinematic redundancy by the mobile platform to perform the tasks. There has been number of works performed which can be found in the literature. In [12] planning and control methodology has been presented along with the model-based controller to eliminate the tracking errors.

The thesis proposes motion control schemes such as improved sliding mode control scheme along with and without disturbance observer, backstepping design control, adaptive backstepping design, kinematic control, dual loop control design, and fault tolerant control.

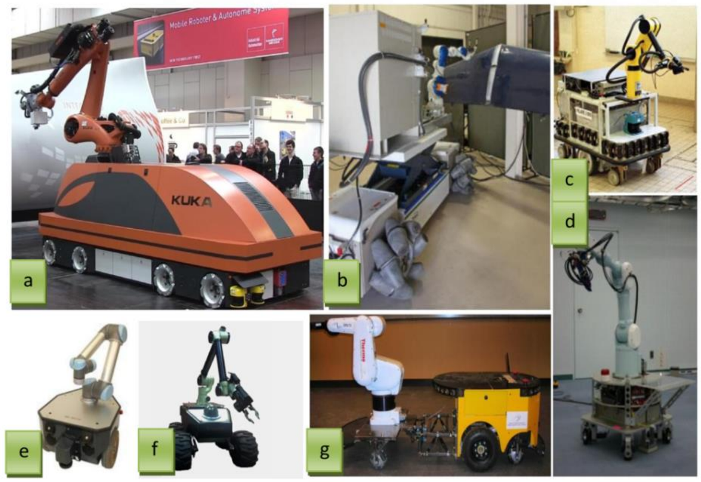

Figure 1.2 Examples of mobile manipulators: (a)- Kuka ”Moiros” for sheet metal manipulation [2], (b)- Southwest Research Institute mobile manipulator [3], (c)- H^2BIS mobile manipulator [3], (d)- ufmrp02 mobile manipulator [5], (e)- MM-500 mobile manipulator [6], (f)- Robotnik XL-Ball mobile manipulator [7], (g)- University of Ontario mobile manipulator [8]

The effectiveness and feasibility of the proposed controllers has been verified on in-house fabricated prototypes. Further the proposed controllers' performances are compared with the traditional motion control schemes in the presence of parameters uncertainty and external disturbances.

1.2 Usage of Robots

Mostly robots perform dirty, dangerous, difficult and repetitive tasks which human prefer not to do. Robots have been made user-friendly nowadays, more intelligent and most important affordable. They can be used in every field such as from industrial manufacturing to the medical field. The benefit of robots has increased their flexibility with being capable of performing a variety of tasks and applications. They are more precise and consistent than human workers. Robots also allow for increased production and profit margin because they can complete tasks faster. Robots have the ability to work around the clock since they do not require vacations, sick days, or breaks. They also make fewer mistakes than humans, saving company's time.

Other benefit of robotics is that they can work in any environment, adding to their flexibility. Robots eliminate dangerous jobs for humans because they can work in hazardous environments. They can handle lifting heavy loads, toxic substances, and repetitive tasks. This has helped companies to prevent many accidents, also saving time and money.

In the medical field robots are used for intricate surgeries such as prostate cancer surgery. Robots can reach and fit where human hands cannot, allowing greater accuracy. Some robotic benefits in the medical field are less invasive procedures and less pain for the patient when recovering. Robots can work faster than robots with consistently, precisely and precisely.

The benefits of robots have opened the door for their use in many fields. Their ability to be customized provides companies the flexibility to use them for a variety of tasks. They are safer to use sometimes for example harmful chemicals and enzymes where humans are not safe to work; robots can work in this type of an environment. According to a paper [13] focus is especially on improved human–robot interaction, and on the reusability of skills within the domain of tasks that are frequently required by the manufacturing industry. Industrial robots often help in reducing cost, improve quality, increasing production rate with higher accuracy level. They manipulate products quickly while performing picking and placing application task. They are designed to work in the harsh environments like in the space, without the air, underwater & in the fire; they can be used instead of the people when the human safety is a concern. They can come in any size required for the task.

1.3 Need of Robust Motion Control

The robotic system is not only a mechanical system; it needs to perform motions using the actuators and sensors. The primary difficulty is because of their nonlinear dynamics, and the system parameters governing the manipulator dynamics are coupled and sometimes time varying. Additionally, the uncertainty of the manipulator parameters and disturbances makes the manipulator control a challenging task for the control engineer. The tracking performance is not only dependent on its mechanical design and rigidity of the structural component but also the robustness of the motion controller performance. According to [15] construction of control systems is one of the major challenges for mobile manipulator for enabling the robot to operate safely in the dynamic environment.

There are various motion control schemes introduced by the researchers in the past which shows the importance of robust control strategy for successful execution of the task in the mobile manipulator. On the other hand, the dynamic model is also not exact because of the unmodeled dynamics, system uncertainties, frictional components and unknown external disturbances.

The conventional control strategies like the motion-based schemes namely proportional-derivative (PD) or proportional-integral-derivative (PID) controllers are more likely to give more tracking error as the inertial values start varying from the position of the optimal control gains. Hence, there is a need of robust controller which can overcome. PID controllers, when used alone, can give poor performance when the PID loop gains must be reduced so that the control system does not overshoot, oscillate or hunt about the control set-point value. In [16] this review paper shows mostly controllers used are in the form PD controller, kinematic and dynamic based controllers, Fuzzy logic controller, and active force controller. All the controllers are not 100% accurate, although a control scheme possesses good performance but still it has some errors. According to [17] there are several methods used for resolving local redundancy based on the determination of joint trajectories from the instantaneous motion needed to follow a desired end-effector path.

The robust control scheme provides satisfactory performance with a simple control structure but produces high control activity at steady state. The main objective of using robust control scheme is to keep the controller stable even in the presence of external disturbances, unmodeled dynamics and other uncertainties.

This thesis focuses on some robust motion control schemes such as backstepping design control, kinematic control dual-loop robust motion control, sliding mode control, adaptive backstepping control. Motion control scheme plays a vital role in gauging the performance and analysing the motion of the task performed by the robotic system. It helps in following the systems trajectory with minimum tracking errors that too in a robust environment, if it is a robust motion control. It forces the moving parts to coordinate in a proper way.

The controller should possess the basic quality of robustness with that it can be adapted easily in any kind of environment. Most of the technology used in mechanical systems of today is a result of development and implementation of motion control schemes. Mostly, motion control of a system includes position control (point to point set point control), velocity control and force control. It has become a part of our daily life. Motion control systems are important for functionality of critical systems in the different fields such as service robots, transportation, medical, machinery, and textile and so on.

1.5 Contributions

- Implementation of proposed robust task-space motion control scheme on a proposed prototype of a redundant 3 dof mobile manipulator with and without presence of parameter uncertainties and external disturbances using a nonlinear PID control along with an uncertainty estimator.

- Proposed an end-effector motion trajectory which is tracked with the help of resolved configuration-space motion without using the Jacobian matrix inverse. Hence recommended a novel resolved kinematic control design scheme for coordinated mobile manipulation of a redundant mobile manipulator.

- Mathematical modelling has been derived for 6dof redundant mobile manipulator which has been used for the computer-based simulations is derived based on a real-time mobile manipulator and the derived model is further verified with an inbuilt gazebo model in a robot operating system (ROS) environment.

- Further, the adaptive backstepping controller design performance is compared with the conventional backstepping control design in both computer-based simulations and in real-time experiments. In addition, the proposed scheme is verified on an in-house fabricated mobile manipulator system

- Usage of Lyapunov's direct method for designing and verifying the system's closed-loop stability and tracking ability of the entire suggested control scheme.

- Introduced a robust double-loop motion control scheme for tracking the end-effector of the vehicle-manipulator system under dynamic variations with the help of redundant feedback. The outer-loop consists of the task-space kinematics and the inner-loop consists of the configuration-space system dynamics. Simulation experiments based on real-time system parameters are accomplished to elucidate the essence of the recommended control scheme

- Computed velocity control is implemented to achieve the ultimate aim to follow the desired operational space pose vector trajectory of the vehicle manipulator with uncertainties and time varying external disturbances

- Kinematic control scheme with proposed Fault Tolerant Control is found quite effective for the four-mecanum wheeled drive mobile robots for both set-point control and trajectory-tracking control. For inverse kinematics pseudo inverse is found less effective than weighted pseudo inverse, error is relatively smaller using weighted pseudo inverse than pseudo inverse.

- Analysis is performed to showcase the behavior of the mobile robot when Fault Tolerant Control is used with the identified faults.

1.6 Organization of the Thesis

This thesis work broadly presents the area of robust motion control scheme designs for kinematically redundant mobile manipulators. It comprises of kinematic modelling, dynamic modelling and motion control of 3 dof and 6 dof mobile manipulators. Further a mecanum wheel base mobile robot behaviour analysis has also been performed when fault tolerant control is introduced with one and two faulty wheels. The effectiveness of the proposed control schemes and their efficacy has been demonstrated using computational simulation and real time prototypes.

The structured outline of the thesis chapters is as follows with their brief description:

Chapter 1: Introduction

Chapter 1 briefly introduces redundant mobile manipulators and various types of all robots. It helps in understanding the usage of robots about how robots can be used in each and every field of our day to day life. This chapter also explains motion control schemes and the requirement of robust motion control design schemes. Redundant mobile manipulators have several applications which have also been mentioned in this chapter.

Chapter 2: The State of the Art

This chapter describes the detailed literature review of the motion control schemes used in the past and existing real time applications used in the redundant mobile manipulator. The different kinds of control strategy opted by the researchers to control the robot motions are presented in this chapter. It also addresses the research gap and the limitations of the various control schemes used in this area.

Chapter 3: Mathematical Modelling of a Generalised Mobile Manipulator

Chapter 3 describes mathematical modelling of the proposed control design schemes. It explains about the kinematics and dynamics of the system.

Chapter 4: Motion Controller Designs

For the motion control of the robot, robust control schemes are proposed, designed and presented in this chapter. Namely first a simplified operational-space control, secondly a resolved kinematic control design and then adaptive backstepping design control has been proposed. Further dual-loop robust motion control and computed velocity control schemes have been proposed and investigated. These controllers' performances are analysed and are compared with the conventional controller designs to illustrate the effectiveness. This chapter illustrates the effectiveness of the control schemes using computer-based simulations. Further, the controller performances and its parameter sensitivity are analysed by variation of its controller parameters (gain constants) and near optimal values are obtained to run the real-time experiments on the in-house fabricated prototype of the proposed robotic system

Chapter 5: Results and Discussions

This chapter summarises the results of the proposed system performance along with the proposed motion controller. Detailed discussion on the working of the controller and prototype with control schemes has been done.

Chapter 6: Conclusions & Future Scope

This chapter consists of the concluding remarks of the proposed work on the usage of motion control scheme on a redundant mobile manipulator. This chapter 6 further discusses the salient features of the proposed motion control schemes. In this chapter discussion has been done on the performances and effectiveness of the various motion control schemes. It also describes the possibility of improvements in the proposed (existing) system which can be considered as scope of future works.

Chapter 2

The State of the Art

2.1. Motion Control Schemes

Motion control is one of the essential aspects in robotics. Controlling redundant mobile manipulators has gained interest in the field of complicated robotic tasks because of its wide range of applications. According to [18] most of the research on controlling the redundant mobile manipulators focused on controlling the end-effector to follow a predefined trajectory, while the mobile platform will follow a trajectory based on certain optimization criteria [19-22] .There are various types of motion control schemes used in this thesis such as sliding mode control, Proportional Integral Derivative control(PID), Proportional Derivative control(PD), adaptive backstepping control, conventional backstepping design control, resolved motion control ,kinematic control joint-space control based in inverse , task-space control based on inverse Jacobian and dual loop control. Researchers have performed various investigations and efforts have been done in the past.

PID controller is one of the most widely used motion control technique used in industries for feedback. Julio et.al [23] in 2001 performed some experiments and demonstrates the good performance and robustness of the of the PID controller. In 2002, T. Kawabe etal proposed a new design method for a robust PID controller with two degrees of freedom which satisfies the robust stability of a closed-loop system against parametric uncertainties of the plant and multiple design specifications for robust performance and it shows good performance. According to a paper in 1995 [25] Simulation studies also show that independent joint PD control gives reasonably good results for the flexible system and is robust to parameter uncertainties. Simulation studies confirm in [26] that the Nonlinear PD control can obtain good trajectory tracking performance.

Sliding mode control (SMC) is strong robustness with respect to system uncertainties and external disturbances. SMC is a special discontinuous control technique applicable to various practical systems [27]. By designing switch functions of state variables or output variables to form sliding surfaces, SMC under matching condition can guarantee that when tracking trajectories reach the sliding surfaces, the switch functions keep the trajectories on the surfaces, thus yielding desired system dynamics. Therefore, it is attractive for many highly nonlinear uncertain systems, such as the holonomic and nonholonomic constrained mechanical systems [28], [29]. According to [30] SMC is designed to be robust to disturbance with a guarantee of the stability of the system. An adaptive sliding mode controller based on the backstepping method applied to the robust trajectory tracking of the wheeled mobile manipulator. In [31] Sliding mode control, taking the advantages of fast response, reduced amount of information, and robustness with respect to system uncertainties and external disturbances, is much more suitable for the control of mobile manipulators. In this paper, focus is on a redundant actuated mobile manipulator. Two control subsystems are proposed to solve the trajectory tracking problem, including the sliding mode control of the mobile platform and the non-singular terminal sliding mode control of the manipulator.

The paper [32] in 2017 recommended a robust adaptive sliding mode control for the trajectory tracking of a nonholonomic wheeled mobile manipulator in task space coordinate. The proposed algorithm is robust adaptive control design where parametric uncertainties and disturbances are compensated by adaptive update technique. Simulation results demonstrate the effectiveness of the robust adaptive based controller in comparison with a robust sliding mode-based controller. Fast response, good transient performance and robustness with regard to parameter variations can be included as the advantages of the sliding mode controller [33]. SMC under matching condition can guarantee that when tracking trajectories reach the sliding surfaces, the switch functions keep the trajectories on the surfaces, thus yielding desired system dynamics. Therefore, it is attractive for many highly nonlinear uncertain systems, such as the holonomic and nonholonomic constrained mechanical systems [33], [35]. It guarantees the stability of the system as well as co-ordinately track the trajectory of the mobile platform and the manipulator with different dynamics effectively. The control scheme is capable of disturbance rejection in the presence of unknown bounded disturbances.

Backstepping control is design technique developed in 1990 which constructs stabilizing control laws for a certain class of nonlinear systems. The recursive backstepping method based on the Lyapunov's direct method-based scheme proposed around 1990s by Krstic, Kanellakopoulos and Kokotovic as discussed in [36]. The primary objective in [37] is to propose a motion control scheme which can track the stated end-effector trajectory in operational-space against internal and external ambiguities. In [38] the paper describes the control problem for a semi-strict nonlinear system depending on unknown parameters, uncertainty, and input constraint. [39] Describes an explicitly novel nonlinear control backstepping based law have been designed to incorporate a continuous-time adaptive backlash inverse model. The controller is a combination of backstepping control and Lyapunov redesign. In [30] when correlated with the adaptive control scheme for uncertain nonlinearities and disturbances, this makes control robust and nonlinear systems approach becomes appealable.

Without requiring any bounds on the unknown parameter in [31] an adaptive backstepping systematic procedure for tracking the motion control design of second-order nonlinear systems is refined. [32]

Discusses the principle of adaptive backstepping, although it can solve the setback of unmeasured states and promise the close-loop system stability. A control design method for nonlinear systems of uncertain class which is robust adaptive is proffered in [33-36] with disturbance observer, actuators uncertainties and backstepping method. Apart from the global stability, this paper [37] also provides L_2 tracking error performance for design A planning and control methodology has been declared in [38] without outraging the non-holonomic constraints. [39- 51] papers introduce a robust adaptive control system for non-holonomic mobile robots for nonlinear systems with uncertainties.

Improved backstepping design in [52] can prevent from repeated differentiation problem which emerges in using the conventional backstepping algorithm. In [53, 53] the main objective is to introduce a dynamic interaction and disturbance observer to compensate with the environment. According to [55] in coordinated control of mobile manipulator there are no studies which consider the effect of dynamic interaction. In [56-61] these papers address the position control with kinematic and dynamic uncertainties as well as the adaptive backstepping design task-space control. According to [62-63] hybrid adaptive-fuzzy controller in the latency of uncertainties and disturbances, together can track the desired trajectory and avoid the obstacles during the trajectory tracking.

In [65-67] robust task-space motion control strategy has been proposed which is able to handle the effects of interactions with the environment. [68-70] discusses about the redundancy resolution which helps in avoiding singularities and joint limits and aids in increasing the Cartesian mechanical rigidity of robot manipulators. In [71, 72] authors tried to comparison between nonlinear controller classic linear kinematic controller where they found nonlinear controller is harder to tune and guarantees whole-body asymptotic stability and linear programming is economical but generates more abrupt control signals. [73-76] These papers analyses work related to mobile manipulators complex task execution to attain the desired trajectory by avoiding high tracking errors which can be executed in operational-space. Lyapunov stability is achieved by fulfilling the constraints and providing a singularity and collision free trajectory of the system.

In [77], the kinematic control scheme based on the inverse kinematic transformation is proposed. In the presence of kinematics and dynamics along with the input disturbances, a task-space tracking control is suggested in [78]. The kinematic control algorithm is implemented and is effectively demonstrated by numerical simulations in [79]. The effectiveness of the real time kinematic and dynamic control of the redundant robots is described in [79, 80]. For manipulation of an object, a proper coordinated motion is required for the robot arm, so reference [81] demonstrates a new control algorithm in this direction. In [82], the work involves the use of pseudo-inverse of the Jacobian matrix and obtains the accurate joint solutions because of using the direct inverse kinematic solutions. In [83], to stabilize and compensate the uncertainties presented in the system, a motion controller based on an adaptive technique has been used for global convergence of trajectory tracking along with the desired internal forces acting on the object. The combined kinematic and computed torque controller which controls the mobile base velocities and also follows the required end-effector trajectory is recommended in [83]. The suggested controller validates the stability of the system by converging to all the errors to zero with the help of Lyapunov's direct method. In [85], the results show the task priority redundancy resolution using the matrix inversion approach based on the damped least squares. In [85], it has been done on robust redundancy resolution algorithm along with a comparative empirical evaluation has also been performed.

Therefore, all these issues in mind, in this thesis, a resolved motion kinematic control scheme is recommended as one of the control schemes in such a way that the mobile base (vehicle) and the manipulator actuation are utilized effectively and achieved dexterous mobile manipulation. In the proposed scheme the vehicle motion is decomposed in such a way that the vehicle coordinate frame and the end-effector frame is maintained with the minimum safe distance. The safe distance is decided based on the dexterous workspace of the manipulator arm. So, the vehicle position and orientation are obtained with the help of line of sight (LoS) motion control strategy along with a minimum safe distance as per the manipulator arm characteristics. The manipulator arm joint positions are obtained through the help of closed-form inverse kinematic solution (which is available readily) based on the vehicle position and its orientation along with the desired operational-space pose vector. In order to certify the suggested control, scheme the computed velocity control law is applied on a real time vehicle- manipulator, namely, JR2 and compared with the conventional operational-space control scheme. In order to get an optimal solution, it is mandatory to employ some constrained optimization techniques and few of them are approached in this manner and they are available in the literature [86-89].

The main target is to introduce a robust double-loop motion control scheme for tracking the end-effector of the vehicle-manipulator system under dynamic variations with the help of redundant feedback. The outer-loop consists of the task-space kinematics and the inner-loop consists of the configuration-space system dynamics. Reference [90] focuses on redundancy resolution schemes and gives the solution for inverse kinematics problem for redundant vehicle-manipulator. Reference [91] illustrates that the internal loop aims for the robustness and the outer loop helps in obtaining the desired trajectory tracking performance. In [92], the task–space tracking errors caused due to mechanical errors can be reduced by the proffered dual integral sliding mode control scheme. Reference [93] describes that the feedback can be taken from the motors as well as the end-effector. The actual feedback is necessary for tracking the performance of the system. Dual-loop control scheme is providing much better results than other controller schemes in terms of reduced tracking errors. Reference [93] discusses the PID controller in inner loop with PID sliding mode in outer loop.

For autonomous robots it is essential to first identify the fault and take suitable remedial to prevent any catastrophe. Some effort has been made to identify faults [95][96] and try to minimize their effect in the performance of mobile robot. Generally, minor faults are compensated in closed loop control by their feedback but so is not the case in open loop. The four-mecanum wheel drive mobile robot, under the failure of one actuator the system remains in full actuation capability and can operate to full potential. This make the system good for testing fault tolerant control (FTC) methods. The behaviour of four-mecanum wheel drive mobile robot without fault, with one-fault, with two-fault and then address the FTC technique using kinematic control scheme for both set-point control and trajectory tracking control (circular profile). There are some existing FTC techniques [95][96][97][98][99] and work which incorporates FTC for performance optimization in [100]. The existing techniques mainly deals with passive and active approach where in one case inherent fault is assumed in the system and the control law is used accordingly while the other tries to minimize the deviation from the desired performance using some pre-built control law or on-board computation. Some effort has been made to use under-actuated mobile platform for inspection purpose [101]. Some FTC techniques incorporates line-of-sight (LOS) [102] in which system becomes under-actuated due to failure of more number of actuators than the state variables. The existing FTC techniques are used in the mobile robot along with kinematic control to achieve the goal configuration within tolerance limit.

The structural uncertainty arises due to the presence of an unknown payload held by the end-effector while state inequality constraints arise due to the existence of (unknown) impediments in the work space. As a result, the parametric uncertainties will exist in both kinematic and dynamic equations of the manipulator system. Furthermore, mobile manipulators possess strong coupled dynamics of mobile platforms and manipulator. Therefore, the design of control system becomes an important topic of research for researchers. Moreover, some of the controllers [103, 103] require inverse and controllers from [105, 106, 107] pseudo-inverse of the Jacobian matrix, respectively, leading to numerical instabilities in a singular neighborhood. The inverse kinematic issue is resolved by a general Jacobian pseudo-inverse approach defined in the autogenously configuration space [108]. Recently, Galicki [109] proposed a motion planning scheme for averting both collisions with obstacles and singular configurations based on optimization criteria. One way to resolve the problem of inverse kinematics is to use the task-space based control approach. Based on this concept, recently the task-space region-reaching control is suggested in [110] for regulating medical mobile manipulator without joint velocity measurement.

2.2 Motivation

Since decades, the focus has been drawn to combine mobile robots with manipulators to perform several applications. For many new applications, such as in-service robotics, industrial robots etc. there is a necessity for the robots to work autonomously in an uncertain environment. There are several challenges when it comes to mobile manipulation. For example, the question arises of how to coordinate the movements between the mobile base and the manipulator is a nontrivial issue. Another issue is how to define and specify the control task. Kinematic redundancy allows the redundant manipulators to perform tasks that require high dexterity. They can use the extra dof in their benefit to avoid their joint limits and the obstacles in the workspace, while still reaching a desired end-effector pose in the task-space. It avoids collision with obstacles (in Cartesian space) or kinematic singularities (in joint space). It increases manipulability in specified directions. It minimizes energy consumption or needed motion torques.

In the recent past, the literature reveals that many researchers have successfully designed motion control algorithms for good tracking performance of fixed manipulators. However, it is strenuous to achieve a good performance in case of a mobile manipulator due to the uncertain nature and dynamic variations of the system. Due to unknown payload which varies with structural uncertainty arises while state inequality arises in the workspace. Hence nowadays for uncertain systems designing a motion control scheme becomes a significant area of research. [72-76] These papers analyses work related to mobile manipulators complex task execution to attain the desired trajectory by avoiding high tracking errors which can be executed in operational-space. Lyapunov stability is achieved by fulfilling the constraints and providing a singularity and collision free trajectory of the system.

To obtain dexterous control of holonomic and nonholonomic mechanical systems [111], our main aim is to control task-space positions and also to overcome parametric uncertainties of the dynamic equation an improved adaptive control has been introduced in our work. Therefore, an improved adaptive backstepping design is proffered as a robust controller. This motion control design assures the global asymptotic stability and tracking error convergence for the slowly varying disturbances and uncertainties. The proposed scheme is effectively demonstrated numerically with the help of real-time mobile manipulator parameters.

On the other hand, a group of researchers are working towards the visual based control of vehicle-manipulators [112-115]. It is comparatively easy in terms of implementation. But it involves complex image processing algorithms which are computationally expensive and cannot be deployed on a low-cost microcontroller.

Further controlling the vehicle-manipulator in its operational-space or inverse kinematic based configuration-space may be the feasible solutions. However, the coordination of the mobile base and manipulator cannot be achieved perfectly. In addition, the vehicle and the manipulator should work in certain manner to increase the productivity. For example, the manipulator arm should work within its dexterous work-volume which increases the overall quality of the performance of the total system. Similarly, deploying an operational-space kinematic control with the help of Moore-Penrose pseudo-inverse in [116,117] of the Jacobian matrix may produce a traceable path, however, in certain occasions the vehicle and the manipulator motions are intersecting. Therefore, it requires proper joint limitation to the manipulator arm. The same situation may arise in the constrained based inverse kinematic solution-based control scheme as well. On above, the numerical instability of the Jacobian matrix inverse may end up with an unstable motion controller.

Even kinematic control of a vehicle-manipulator through the help of reinforcement learning has been done in the recent past [121]. But in the computational point of view, these techniques require very high computing facilities and implicate an expensive system.

Therefore, all these issues in mind, in this work, a resolved motion kinematic control scheme is recommended in such a way that the mobile base (vehicle) and the manipulator actuation are utilized effectively and achieved dexterous mobile manipulation. In the proposed scheme the vehicle motion is decomposed in such a way that the vehicle coordinate frame and the end-effector frame is maintained with the minimum safe distance. The safe distance is decided based on the dexterous workspace of the manipulator arm. So, the vehicle position and orientation is obtained with the help of line of sight (LoS) motion control strategy along with a minimum safe distance as per the manipulator arm characteristics. The manipulator arm joint positions are obtained through the help of closed-form inverse kinematic solution (which is available readily) based on the vehicle position and its orientation along with the desired operational-space pose vector. The closed-form inverse kinematics of the manipulator arm is not discussed, since the focus of the paper is related to coordinate motion control of a vehicle-manipulator system.

Therefore, the desired operational-space is resolved as desired configuration-space variables of the vehicle-manipulator. To certify the suggested control, scheme the computed velocity control law is applied on a real time vehicle- manipulator, namely, JR2 and compared with the conventional operational-space control scheme. To get an optimal solution, it is mandatory to employ some constrained optimization techniques and few of them are approached in this manner and they are available in the literature [86-88,117].

As mentioned above, in this work, a novel kinematic control scheme is introduced, and its overall performance is compared to the conventional scheme. It has the capability to incorporate all kinematic constraints and resolves redundancy [118]. Several redundancy resolution schemes have been reviewed in [119] with a comparative empirical evaluation. The advantage of the proposed resolved configuration space-motion is that to track the given operational-space poses trajectory it does not require a Jacobian matrix inverse or pseudo inverse [120]. This work also discusses the asymptotic convergence property of the controllers which assure the stability of the system through the help of Lyapunov direct method as discussed in [120]. This control design handles all the uncertain parameters, disturbances and input constraints in the system. In this work, two performance quantifiers are used and compared numerically between conventional operational-space kinematic control scheme and resolved motion kinematic control scheme in configuration-space.

In the real-time applications and motion control of kinematically redundant systems, a robust double-loop motion control scheme for tracking the end-effector of the vehicle-manipulator system under dynamic variations with the help of redundant feedback is introduced. The outer-loop consists of the task-space kinematics and the inner-loop consists of the configuration-space system dynamics. This work also discusses the tracking performance when uncertainties and disturbances arise during the motion and contact of the vehicle-manipulator with the environment. The main aim of the proposed method is to simultaneously control the velocity of the mobile base and the motion of the end-effector under the effect of parametric uncertainties, coupling effects and external disturbances. In some cases, mobile robot might be used in hazardous environment such as rescuing activities, scientific experiments in critical conditions or long-term operation, where the chance of the failure of the actuators increases drastically. Therefore, it is needed to increase their robustness against possible actuator failure. In some cases, actuator failure causes unnecessary accelerations and forces which are highly dangerous for the mobile robot as well as people nearby. So, for a kinematic redundant mobile manipulator it is vital to introduce a fault tolerant control which can identify the faults of actuators while functioning and minimize the effect in actuator performance.

2.3 Objectives of Work

The main objective of the thesis is to investigate various robust motion control designs for a kinematic redundant mobile manipulator. The objectives are:

- The proposed control law incorporates a feed-forward compensation term used to reinforce the control activity by canceling the effects known disturbances from known reference acceleration;
- A decentralized PID control law is introduced as a feedback part to enlarge the stability of the entire system which would improve

transient performance; and a simple and effective estimation approach to estimate the perturbations from the dynamics of the PID law to negate for unmodeled dynamics of the 3dof Mobile Manipulator and effect of unknown external disturbances.

- An improved adaptive based backstepping design control scheme is proposed which shows better performance when compared with the conventional backstepping control scheme under kinematic and dynamic constraints.
- Motion control design assures the global asymptotic stability and tracking error convergence for the slowly varying disturbances and uncertainties. The proposed scheme is effectively demonstrated numerically with the help of real-time mobile manipulator parameters.
- The suggested backstepping design with a nonlinear disturbance observer evaluates the disturbance vector based on the identified dynamics of the system (in general, imprecise parameters of the system).
- The feasibility, performance and robustness of the suggested controller are demonstrated and investigated numerically with the help of computer-based simulations. The mathematical model used for the computer-based simulations is derived based on a real-time mobile manipulator and the derived model is further verified with an inbuilt gazebo model in a robot operating system (ROS) environment.
- Lyapunov’s method is used for designing the proposed control strategy which also helps to verify the closed-loop stability of the system.
- A comparative analysis of conventional and robust nonlinear adaptive backstepping control method for the desired operational-space motion control of a simple spatial 6-dof wheel-based vehicle-manipulator system in real-time.

- A resolved kinematic motion control approach is analyzed, and the performance is compared with the well-known operational-space kinematic control scheme.
- The proposed control scheme aims to track the given operational-space (end-effector) motion trajectory with the help of resolved configuration-space motion without using the Jacobian matrix inverse or pseudo inverse.
- A performance investigation of 6 dof vehicle-manipulator's operational-space position tracking is executed by extensive real-time experiments based on robot operating system (ROS) inbuilt package.
- Four-mecanum wheeled drive mobile robot wheels' configurations that will give near desired performance with one fault and two faults for both set-point control and trajectory-tracking (circular profile) using kinematic motion control scheme within the tolerance limit.
- A robust double-loop motion control scheme is applied for the end-effector trajectory tracking of the 9 dof spatial JR2 vehicle-manipulator system.

Motion control designs introduced in this thesis are successfully verified with their robustness and sensitivity analysis has been performed. Their performance analysis is also shown and compared with the conventional control schemes. The main aim of the motion control schemes is that the error should converge to zero with minimum energy consumption. It should provide shield against all the parametric and dynamic uncertainties and withstand while all the external disturbances occur. In the next chapter mathematical modelling consisting of the kinematics and dynamics has been discussed for the generalised n-dof systems.

Chapter 3

Mathematical Modelling of a Generalized Mobile Manipulator

3.1 Generalized Model

Mathematical modelling generally deals with the description of the system in many forms such as dynamic model or equations of motion, kinematic or geometric model, and differential equations. n this thesis work the term generalized means, a mobile manipulator consists of a 3-dof mobile base (planar or ground-based) with a n-dof manipulator arm. Figure 3.1 shows the line or conceptual diagram of a generalized mobile manipulator with n number of links.

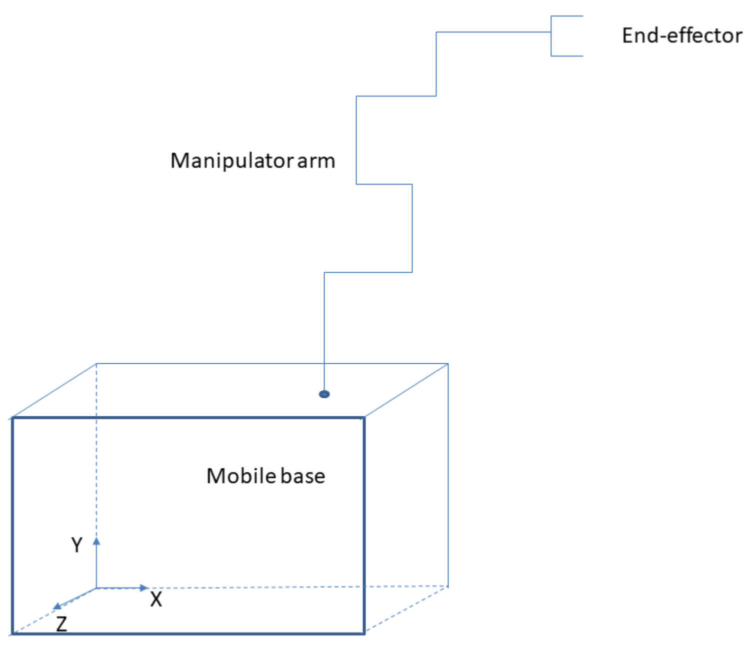

Figure 3.1 Line diagram of a mobile manipulator with n-links

Mobile manipulators mostly perform a pick and place or certain manipulation tasks in three dimensional space which naturally leads to a need for representing the position and orientation of the system. However, the mobile manipulator is a multibody system and involves various frames and their mapping. This chapter concentrates on the study of position, velocity, acceleration known as kinematics on the relations between the motions and the forces and torques that cause them constitute the problem of dynamics. Mathematical model or dynamic simulation model helps in computing the position and orientation of the manipulator's end-effector relative to the base of the manipulator as a function of the joint variables. We will describe all positions and orientations with respect to the with respect to other Cartesian coordinate systems that are (or could be) defined relative to the cartesian system. To describe a motion of the system effectively, set of reference points associated with coordinate frames (simply reference frames) are used to locate and orient the system. Mostly there are two types of reference frames namely inertial and non-inertial frame of reference comes under observational reference frame which lays emphasis on state of motion and implies that the observer is at the rest(fixed) in frame or moving with a constant velocity . In inertial frame of reference, zero net force acts on the body, such a body is at rest and fixed to the environment. On the contrary, the non-inertial frame of references undergoes acceleration with respect to the inertial frame. So a moving frame is a non-inertial reference frame which can translate or rotate along with the body motion. A mobile manipulator is a set of frames, links, each one capable of motion, and velocity is computed starting from the vehicle base to end effector. So with the help of the inertial fixed frame and non-inertial frames such vehicle base (moving) frame, end effector or tool frame the mobile manipulator system position and orientation can be described. Depending on the application of the robot, the end-effector could be a gripper, a welding torch, an electromagnet, or another device. We generally describe the position of the manipulator by giving a description of the tool frame which is attached to the end-effector, relative to the base frame which is attached to the non-moving base of the manipulator.

The characterization of the system which uniquely defines the system configuration refers to generalized coordinates. For example for a 6 dof robotic arm, there are 6 state variables which defines the position of the robot. There are some spaces namely configuration or joint space and operational or task space, which help in describing the system configuration. Configuration space of the robot is the set of all possible positions and orientations for each rigid link of the robot. For the robotic manipulator, it can be assumed that its configuration is completely determined by its joint parameters.. Task space (or Cartesian space or operational space) is defined by the position and orientation of the end effector of a robot. Task space is the cartesian space where the operation of robot is required. It has X,Y and Z ortho normal axes and roll, pitch and yaw rotations about each axes. To relate joint velocities (configuration space) to Cartesian velocities (operational space) of the tip of the arm Jacobians is used. Jacobian is a multidimensional form of the derivative which helps in mapping joint velocities (configurational space) to the end-effector velocities (operational space) .

The existence or non-existence of the kinematic solution defines the workspace of a given manipulator. The workspace of a manipulator arm is the set of all positions that it can reach. It is that volume of space that the end-effector of the manipulator can reach. For a solution to exist, the specified goal point must lie within the workspace. Sometimes, it is useful to consider two definitions of workspace: Dextrous workspace is that volume of space that the robot end-effector can reach with all orientations. That is, at each point in the dextrous workspace, the end-effector can be arbitrarily oriented. The reachable workspace is that volume of space that the robot can reach in at least one orientation.

Mobile manipulator consists of the chain of bodies, joints and links which need to be described. To compute the position and orientation to the tool frame relative to the base frame forward kinematics is required. Forward kinematics can be described kinematically by knowing the four parameters called Denavit Hartenberg parameters [122]. Using Denavit Hartenberg parameters method, kinematics model can be established for any type of mobile manipulator with the n-links The way in which the motion of the manipulator arises from torques applied by the actuators, or from external forces applied to the manipulator. There are two popular approaches to obtain equations of motion of a robot firstly energy based approach namely Lagrange-Euler which is simple and symmetric. Secondly momentum/force approach called Newton-Euler recursive method [124] which is efficient, derivation is simple but messy, it involves vector cross product and allows real-time control.

Let us consider an example of JR2 omni-directional mecanum base autonomous mobile manipulator designed for industrial purposes [123]. JR2 has been developed by Robotnik, Gaitech and Smokie Robotics. The suggested vehicle manipulator consists of summit XL steel base comprises of four mecanum wheels and Aubo-ouri5 manipulator arm with six rotary joints mounted at the top of the XL steel base.

3.2 Kinematic and Dynamic Model of 9dof JR2 Mobile Manipulator

3.2.1 Kinematic Model of 9 dof Mobile Manipulator

In this work, the vehicle-manipulator considered for the motion analysis constitutes a six-link serial manipulator anchored on a four-mecanum wheeled mobile platform. The mobile platform of the vehicle-manipulator is driven by the four independent motored wheels. The photographic image along with the generalized frames of the vehicle-manipulator is shown in Figure 3.2 where, O (0, 0, 0) is the earth-fixed inertial frame. B (x_B, y_B, z_B) is the mobile base (moving) frame and end-effector frame is denoted as

$\mathrm{T}(x_t, y_t, z_t)$. The kinematic frame arrangement of the vehicle-manipulator is shown in Fig.3.3. $\boldsymbol{\eta} \in \Re^{9\times1}$ is the configuration (joint) space vector of position variables, $\boldsymbol{\eta} = [\boldsymbol{\eta}_v \quad \boldsymbol{\eta}_m]^{\mathrm{T}}$. $\boldsymbol{\eta}_v \in \Re^{3\times1}$ is the vehicle base positions and orientation vector and given as: $\boldsymbol{\eta}_v = [x_v \quad y_v \quad \theta_v]^{\mathrm{T}}$ $\boldsymbol{\eta}_m \in \Re^{6\times1}$ is the vector of manipulator rotary joint angles and given as: $\boldsymbol{\eta}_m = [\theta_1 \quad \theta_2 \quad \theta_3 \quad \theta_4 \quad \theta_5 \quad \theta_6]$ where, $\theta_1, \theta_2, \theta_3, \theta_4, \theta_5$ and θ_6 are the joint angles of the manipulator interrelated with serial links.

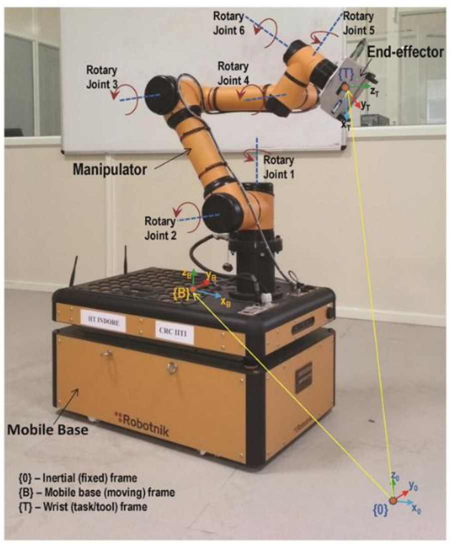

Figure 3.2 Photographic image of the JR2 vehicle-manipulator

However, the actuator inputs are with respect to the vehicle frame, therefore configuration-space velocity vector can be expressed as:

$$\dot{\boldsymbol{\eta}} = \mathbf{J}_1(\boldsymbol{\eta})\boldsymbol{\xi} \tag{3.1}$$

$\boldsymbol{\xi} = [\boldsymbol{\xi}_{\mathbf{b}} \quad \boldsymbol{\xi}_{\mathbf{m}}]^{\mathrm{T}} \in \Re^{9\times1}$ is the control inputs vector in body-fixed coordinate frame or command velocities, where $\boldsymbol{\xi}_{\mathbf{b}} \in \Re^{3\times1}$ is the vector of velocity inputs of the vehicle and $\boldsymbol{\xi}_{\mathbf{m}} \in \Re^{6\times1}$ is the joint velocities vector of the serial manipulator.

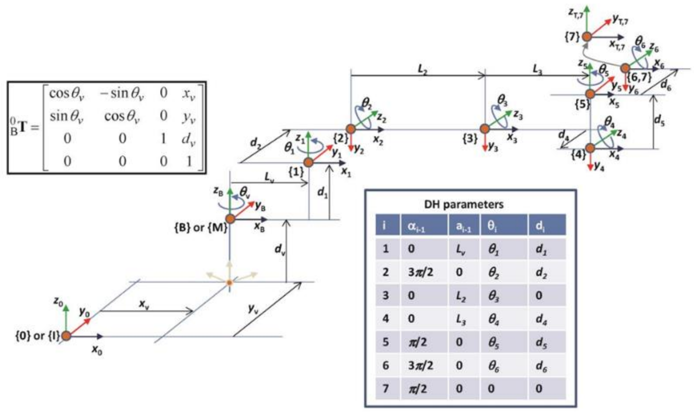

Figure 3.3 Systematic frame arrangements along with kinematic parameters of the JR2 vehicle-manipulator

$\mathbf{J}_1(\boldsymbol{\eta}) \in \Re^{9\times 9}$ is the Jacobian matrix of the vehicle-manipulator which maps the configuration-space velocities from the body-fixed frame to the inertial frame. The proposed vehicle-manipulator constitutes 3 degree of freedom (dof) of vehicle base and a 6-dof manipulator arm. The cylindrical-shaped manipulator links are considered with serial arrangement. Based on the mobile manipulator link parameters in Fig.3.3, the homogeneous transformation matrix [124] which is derived, that specifies the location of the end effector with respect to the base coordinate system, is expressed as:

$$ {}^{0}_{7}T = \begin{bmatrix} & {}^{0}_{7}R & & {}^{0}_{7}P \\ 0 & 0 & 0 & 1 \end{bmatrix} \tag{3.2} $$

$$ T^{k-1}_{k} = \begin{bmatrix} \cos\theta_k & -\sin\theta_k & 0 & a_{k-1} \\ \sin\theta_k \cos a_{k-1} & \cos\theta_k \cos a_{k-1} & -\sin a_{k-1} & -\sin a_{k-1} d_k \\ \sin\theta_k \sin a_{k-1} & \cos\theta_k \sin a_{k-1} & \cos a_{k-1} & \cos a_{k-1} d_k \\ 0 & 0 & 0 & 1 \end{bmatrix} \tag{3.3} $$

The matrix ${}^{0}_{7}R$ and the vector ${}^{0}_{7}P = [P_X \quad P_Y \quad P_Z]^T$ are the rotational matrix and the position vector from the base coordinates to the end effector, respectively. The vehicle-manipulator's kinematic model is formulated and the forward kinematic solution using the Denavit-Hartenberg formulation and the forward kinematic solution of the vehicle-manipulator is expressed below:

$$\mu = \begin{bmatrix} L_v - (d_2 + d_4)\sin\theta_1 + (L_3\cos(\theta_2+\theta_3) + L_2\cos\theta_2)\cos\theta_1 \\ (d_2 + d_4)\cos\theta_1 + (L_3\cos(\theta_2+\theta_3) + L_2\cos\theta_2)\sin\theta_1 \\ d_1 - L_3\sin(\theta_2+\theta_3) - L_2\sin\theta_2 \end{bmatrix} \tag{3.4}$$

3.2.2 Dynamic Model of 9 dof Mobile Maniplator

The Newton-Euler recursive method is used for deriving the equation of motion of the vehicle-manipulator and it can be presented in the matrix and vector form. Detailed derivation for any n -links of manipulator am is as follows:

Outward iterations for computing velocities and acceleration of the joints($\theta, \dot{\theta}, \ddot{\theta}$) are:

First of all it is necessary to compute the rotational velocity and linear and rotational acceleration of the centre of mass of each link of the manipulator at any given instant. Start outward to link n and moves successfully link to link

So that computations will be performed in an iterative way. ω_i is the angular velocity vector, here i denotes the corresponding joint axis (k = 1, 2, 3) and ${}^{i}_{i+1}R$ the rotation matrix, , So the rotational velocity will be:

$${}^{i+1}\omega_{i+1} = {}^{i+1}_{i}R\,{}^{i}\omega_i + \dot{\theta}_{i+1}\,{}^{i+1}\hat{Z}_{i+1} \tag{3.5}$$

For rotary joint the angular acceleration is as follows:

$${}^{i+1}\dot{\omega}_{i+1} = {}^{i+1}_{i}R\,{}^{i}\dot{\omega}_i\;{}^{i+1}_{i}R\,{}^{i}\omega_i \times \dot{\theta}_{i+1}\,{}^{i+1}\hat{Z}_{i+1} + \ddot{\theta}_{i+1}\,{}^{i+1}\hat{Z}_{i+1} \tag{3.6}$$

Then for prismatic joint it is:

$$ {}^{i+1}\dot{\omega}_{i+1} = {}^{i+1}_{i}R\,{}^{i}\omega_i \tag{3.7} $$

Now, computing linear acceleration as:

$$ {}^{i+1}\dot{v}_{i+1} = {}^{i+1}_{i}R[{}^{i}\omega_i \times {}^{i}P_{i+1} + {}^{i}\omega_i \times ({}^{i}\omega_i \times {}^{i}P_{i+1}) + {}^{i}\hat{v}_i] \tag{3.8} $$

Similarly for prismatic joint:

$$ {}^{i+1}\dot{v}_{i+1} = {}^{i+1}_{i}R[{}^{i}\omega_i \times {}^{i}P_{i+1} + {}^{i}\omega_i \times ({}^{i}\omega_i \times {}^{i}P_{i+1}) + {}^{i}\hat{v}_i] + 2\,{}^{i+1}\omega_{i+1} \times \dot{d}_{i+1}\,{}^{i+1}\hat{Z}_{i+1} + \ddot{d}_{i+1}\,{}^{i+1}\hat{Z}_{i+1} \tag{3.9} $$

We also require the linear acceleration of the centre of mass of each link so it is shown below:

$$ {}^{i}v_{ci} = {}^{i}\dot{\omega}_i \times {}^{i}P_{ci}) + {}^{i}\omega_i \times {}^{i}\omega_i + {}^{i}P_{ci}) + {}^{i}\hat{v}_i] \tag{3.10} $$

Forces and torques acting on the centre of each link is:

$$ \begin{aligned} F_i &= m\hat{v}_{ci} \\ N_i &= {}^{ci}I\dot{\omega}_i + \omega_i \times {}^{ci}I\omega_i \end{aligned} \tag{3.11} $$

Inward iterations for computing forces and torques are:

f_i = force exerted on the link i by link i-1

n_i =torque exerted on the link i by link i-1

Forces and torques exerting on the link about the centre of the mass are:

$$ {}^{i}F_i = {}^{i}f_i - {}_{i+1}^{i}R\,{}^{i+1}f_{i+1} \tag{3.12} $$

$$ {}^{i}N_i = {}^{i}n_i - {}_{i+1}^{i}R\,{}^{i+1}n_{i+1} - {}^{i}P_{ci} \times {}^{i}F_i - {}^{i}P_{i+1} \times {}_{i+1}^{i}R\,{}^{i+1}f_{i+1} \tag{3.13} $$

The required joint torques are found by taking the Z component of the torque applied by one link on its neighbour:

$$ \tau_i = {}^{i}n_i^{T}\,{}^{i}\hat{Z}_i \tag{3.14} $$

For prismatic joint:

$$\tau_i = {}^i f_i^T \, {}^i\hat{Z}_i \tag{3.15}$$

In order to express the dynamic equations of a manipulator in a single equation, equation (3.16) shows the structure of the equation which is as follows :

$$\tau = M(\theta)\ddot{\theta} + V(\theta,\dot{\theta}) + G(\theta) \tag{3.16}$$

where $M(\theta)$ is then $n \times n$ mass matrix of the manipulator, $V(\theta,\dot{\theta})$ is an $n \times 1$ vector of centrifugal and Coriolis terms, and $G(\theta)$ is an $n \times 1$ vector of gravity terms.

The recursive Newton-Euler dynamics algorithm for all links, symbolically, yields the equations of motion for the mobile manipulator, it is written as follows:

$$\mathbf{M}(\boldsymbol{\eta})\dot{\boldsymbol{\xi}} + \mathbf{n}(\boldsymbol{\eta},\boldsymbol{\xi}) + \mathbf{g}(\boldsymbol{\eta}) = \boldsymbol{\sigma} \tag{3.17}$$

$$\ddot{\boldsymbol{\eta}} = \mathbf{J}_1(\boldsymbol{\eta})\dot{\boldsymbol{\xi}} + \dot{\mathbf{J}}_1(\boldsymbol{\eta})\dot{\boldsymbol{\eta}} \tag{3.18}$$

$\dot{\boldsymbol{\eta}} \in \Re^{9\times1}$, $\ddot{\boldsymbol{\eta}} \in \Re^{9\times1}$ are the configuration (joint) space velocities and accelerations vector. $\mathbf{M}(\boldsymbol{\eta})\dot{\boldsymbol{\xi}}$ is the vector of inertial forces and moments of the vehicle-manipulator, $\mathbf{n}(\boldsymbol{\eta},\boldsymbol{\xi})$ is the dissipative and non-conservative forces vector which includes frictional, Coriolis and centripetal effects of the vehicle-manipulator, the vector of gravity effects of the vehicle-manipulator is written as $\mathbf{g}(\boldsymbol{\eta})$. $\boldsymbol{\sigma} = [\boldsymbol{\sigma}_v \quad \boldsymbol{\sigma}_m]^{\mathrm{T}} \in \Re^{9\times1}$ is the control inputs vector, where $\boldsymbol{\sigma}_v \in \Re^{3x1}$ is the inputs of the mobile base vector and $\boldsymbol{\sigma}_m \in \Re^{3x1}$ is the input torques vector of the serial manipulator attached on a mobile base. The vector of inputs can be further considered as two variables by considering control inputs and disturbances.

$$\boldsymbol{\sigma} = \boldsymbol{\sigma}_{con} + \boldsymbol{\sigma}_{dis} \tag{3.19}$$

$$\boldsymbol{\sigma}_{dis} = \boldsymbol{\sigma}_{edis} + \boldsymbol{\sigma}_{idis} \tag{3.20}$$

$$\boldsymbol{\sigma}_{idis} = \left(\hat{\mathbf{M}}(\boldsymbol{\eta}) - \mathbf{M}(\boldsymbol{\eta})\right)\dot{\boldsymbol{\xi}} + \left(\hat{\mathbf{n}}(\boldsymbol{\eta},\boldsymbol{\xi}) - \mathbf{n}(\boldsymbol{\eta},\boldsymbol{\xi})\right) + \left(\hat{\mathbf{g}}(\boldsymbol{\eta}) - \mathbf{g}(\boldsymbol{\eta})\right) - \mathbf{F}(\boldsymbol{\eta},\boldsymbol{\xi}) + \boldsymbol{\delta} \tag{3.21}$$

where, $\hat{\mathbf{M}}(\boldsymbol{\eta})$, $\hat{\mathbf{n}}(\boldsymbol{\eta},\boldsymbol{\xi})$ and $\hat{\mathbf{g}}(\boldsymbol{\eta})$ are the noted (inaccurate) model equations of the vehicle-manipulator. $\mathbf{F}(\boldsymbol{\eta},\boldsymbol{\xi})$ is the frictional effects vector which comprises of static, coulomb and viscous frictional effects. $\boldsymbol{\delta}$ is the internal disturbances vector acquainted with the system due to measurement and process noises. $\boldsymbol{\sigma}_{edis}$ is the external disturbances vector acting. on the vehicle-manipulator $\boldsymbol{\sigma}_{idis}$ is the internal disturbances vector due to parametric and frictional effects, disturbances and system uncertainties arises due to measurement and process noises.

3.2.2.1. Actuator Inputs and its Allocations

While correlating the single force actuator inputs with the generalized input vector of the suggested kinematically redundant vehicle-manipulator, the input (control) vector can be rewritten as follows:

$$\boldsymbol{\sigma}_{con} = \mathbf{B}\boldsymbol{\kappa} \tag{3.22}$$

where, $\mathbf{B} \in \Re^{6\times10}$ is the actuator configuration matrix and $\boldsymbol{\kappa} \in \Re^{10\times1}$ is the actuator input vector. The recommended vehicle-manipulator has four actuators (individual wheel motors) inputs in its mobile platform and three rotary actuators as actuator inputs at the manipulator.

Putting value of (3.21) into (3.17) and reorganizing the terms, we have,

$$\dot{\boldsymbol{\xi}} = \mathbf{M}(\boldsymbol{\eta})^{-1}(\mathbf{B}\boldsymbol{\kappa} - \mathbf{n}(\boldsymbol{\eta},\boldsymbol{\xi}) + \mathbf{g}(\boldsymbol{\eta}) + \boldsymbol{\sigma}_{dis}) \tag{3.23}$$

The desired manipulator behaviour is well-chosen and presented in the Cartesian (operational) space. The operational-space position, velocity and acceleration vectors can be insinuated below:

$$\begin{aligned}
&\boldsymbol{\mu} = \text{fun}(\boldsymbol{\eta}) \\
&\dot{\boldsymbol{\mu}} = \mathbf{J}_2(\boldsymbol{\eta})\dot{\boldsymbol{\eta}} = \mathbf{J}_2(\boldsymbol{\eta}) = \mathbf{J}_1(\boldsymbol{\eta})\boldsymbol{\xi} \\
&\dot{\boldsymbol{\eta}} = \mathbf{J}_1(\boldsymbol{\eta})\boldsymbol{\xi} \\
&\ddot{\boldsymbol{\mu}} = \mathbf{J}_2(\boldsymbol{\eta})\ddot{\boldsymbol{\eta}} + \dot{\mathbf{J}}_2(\boldsymbol{\eta})\dot{\boldsymbol{\eta}} \\
&\ddot{\boldsymbol{\mu}} = \mathbf{J}_1(\boldsymbol{\eta})\mathbf{M}(\boldsymbol{\eta})^{-1}(\mathbf{B}\boldsymbol{\kappa} - \mathbf{n}(\boldsymbol{\eta},\boldsymbol{\xi}) + \mathbf{g}(\boldsymbol{\eta}) + \boldsymbol{\sigma}_{dis}) + \dot{\mathbf{J}}_2(\boldsymbol{\eta})\dot{\boldsymbol{\eta}}
\end{aligned} \tag{3.24}$$

Where, $\boldsymbol{\mu} \in \Re^{6x1}$ is the operational-space position vector $\boldsymbol{\mu} = [x \quad y \quad z \quad \alpha \quad \beta \quad \gamma]^T$. $\mathbf{J}_1(\boldsymbol{\eta}) \in \Re^{6\times 9}$ is the Jacobian matrix. However, the vehicle-manipulator has two coordinate frames and the configuration (inertial-fixed) space velocities can be mapped with body-fixed (moving) frame velocities as:

$$\dot{\boldsymbol{\eta}} = \mathbf{J}_1(\boldsymbol{\eta})\boldsymbol{\xi} \tag{3.25}$$

where, $\boldsymbol{\xi} \in \Re^{6x1}$ is the body-fixed frame velocities. Therefore, the operational-space velocities can be rewritten with body-fixed velocities as follows:

$$\dot{\boldsymbol{\mu}} = \mathbf{J}_1(\boldsymbol{\eta})\mathbf{J}_2(\boldsymbol{\eta})\boldsymbol{\xi} = \mathbf{J}(\boldsymbol{\eta})\xi \tag{3.26}$$

Hence kinematics and dynamics of various mobile manipulators with n number of links can been studied as discussed so far in this chapter. Further in the next chapter some motion controller designs studied in this research work have been presented.

Chapter 4

Motion Controller Design

4.1 Introduction

To control the kinematic redundant mobile manipulator with minimal tracking errors and provide an effective performance (that is, at a satisfactory designed level) on the repetitive task-specific motions, the motion controller should be synthesized with all constraints and found the optimum controller design. Controllers are implemented to achieve the aim to follow the desired operational-space pose vector (spatial) trajectory of the vehicle manipulator with uncertainties and time varying external disturbances. System parameters are considered as accurate according to the literature review and disturbances are measured by sensors directly. The optimum controller should overcome the system uncertainties, process and measurement noises, and further reject the unknown disturbances from the external factors. The major objective of the controller is that the zero-error convergence and the controller should overcome and adapt itself from all the issues associated with the system that is, variations in parameters, frictional effects, external and internal disturbances, unmodeled dynamics, etc. This chapter describes the controller design of this motion controller along with its closed-loop system stability analysis.

4.2 Proposed Motion Control Scheme

A robust control methodology helps to deal with system uncertainties due its own parameters, friction, internal measurement noise, payload variations and external disturbances. The accurate state estimation with these uncertainties is still difficult and certain parameters are still more difficult to measure. Most of the existing controllers assume all the parameter to be known but real-time parameters are difficult to estimate and almost impossible to obtain an exact dynamic model of a mobile manipulator due to unavoidable reasons. Good performance cannot be achieved without incorporating advanced controllers. In this thesis various controllers are introduced such as conventional Joint-space control based on inverse kinematics, operational-space end effector position and orientation trajectory tracking control based on Inverse Jacobian, , dual-loop control, resolved motion control, kinematic control, adaptive backstepping and conventional backstepping. These motion control schemes show effective and feasible results when compared with the conventional and recently control schemes. Let us discuss some of the motion control schemes.

4.2.1 Operational-space End Effector Position Trajectory Tracking Control

In this, a robust nonlinear control method is suggested to perfectly follow a desired task space position trajectory of the MM for all possible values of 7 uncertainties and time-varying external disturbances. The idea used in selecting control law is that the tracking errors must converges to zero and stays thereafter even in presence of lumped disturbance and provide strong robustness, excellent transient performance and speedy response. The proposed control law can be divided into three parts as:

- The first control term, η_{ct} is obtained by feedback linearization technique, known as computed torque control. This control approach transforms the nonlinear system into a linear error dynamic. This control term consists of $(\ddot{\mu}d)$ as a feed-forward part responsible for cancelling the effects of known disturbances and $\left(-2\Gamma\dot{\tilde{\mu}} - \Gamma^2\ \tilde{\mu}\right)$ as a feedback part which stabilizes the tracking error dynamics. However, this control alone does not guarantee robustness and stability for all possible values of time-varying uncertainties and external disturbances.

- Hence the second control term considered here, η_{PID} is a PID type controller which helps in enhancing the stability of the whole system. As a result, it advances the transient response of the closed loop system.
- The third term, η_{est} is a disturbance estimator, used to compensate for the error which occurs due to the estimation of perturbations. This estimator estimates all the uncertainties including external disturbances and unknown nonlinear dynamics of the manipulator based on the perturbation from the dynamics of the PID controller.

Therefore, at every sampling period, the control input compensates for the uncertainty that exists during task space trajectory tracking of MM. Thus, eliminates the need of information of the bounds of perturbation vector in prior.

Consequently, the proposed control law can be stated as follows.

$$\eta = A_w^{+} \left(\ddot{\mu}r - K_c sign(\chi)^{\gamma} - \hat{\delta} - \hat{\nu} \right) \tag{4.1}$$

where, $\ddot{\mu}r = \ddot{\mu}d - 2\Gamma\dot{\tilde{\mu}} - \Gamma^2 \tilde{\mu}$

$$\chi = \dot{\tilde{\mu}} + 2\Gamma\tilde{\mu} + \Gamma^2 \int \tilde{\mu} dt$$

$$\dot{\tilde{\mu}} = \dot{\mu}d - \dot{\mu}$$

$$\tilde{\mu} = \mu d - \mu;$$

$$\hat{\delta} = K_o \int \chi dt$$

K_c and K_o are the controller and estimator gain matrices of the proposed controller, respectively and chosen as constant symmetric positive definite (SPD) matrices. $\ddot{\mu}r$ is the vector of reference acceleration. μd , $\dot{\mu}d$, and $\ddot{\mu}d$ are the given desired task space position, velocity and acceleration vectors, respectively. Γ is a positive diagonal matrix. χ is the decentralized PID control input vector. $\hat{\nu}$ is the estimated vector of nonlinear terms (based on approximated model parameter values) of the manipulator. γ is the positive fractional coefficient and ranging from, $0.5 < \gamma < 2$. $\hat{\delta}$ is the estimated uncertainty and disturbance vector.

4.2.1.1 Stability Analysis

In this subsection, the Lyapunov stability analysis tool is employed to show the asymptotic convergence property of the proposed controller. To ensure the asymptotic stability of system, the following assumptions are considered in the controller design.

Assumption 1. The controller and estimator gain matrices namely K_c, K_o and Γ are constant SPD matrices, by design, i.e.

$$\begin{aligned} K_c &= K_c^T > 0 \\ K_o &= K_o^T > 0 \\ and\ \Gamma &= \Gamma^T > 0 \end{aligned} \tag{4.2}$$

Assumption 2. The value of the lumped disturbance is arbitrarily large and slowly varying with time i.e. $\dot{\delta} = 0$

Consider the Lyapunov candidate to be

$$V = \frac{1}{2}\chi^T \chi + \frac{1}{2}\tilde{\delta}^T K_o^{-1}\tilde{\delta} \tag{4.3}$$

where, $\tilde{\delta}$ is the vector of the lumped uncertainty estimation error and can be denoted as

$$\tilde{\delta} = \hat{\delta} - \delta \tag{4.4}$$

Taking derivative of Eq. (4.3) results into,

$$\dot{V} = \chi^T \dot{\chi} + \tilde{\delta}^T K_o^{-1}\dot{\tilde{\delta}} \tag{4.5}$$

where, $\dot{\chi}$ is the change in the control efforts given by the PID control term and is obtained as:

$$\dot{\chi} = \ddot{\tilde{\mu}} + 2\Gamma\dot{\tilde{\mu}} + \Gamma^2\tilde{\mu} \tag{4.6}$$

$$\dot{\chi} = \ddot{\tilde{\mu}} + 2\Gamma\dot{\tilde{\mu}} + \Gamma^2\tilde{\mu} \tag{4.7}$$

From Eq. (4.1) and Eq. (4.7), we can write

$$\dot{\chi} = \ddot{\mu} - \ddot{\mu}_r \tag{4.8}$$

Now putting the value of $\ddot{\mu}$ from Eq. (4.7) into Eq. (4.8) leads to,

$$\dot{\chi} = -K_c sign(\chi)^{\gamma} - \tilde{\delta} \tag{4.9}$$

The time derivative of the estimated uncertainty term is given as

$$\dot{\hat{\delta}} = K_o\chi \tag{4.10}$$

Substitute Eq. (4.9) and Eq. (4.10) into Eq. (4.5), we have

$$\dot{V} = -\chi^T K_c sign(\chi)^{\gamma} - \tilde{\delta}^T K_o^{-1}\dot{\delta} \tag{4.11}$$

As stated in assumption 2, if the uncertainties are slowly time-varying then $\dot{\delta}$ is zero or negligible i.e. $\dot{\hat{\delta}} \approx 0$. Therefore Eq. (4.11) takes the form

$$\dot{V} = -\chi^T K_c sign(\chi)^{\gamma} \leq 0 \tag{4.12}$$

Since, the controller gain matrices Kc and Γ are constant SPD matrices, by design the complete system is asymptotically stable. This implies that the task space trajectory tracking errors will converge to zero asymptotically. Let S be the set of all points where $\dot{V} = 0$ as follows:

$$S = \{x \in \Re \mid \dot{V} = 0\} \quad (4.13)$$

The set is satisfied by $S = \{x \in \Re \mid \chi = 0\}$. If, $\chi(t) = 0$ then $\ddot{\mu} = 0$. This implies that no solution can stay identically in S other than $\tilde{\delta}(t) = 0$. Hence, Lyapunov's direct method and Barbalats Lemma, the tracking error converges to zero asymptotically i.e.

$$\lim_{t\to\infty} \chi(t) = 0, \lim_{t\to\infty} \mu(t) = 0, \lim_{t\to\infty} \dot{\tilde{\mu}}(t) = 0 \quad (4.14)$$

Remark 1. If the lumped disturbance term δ is fast varying with time, then a enough condition for $\dot{V}$ to be negative definite is

$$\tilde{\delta}^T K_o^{-1} \dot{\delta} \geq 0 \quad (4.15)$$

As mentioned in assumption 1 the estimator and controller gain matrices (K_o, K_c and Γ) are constant SPD matrices, ideally inequality in Eq. (3.2) can always be satisfied. However, if in the worst-case scenario, $\tilde{\delta}^T K_o^{-1} \dot{\delta} < 0$ then Eq. becomes:

$$\dot{V} = -\chi^T K_c sign(\chi)^\gamma + \in \quad (4.16)$$

where $\in = -\tilde{\delta}^T K_o^{-1} \dot{\delta}$ is a small positive scalar value. In this case, the task-space tracking errors can be minimized arbitrarily by appropriate choice of design parameters (K_c and K_o) and the uniform ultimate boundedness is guaranteed.

4.2.1.2 Description of the System and Task for Operational-space End Effector Position Tracking Control

To demonstrate the potency of the proposed control method on the proposed robotic system, extensive computer-based simulations were performed. The proposed manipulator system is composed of 3-dof PRRR serial manipulator mounted on 3-dof mobile base. The specifications of the MM used for this study are presented in Table 4.1. The control activity of the proposed control method is validated by choosing complex trajectory tracking task under the effect of lumped disturbance with and without disturbance estimator. The test case chosen such that the manipulator will start moving from its home position and revisit back to the same position after traveling a defined desired complex path. While performing this task the manipulator at home position would picks an object of unknown mass (for example, weigh of 2 kg payload is considered here for simulation), carry this unknown mass along its defined path and drops an object at a desired location point.

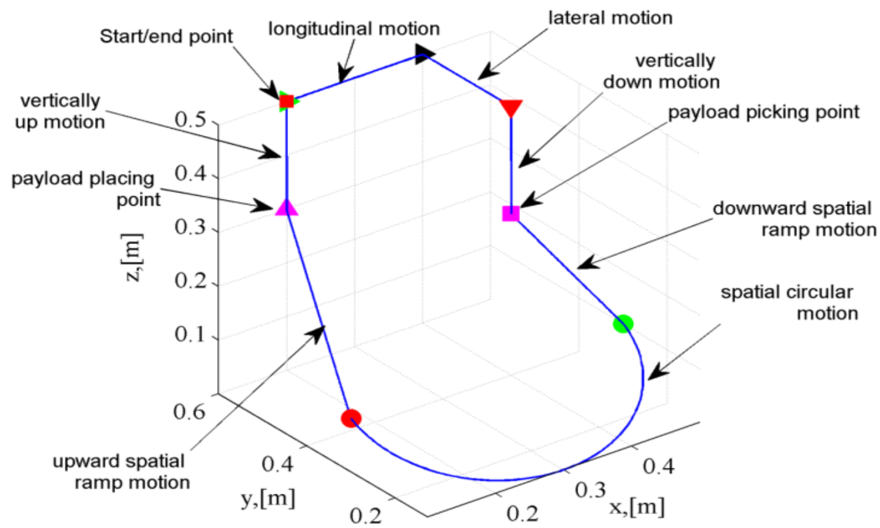

Figure 4.1 Desired end-effector (task space) trajectory from the mobile base top used for the simulations

The complex path consists of a vertically downward motion where the end-effector picks an object of unknown mass, a down- ward spatial ramp followed by a spatial circular motion, upward spatial ramp motion where end-effector drops the payload and ending with by following longitudinal motion and lateral motion as depicted in Figure 5.1.

4.2.2 Operational-space End Effector Position and Orientation Trajectory Tracking Control

Operational-space end effector trajectory tracking pose control is introduced where both positions and orientations has been considered. An improved backstepping design is presented to follow accurately a given desired operational-space position trajectory of the mobile manipulator in the latency of system disturbances and ambiguities. Backstepping is a versatile nonlinear control technique which is simple to design, since it indulges a recursive method to forge the nonlinear control law along with the admissible Lyapunov functions. Furthermore, it has weightiness of rejecting all the unstable nonlinearities, whereas safeguarding the nonlinearities in the system that can be utilized to stabilize it, thus it is truly different from other nonlinear control techniques. The suggested backstepping design with a nonlinear disturbance observer evaluates the disturbance vector based on the identified dynamics of the system (in general, imprecise parameters of the system. The proffered observer surmises the disturbance vector which compensates the next step response based on current state measurements. Two different controllers are used namely a conventional backstepping and the proposed adaptive backstepping control for analyzing the desired trajectory performance. The control laws can be stated as:

Conventional Backstepping Design:

$$\boldsymbol{\tau}_{ct} = \hat{\mathbf{M}}(\mathbf{x}_1)\left(\mathbf{J}^{+}\left(\mathbf{x}_1\right)\left(\ddot{\mathbf{x}}_{1d} + \mathbf{K}_1\dot{\mathbf{e}}_1\right) + \dot{\mathbf{J}}^{+}\left(\mathbf{x}_1\right)\left(\dot{\mathbf{x}}_{1d} + \mathbf{K}_1\mathbf{e}_1\right) + \mathbf{K}_2\mathbf{e}_2 + \mathbf{J}^{\mathrm{T}}\left(\mathbf{x}_1\right)\mathbf{e}_1\right) + \hat{\boldsymbol{\eta}}\left(\mathbf{x}_1, \mathbf{x}_2\right) \quad (4.17)$$

Adaptive Backstepping Design:

$$\boldsymbol{\tau}_{ct} = \hat{\mathbf{M}}(\mathbf{x}_1)\begin{pmatrix}\mathbf{J}^{+}\left(\mathbf{x}_1\right)\left(\ddot{\mathbf{x}}_{1d} + \mathbf{K}_1\dot{\mathbf{e}}_1\right) + \dot{\mathbf{J}}^{+}\left(\mathbf{x}_1\right)\left(\dot{\mathbf{x}}_{1d} + \mathbf{K}_1\mathbf{e}_1\right) \\ +\mathbf{K}_2\mathbf{e}_2 + \mathbf{J}^{\mathrm{T}}\left(\mathbf{x}_1\right)\mathbf{e}_1\end{pmatrix} + \hat{\boldsymbol{\eta}}\left(\mathbf{x}_1, \mathbf{x}_2\right) - \hat{\boldsymbol{\tau}}_{dis} \quad (4.18)$$

4.2.2.1 Stability analysis and Disturbance observer

Assumption 1: Controller gain matrix and observer gain matrix are believed to be symmetric positive definite matrices. i.e.,

$$\mathbf{K}_1 = \mathbf{K}_1^{\mathrm{T}} > 0; \mathbf{K}_2 = \mathbf{K}_2^{\mathrm{T}} > 0; \mathbf{K}_3 = \mathbf{K}_3^{\mathrm{T}} > 0; \tag{4.19}$$

For simplicity, in this numerical investigation these gains are assumed as positive diagonal matrices, as follows:

$$\begin{aligned} &\mathbf{K}_1 = k_1\mathbf{I}_{3\times3}; \mathbf{K}_2 = k_2\mathbf{I}_{6\times6}; \mathbf{K}_3 = k_3\mathbf{I}_{6\times6}; \\ &\text{where, } k_1 > 0, k_2 > 0, k_3 > 0. \end{aligned} \tag{4.20}$$

Assumption 2: The total lumped disturbance vector value is capriciously large, bounded (since, the actuators have limited capabilities, it is assumed that the disturbances are bounded) and gradually changing with time i.e. $\dot{\boldsymbol{\tau}}_{dis} \approx 0$.

The system is bounded to follow the given operational-space position trajectory and the desired operational-space trajectory is considered as $\boldsymbol{\mu}_d$. The system dynamic model can be rewritten as two single order sub-systems in a control-affine form as follows:

$$\begin{aligned} &\dot{\mathbf{x}}_1 = \dot{\boldsymbol{\mu}} = \mathbf{J}\left(\mathbf{x}_1\right)\ \mathbf{x}_2 \\ &\dot{\mathbf{x}}_2 = \dot{\mathbf{q}} = \mathbf{M}(\mathbf{x}_1)^{-1}(\mathbf{B}\boldsymbol{\kappa} - \boldsymbol{\eta}\left(\mathbf{x}_1, \mathbf{x}_2\right) + \boldsymbol{\tau}_{dis}) \end{aligned} \tag{4.21}$$

Here, $\mathbf{x}_1 = \boldsymbol{\mu}$ and $\mathbf{x}_2 = \mathbf{q}$ are the state variables and they will be available as state feedback signals to the motion controller. $\mathbf{x}_1 = \begin{bmatrix} x & y & z \end{bmatrix}^{\mathrm{T}}$ and $\mathbf{x}_2 = \begin{bmatrix} u & v & r & \dot{\theta}_1 & \dot{\theta}_2 & \dot{\theta}_3 \end{bmatrix}^{\mathrm{T}}$. For the proper choice of $\mathbf{x}_2$ can stabilize the first subsystem and allow the sub-system $\boldsymbol{\mu}$ to track the given desired position trajectory, $\boldsymbol{\mu}_d$. However, $\mathbf{x}_2$ is the state vector and available as feedback to the controller and controller cannot choose any values. Therefore, the controller chooses a virtual control vector called $\mathbf{x}_2^{vc}$ and the state $\mathbf{x}_2$ should follows the given, $\mathbf{x}_2^{vc}$. This action can be controlled by the second sub-system with a proper input vector. From these actions, the closed-loop system contains three error state vectors namely,

$$\begin{aligned}
\mathbf{e}_1 &= \mathbf{x}_{1d} - \mathbf{x}_1 \\
\mathbf{e}_2 &= \mathbf{x}_2^{vc} - \mathbf{x}_2 \\
\mathbf{e}_3 &= \boldsymbol{\tau}_{dis} - \hat{\boldsymbol{\tau}}_{dis}
\end{aligned} \tag{4.22}$$

where, $\mathbf{x}_{1d}$ is the desired operational-space position vector $\boldsymbol{\mu}_d$. $\mathbf{x}_2^{vc}$ is the virtual control input vector or in other words virtual reference vector of velocities. $\hat{\boldsymbol{\tau}}_{dis}$ is the estimated disturbances vector . In order to design the motion control for the mobile manipulator, consider a positive Lyapunov's candidate function as follows:

$$V\left(\mathbf{e}_1, \mathbf{e}_2, \mathbf{e}_3\right) = \frac{1}{2}\left(\mathbf{e}_1^{\mathrm{T}}\mathbf{e}_1 + \mathbf{e}_2^{\mathrm{T}}\mathbf{e}_2 + \mathbf{e}_3^{\mathrm{T}}\mathbf{K}_3^{-1}\mathbf{e}_3\right) \tag{4.23}$$

Where, $\mathbf{K}_3$ is a design matrix and assumed as a symmetric positive definite matrix. . Here $V\left(\mathbf{e}_1, \mathbf{e}_2, \mathbf{e}_3\right) \geq 0$ as it is the sum of the individual positive values.

On differentiating the Lyapunov's candidate function analogous to time in together with state trajectories, it gives,

$$\dot{V}\left(\mathbf{e}_1, \mathbf{e}_2, \mathbf{e}_3\right) = \mathbf{e}_1^{\mathrm{T}}\dot{\mathbf{e}}_1 + \mathbf{e}_2^{\mathrm{T}}\dot{\mathbf{e}}_2 + \mathbf{e}_3^{\mathrm{T}}\mathbf{K}_3^{-1}\dot{\mathbf{e}}_3 \tag{4.24}$$

Where $\dot{\mathbf{e}}_1, \dot{\mathbf{e}}_2$ and $\dot{\mathbf{e}}_3$ are the error derivatives. The error derivatives can be written as follows:

$$\dot{\mathbf{e}}_1 = \dot{\mathbf{x}}_{1d} - \dot{\mathbf{x}}_1; \dot{\mathbf{e}}_2 = \dot{\mathbf{x}}_2^{vc} - \dot{\mathbf{x}}_2; \dot{\mathbf{e}}_3 = \dot{\boldsymbol{\tau}}_{dis} - \dot{\hat{\boldsymbol{\tau}}}_{dis}; \tag{4.25}$$

$$\dot{\mathbf{e}}_1 = \dot{\mathbf{x}}_{1d} - \mathbf{J}(\mathbf{x}_1)\mathbf{x}_2, \mathbf{x}_2 = \mathbf{x}_2^{vc} - \mathbf{e}_2$$
$$\dot{\mathbf{e}}_1 = \dot{\mathbf{x}}_{1d} - \mathbf{J}(\mathbf{x}_1)\mathbf{x}_2^{vc} + \mathbf{J}(\mathbf{x}_1)\mathbf{e}_2 \tag{4.26}$$

By choosing proper stabilizing function to the virtual control input in (4.27) as follows:

$$\mathbf{x}_2^{vc} = \mathbf{J}^{+}(\mathbf{x}_1)(\dot{\mathbf{x}}_{1d} + \mathbf{K}_1\mathbf{e}_1), \mathbf{K}_1 = \mathbf{K}_1^{\mathrm{T}} > 0 \tag{4.27}$$

where, $\mathbf{J}^{+}(\mathbf{x}_1)$ is the pseudo inverse of the Jacobian matrix. Substituting (4.27) in (4.26), gives,

$$\dot{\mathbf{e}}_1 = -\mathbf{K}_1\mathbf{e}_1 + \mathbf{J}(\mathbf{x}_1)\mathbf{e}_2 \tag{4.28}$$

Similarly, error derivative of $\dot{\mathbf{e}}_2$ can be indicated as follows:

$$\dot{\mathbf{e}}_2 = \mathbf{J}^{+}(\mathbf{x}_1)(\ddot{\mathbf{x}}_{1d} + \mathbf{K}_1\dot{\mathbf{e}}_1) + \dot{\mathbf{J}}^{+}(\mathbf{x}_1)(\dot{\mathbf{x}}_{1d} + \mathbf{K}_1\mathbf{e}_1) - \mathbf{M}(\mathbf{x}_1)^{-1}(\mathbf{B}\boldsymbol{\kappa} - \boldsymbol{\eta}(\mathbf{x}_1, \mathbf{x}_2) + \boldsymbol{\tau}_{dis}) \tag{4.29}$$

Choose a control vector as follows:

$$\boldsymbol{\tau}_{ct} = \mathbf{B}\boldsymbol{\kappa} = \hat{\mathbf{M}}(\mathbf{x}_1)\begin{pmatrix} \mathbf{J}^{+}(\mathbf{x}_1)(\ddot{\mathbf{x}}_{1d} + \mathbf{K}_1\dot{\mathbf{e}}_1) + \dot{\mathbf{J}}^{+}(\mathbf{x}_1)(\dot{\mathbf{x}}_{1d} + \mathbf{K}_1\mathbf{e}_1) \\ +\mathbf{K}_2\mathbf{e}_2 + \mathbf{J}^{\mathrm{T}}(\mathbf{x}_1)\mathbf{e}_1 \end{pmatrix} + \hat{\boldsymbol{\eta}}(\mathbf{x}_1, \mathbf{x}_2) - \hat{\boldsymbol{\tau}}_{dis} \tag{4.30}$$

Where, K_2 is the controller gain matrix and it is presumed as a symmetric positive definite matrix. i.e., $K_2 = K_2^T > 0$. Substituting values, it gives,

$$\dot{\mathbf{e}}_2 = -\mathbf{J}^{\mathrm{T}}(\mathbf{x}_1)\mathbf{e}_1 - \mathbf{K}_2\mathbf{e}_2 - \mathbf{e}_3 \tag{4.31}$$

The error derivative of $\dot{\mathbf{e}}_3$ is given as:

$$\dot{\mathbf{e}}_3 = \dot{\boldsymbol{\tau}}_{dis} - \dot{\hat{\boldsymbol{\tau}}}_{dis} \tag{4.32}$$

Where choose an adaptive law based on velocity feedback as follows:

$$\hat{\boldsymbol{\tau}}_{dis} = \mathbf{K}_3\hat{\mathbf{M}}(\mathbf{x}_1)\mathbf{x}_2 + \mathbf{x}_3 \tag{4.33}$$

$$\dot{\mathbf{x}}_3 = -\mathbf{K}_3\left(\boldsymbol{\tau}_{ct} - \hat{\boldsymbol{\eta}}\left(\mathbf{x}_1, \mathbf{x}_2\right) + \hat{\boldsymbol{\tau}}_{dis} + \mathbf{e}_2\right) - \mathbf{K}_3\dot{\hat{\mathbf{M}}}(\mathbf{x}_1)\mathbf{x}_2 \tag{4.34}$$

Substituting (4.27) in (4.26), gives

$$\dot{\mathbf{e}}_3 = \dot{\boldsymbol{\tau}}_{dis} - \mathbf{K}_3\left(\mathbf{e}_3 - \mathbf{e}_2\right) \tag{4.35}$$

Since, the mobile manipulator moves slowly, and its disturbance vector is also slowly varying, i.e. $\dot{\tau}_{dis} \approx 0$. This assumption reduces (4.27) as follows:

$$\dot{\mathbf{e}}_3 = -\mathbf{K}_3\left(\mathbf{e}_3 - \mathbf{e}_2\right) \tag{4.36}$$

Substituting it gives,

$$\dot{V}\left(\mathbf{e}_1, \mathbf{e}_2, \mathbf{e}_3\right) = -\left(\mathbf{e}_1^{\mathrm{T}}\mathbf{K}_1\mathbf{e}_1 + \mathbf{e}_2^{\mathrm{T}}\mathbf{K}_2\mathbf{e}_2 + \mathbf{e}_3^{\mathrm{T}}\mathbf{e}_3\right) \tag{4.37}$$

The time derivative of the Lyapunov candidate function is negative definite which means, the chosen control design is globally asymptotically stable, and the error tends to become zero asymptotically.

If the disturbance vector $\dot{\tau}_{dis}$ is not slowly varying and it is bounded, the choice of K_3 can guarantees the stability of the system.

$$\dot{V}\left(\mathbf{e}_1, \mathbf{e}_2, \mathbf{e}_3\right) = -\left(\mathbf{e}_1^{\mathrm{T}}\mathbf{K}_1\mathbf{e}_1 + \mathbf{e}_2^{\mathrm{T}}\mathbf{K}_2\mathbf{e}_2 + \mathbf{e}_3^{\mathrm{T}}\mathbf{e}_3\right) + \mathbf{e}_3^{\mathrm{T}}\mathbf{K}_3^{-1}\dot{\boldsymbol{\tau}}_{dis} \tag{4.38}$$

4.2.2.2 Description of the System and Task for Operational-space End Effector Position and Orientation Trajectory Tracking Control

To authenticate the usefulness of the suggested motion control design, a performance investigation of the mobile manipulator's operational-space position tracking is executed by using the MATLAB/Simulink package. The specifications and the physical parameters of the mobile manipulator which are used for this study presented in Table 4.1. The dynamic parameters considered for the simulations are obtained as per the real-time mobile manipulator namely JR2. The motion control strategy of the current JR2 is not compatible for the users. Further, the proposed operational-space position tracking control requires the positional vector feedback of the wrist (position vector of the fourth joint of the JR2), which is not available at this time.

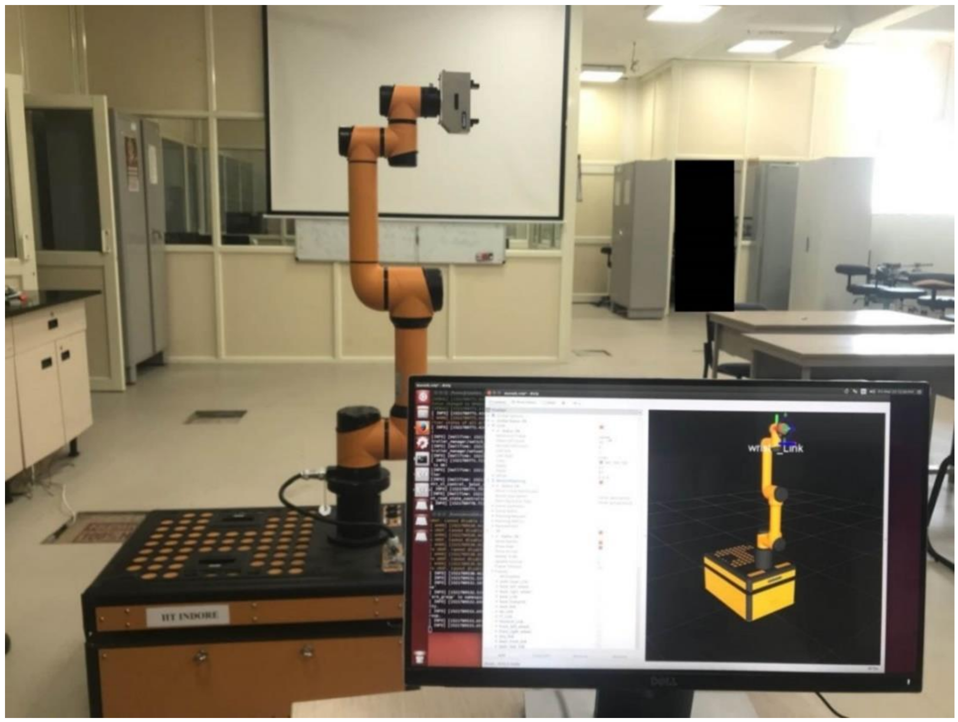

Figure 4.2 Real time image of JR2 mobile manipulator in the MoveIt Software

Therefore, although the real-time robot available with the authors, the real-time validation could not perform and present in this paper. Moreover, the real-time enactment of the designed controller on a real-time mobile manipulator is considered as a future work and it will be available in near future.

Table 4.1 Technical specifications of the JR2 mobile manipulator

Specifications	**Values**
Size of the mobile base	800 mm x550 mm x320 mm
Maximum speed of the mobile base	3 m/s
Number of wheels	3
Number of manipulator axes	6
Work envelope of the manipulator	0.629 m^3
Horizontal distance between the vehicle frame to the manipulator base (L_v)	0.3 m
Vertical distance between the vehicle frame to the manipulator base (d_1)	0.258 m
Vehicle frame from the ground (height) (d_v)	0.32 m
Joint distance of the manipulator's second frame (d_2)	0.15 m
Joint distance of the manipulator's fourth frame (d_3)	0.109 m
Max. payload for the manipulator	2 kg
Length of the manipulator second link ($L2$)	0.308 m
Length of the manipulator third link (L_3)	0.372 m

The photography image of the JR2 mobile manipulator along with its working environment is presented in Figure 4.2. The JR2 consists of an open architecture Robot operating system and Player/Stage Embedded PC with Linux Real Time RBK-IMU (integrated IMU + MAGNETOMETER + GYRO) with RBK-Rotary encoders. The photographic image shows the

JR2 vehicle-manipulator along with its kinematic control package, namely, the MoveIt software in the lab environment. MoveIt is most widely used state of the art software used for the mobile manipulation and establishing modern advances in the motion planning. However, the derived dynamic model is verified in the virtual robot model in Gazebo package environment and the JR2 mobile manipulator in the virtual background is presented in Figure 4.3.

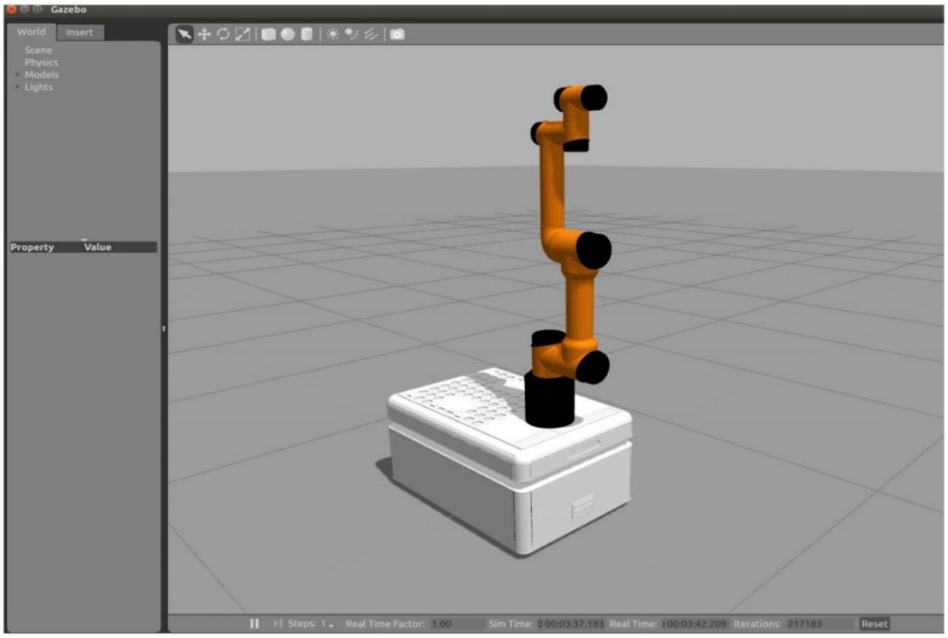

Figure 4.3 JR2 Mobile Manipulator Model in the Gazebo Software

Gazebo is a group of robot operating systems (ROS) packages provides a realistic simulation environment with obstacles and many other objects to test our robot in unknown conditions. The derived model is almost matching with the virtual system motion in both forward and inverse dynamic cases. The mobile manipulator will begin from its home position and bounded to track an eight-shaped spatial position trajectory as given in Figures.4.4 and 4.5. Figure 4.3 describes the desired complex spatial operational space position trajectory for the performance evaluation.

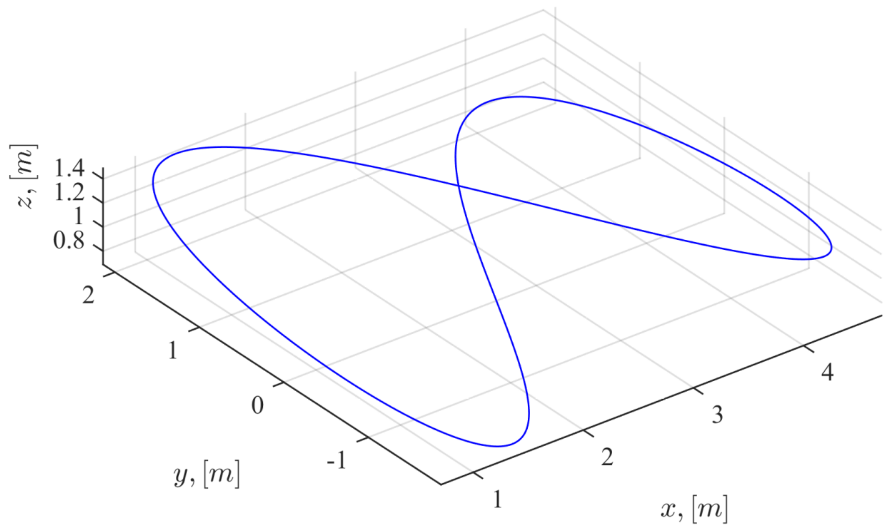

Figure 4.4 Desired complex spatial operational-space position trajectory for the performance evaluation

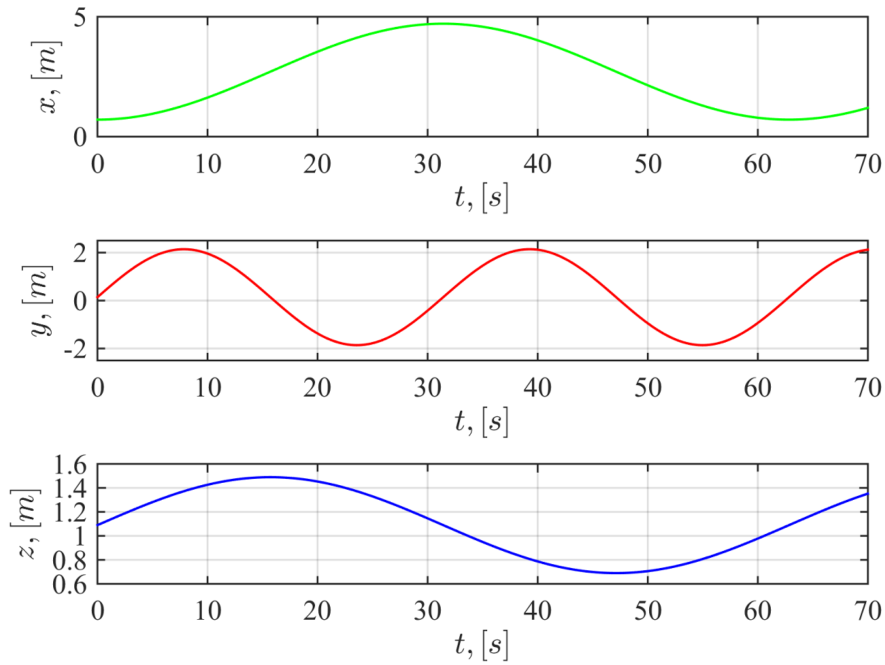

Figure 4.5 Desired operational-space positions time trajectories for the performance evaluation

Figure 4.5 displays the desired operational-space positions time trajectories for the performance evaluation For any mobile base systems, achieving a complex profile pattern as shown in Figure 4.3 is a very complicated and challenging task. The proposed controller follows the given complex pattern successfully which is commonly used in industries for better reliability.

4.2.3 Resolved Motion Control

In this research work, desired trajectory is resolved in configuration-space and kinematic control. The computed velocity control is implemented to achieve the aim to follow the desired operational-space pose vector (spatial) trajectory of the vehicle manipulator with uncertainties and time varying external disturbances. System parameters are considered as accurate according to the literature review and disturbances are measured by sensors directly. The recommended controller along with a nonlinear disturbance observer assesses the disturbance vector depends on the identified system dynamics (normally, imprecise parameters of the system), accessible displacement and velocity measurements (with sensor noises). The main target of the recommended controller is that the tracking errors must converge to zero and the controller should overcome and adapt itself from all the issues associated with the system that is, variations in parameters, frictional effects, external and internal disturbances, Unmodeled dynamics, etc. To perform motion control, two kinematic control schemes are discussed in this article. The control laws used in the research article can be discussed as:

A. Conventional operational-space velocity control:

$$\boldsymbol{\xi} = \mathbf{J}(\boldsymbol{\eta})^{+}\left(\dot{\boldsymbol{\rho}}_{\mathrm{d}} + \mathbf{K}\tilde{\boldsymbol{\rho}}\right) \tag{4.39}$$

where $\mathbf{J}(\boldsymbol{\eta})^{+} \in \Re^{9\times 6}$ is the pseudo inverse of the Jacobian matrix. Jacobian is a non-square matrix. As it is a task space kinematic control so $\mathbf{J}(\boldsymbol{\eta})$ need to be inverted. Hence, we are using Moore–Penrose inverse. $\dot{\boldsymbol{\rho}}_{\mathrm{d}}$ is the vector of desired operational-space velocities $\tilde{\boldsymbol{\rho}} = \boldsymbol{\rho}_\mathrm{d} - \boldsymbol{\rho}$ is the vector of operational-space pose errors. $\boldsymbol{\rho}_\mathrm{d}$ is the desired operational space pose vector. $\boldsymbol{\rho}$ is the actual operational-space pose vector. $\mathbf{K}$ is the controller gain matrix and chosen as a symmetric positive definite matrix, that is, $\mathbf{K} = \mathbf{K}^\mathrm{T} > 0$.

B. Resolved operational-space motion to the configuration-space velocity control

$$\boldsymbol{\xi} = \mathbf{J}_1(\boldsymbol{\eta})^\mathbf{T}\left(\dot{\boldsymbol{\eta}}_\mathrm{d} + \boldsymbol{\Lambda}\tilde{\boldsymbol{\eta}}\right) \tag{4.40}$$

where $\mathbf{J}_1(\boldsymbol{\eta})^\mathrm{T} = \mathbf{J}_1(\boldsymbol{\eta})^{-1} \in \Re^{9\times 9}$ is the inverse of the vehicle Jacobian matrix. $\dot{\boldsymbol{\eta}}_\mathrm{d}$ is the vector of desired inertial frame (earth-fixed) configuration-space velocities which is obtained from the desired operational-space velocities. $\tilde{\boldsymbol{\eta}} = \boldsymbol{\eta}_\mathrm{d} - \boldsymbol{\eta}$ is the vector of configuration-space pose errors. $\boldsymbol{\eta}_\mathrm{d}$ is the desired configuration-space pose vector which is resolved from the operational-space pose vector. $\boldsymbol{\eta}$ is the actual configuration-space pose vector. $\boldsymbol{\Lambda}$ is the controller gain matrix and chosen as a symmetric positive definite matrix, i.e. $\boldsymbol{\Lambda} = \boldsymbol{\Lambda}^\mathrm{T} > 0$

$$\boldsymbol{\eta}_\mathrm{d} = \begin{bmatrix} \boldsymbol{\eta}_\mathrm{dv} \\ \boldsymbol{\eta}_\mathrm{dm} \end{bmatrix} \tag{4.41}$$

where, $\boldsymbol{\eta}_\mathrm{dv} = [x_\mathrm{dv} \quad y_\mathrm{dv} \quad \theta_\mathrm{dv}]^\mathrm{T}$ is the vector of desired positions and orientation of the vehicle. $\boldsymbol{\eta}_\mathrm{dm} = [\theta_\mathrm{1dm} \quad \theta_\mathrm{2dm} \quad \theta_\mathrm{3dm} \quad \theta_\mathrm{4dm} \quad \theta_\mathrm{5dm} \quad \theta_\mathrm{6dm}]^\mathrm{T}$ is the vector of desired joint angles of the spatial manipulator arm. These desired configuration-space variables can be obtained from the desired operational-space pose vector with the help of inverse kinematics. However, the vehicle-manipulator system is a kinematically redundant system and there are multiple solutions exist.]. In this work, it is resolved in two steps, the first step is finding the vehicle positions and orientation with the help of line of sight method along with the dexterous workspace of the manipulator and the second step is finding the inverse kinematic solutions of the spatial manipulator. After the first step operation, the remaining equations are equal to the number of unknowns, i.e., there are six independent equations with six unknowns. Therefore, the solution is obtained with the help of analytical relations and based on the manipulator theory; the closed-form solution is available for the manipulator which is considered for the analysis. In this work, the inverse kinematic solution of the manipulator arm is not discussed as it is not the core research content of this work. Moreover, the inverse kinematic solution of the manipulator can be obtained using the partial Jacobian matrix inverse (i.e., using the Jacobian matrix of the manipulator arm alone).

The vector of desired positions and orientation of the vehicle can be obtained as follows:

$$
\begin{aligned}
\theta_{\mathrm{vd}} &= \operatorname{atan} 2\left(\dot{y}_{\mathrm{d}}, \dot{x}_{\mathrm{d}}\right) \\
x_{\mathrm{vd}} &= x_{\mathrm{d}} - R_{\min} \cos \theta_{\mathrm{vd}} \\
y_{\mathrm{vd}} &= y_{\mathrm{d}} - R_{\min} \sin \theta_{\mathrm{vd}}
\end{aligned}
\tag{4.42}
$$

where, $R_{\min}$ is the minimum safe radial distance between the vehicle frame and the end-effector frame. The minimum safe radial distance can be decided based on the manipulator dexterous workspace. The vector of desired joint angles of the manipulator can be obtained as follows:

$$
\boldsymbol{\eta}_{\mathrm{dm}} = fun(\boldsymbol{\mu}) \tag{4.43}
$$

where, $\boldsymbol{\mu}$ is the manipulator pose vector from its base frame and it is resolved from the original operation-space pose vector and the desired positions and the orientation of the vehicle. Simple conventional base velocity control and resolved based operational space motion are compared and evaluated. Both the controllers are almost equal and providing same result while kinematic control. If motion control dynamics is available, then it can be extended up to dynamic control. Further, it can be expressed as per the proposed method as follows:

$$\boldsymbol{\mu} = \begin{bmatrix} (R_{\mathrm{min}} - l_{\mathrm{v}})\cos\theta_{\mathrm{vd}} \\ (R_{\mathrm{min}} - l_{\mathrm{v}})\sin\theta_{\mathrm{vd}} \\ z_{\mathrm{d}} - d_{\mathrm{v}} \\ \alpha_{\mathrm{d}} \\ \beta_{\mathrm{d}} \\ \gamma_{\mathrm{d}} \end{bmatrix} \tag{4.44}$$

4.2.3.1 Stability Analysis

The proposed controller closed loop asymptotic stability is verified by Lyapunov direct method. The below mentioned presumptions are well-chosen to assure the asymptotic convergence of disturbance and trajectory tracking response in the overall closed-loop system:

Assumption 1: The controller gain matrices and chosen symmetric positive definite matrix which is given as:

$$\boldsymbol{\Lambda} = \boldsymbol{\Lambda}^{\mathrm{T}} > 0; \mathbf{K} = \mathbf{K}^{\mathrm{T}} > 0; \tag{4.45}$$

In this numerical investigation these gains are assumed as positive diagonal matrices for simplicity, as follows:

$$\boldsymbol{\Lambda} = k_1 \mathbf{I}_{9\times 9}; \mathbf{K} = k_2 \mathbf{I}_{6\times 6};$$

$$k_1 > 0, k_2 > 0; \tag{4.46}$$

Here, $\dot{\tilde{\boldsymbol{\eta}}} = \dot{\boldsymbol{\eta}}_{\mathrm{d}} - \dot{\boldsymbol{\eta}}$ is the vector of configuration-space velocity errors.

$\dot{\boldsymbol{\eta}}_{\mathrm{d}}$ is the desired configuration-space velocity vector which is resolved from the operational-space velocity vector. $\dot{\boldsymbol{\eta}}$ is the vector of actual configuration-space velocity.Chosen Lyapunov candidate function for the proposed resolved motion control scheme is mentioned below:

$$V_1(\tilde{\boldsymbol{\eta}}) = \frac{1}{2}\tilde{\boldsymbol{\eta}}^{\mathrm{T}}\tilde{\boldsymbol{\eta}} \tag{4.47}$$

Further differentiating with respect to time along with state trajectories, it gives,

$$\dot{V}_1(\tilde{\boldsymbol{\eta}}) = \tilde{\boldsymbol{\eta}}^{\mathrm{T}}\dot{\tilde{\boldsymbol{\eta}}} \tag{4.48}$$

$$\dot{\boldsymbol{\eta}} = \mathbf{J}_1(\boldsymbol{\eta})\boldsymbol{\xi} \tag{4.49}$$

$$\boldsymbol{\xi} = \mathbf{J}^{-1}(\boldsymbol{\eta})[\dot{\boldsymbol{\eta}}_d + k_1\tilde{\boldsymbol{\eta}}] \tag{4.50}$$

$$\dot{\tilde{\boldsymbol{\eta}}} = \dot{\boldsymbol{\eta}}_d - [\dot{\boldsymbol{\eta}}_d + k_1\tilde{\boldsymbol{\eta}}] = -k_1\tilde{\boldsymbol{\eta}} \tag{4.51}$$

Substituting (4.49) in (4.43), it becomes

$$\dot{V}_1(\tilde{\boldsymbol{\eta}}) = -\tilde{\boldsymbol{\eta}}^{\mathrm{T}}k_1\tilde{\boldsymbol{\eta}} \tag{4.52}$$

Lyapunov candidate function for the conventional operational-space control scheme, as follows:

$$V_2(\tilde{\boldsymbol{\mu}}) = \frac{1}{2}\tilde{\boldsymbol{\rho}}^{\mathrm{T}}\tilde{\boldsymbol{\rho}} \tag{4.53}$$

After differentiating with respect to time along with state trajectories, it gives,

$$\dot{V}_2(\tilde{\boldsymbol{\mu}}) = \tilde{\boldsymbol{\rho}}^{\mathrm{T}}\dot{\tilde{\boldsymbol{\rho}}} \tag{4.54}$$

Operational space velocity errors will be the difference between desired operational space velocities and actual operational space velocities which is stated as:

$$\dot{\tilde{\boldsymbol{\rho}}} = \dot{\tilde{\boldsymbol{\rho}}} - \dot{\boldsymbol{\rho}} \tag{4.55}$$

$$\dot{\boldsymbol{\rho}} = \mathbf{J}_{\mathbf{1}}(\boldsymbol{\eta})\boldsymbol{\xi} = \mathbf{J}_{\mathbf{2}}(\boldsymbol{\eta})\dot{\boldsymbol{\eta}}$$

(4.54) $\dot{\boldsymbol{\rho}} = \mathbf{J}_2(\boldsymbol{\eta})\mathbf{J}_1(\boldsymbol{\eta})\boldsymbol{\xi} = J(\boldsymbol{\eta})\boldsymbol{\xi}$ (4.55)

$$\boldsymbol{\xi} = \mathbf{J}^{+}(\boldsymbol{\eta})[\dot{\boldsymbol{\rho}}_d + k_2\tilde{\boldsymbol{\rho}}] \tag{4.56}$$

Substituting (4.56) in (4.52), it becomes

$$\dot{V}_2(\tilde{\boldsymbol{\mu}}) = -(\tilde{\boldsymbol{\rho}}^{\mathrm{T}} k_{\mathbf{2}}\tilde{\boldsymbol{\rho}}) \tag{4.57}$$

The Lyapunov candidate function's time derivatives are negative definite (strictly) which means that chosen control designs are globally asymptotically stable and the tracking errors converge to zero asymptotically. The controller parameters of the controller schemes, namely, k_1 and k_2. These values are tuned in such a way that the controller performances are almost same in the real-time environment with the help of MoveIt**.**

4.2.3.2 Description of the System and Task for Resolved Motion Control

To validate the usefulness of the suggested motion control design, a performance investigation of the vehicle-manipulator's operational-space position tracking is executed by extensive real-time experiments based on robot operating system (ROS) inbuilt package. For quantification measurement, it is validated by performing the robustness and sensitivity analyses. Kinematic control is a high-level user-friendly control where optimized values are considered. The proffered vehicle manipulator comprises of 6-dof manipulator attached on a 3-dof vehicle base**.** The specifications along with the geometrical and other parameters of the vehicle-manipulator which are used for this study presented in Table 4.2. Vehicle joint positions have small sensor (measurement) noises and filter design is out of scope for the current work. However, the JR2 system has a reliable sensor system based on an inbuilt extended Kalman filter fused with multiple sensors namely, odometer, motor encoders, accelerometer and rate-gyros. Since, the inner-loop control of the JR2 is hard-coded and has an inbuilt proportional-integral-derivate (PID) tuned based on hardware (wired), the motion control strategy of the current JR2 is not compatible for the users. However, the kinematic level controller is quite open and flexible, the inbuilt PID control takes the user given velocity inputs and control the system in dynamic level. The JR2 consists of an open architecture ROS and Player/Stage Embedded PC with Linux Real Time RBK-IMU (integrated IMU + MAGNETOMETER + GYRO) with RBK-Rotary Encoders. The photography image of the JR2 vehicle-manipulator along with its kinematic control package, namely, the MoveIt software in the lab environment is shown in Figure 4.6.

Table 4.2 Geometrical Parameters of the JR2 mobile manipulator

Specifications	**Values**
Size of the mobile base	800 mm x550 mm x320 mm
Maximum speed of the mobile base	3 m/s
Number of wheels	3
Number of manipulator axes	6
Work envelope of the manipulator	0.629 m^3
Horizontal distance between the vehicle frame to the manipulator base (L_v)	0.3 m
Vertical distance between the vehicle frame to the manipulator base (d_1)	0.258 m
Vehicle frame from the ground (height) (d_v)	0.32 m

Joint distance of the manipulator's second frame (d_2)	0.15 m
Joint distance of the manipulator's fourth frame (d_3)	0.109 m
Joint distance of the manipulator's fifth frame (d_5)	0.102 m
Joint distance of the manipulator's sixth frame (d_6)	0.0825 m
Length of the manipulator second link (L_2)	0.308 m
Length of the manipulator third link (L_3)	0.372 m

We are performing kinematic control with the help of MoveIt which is enabled to JR2. MoveIt is most widely used state of the art software used for the mobile manipulation and establishing modern advances in the motion planning. In order to validate the proposed scheme along with the conventional scheme, we have taken four different profiles. The vehicle-manipulator will start moving from its original position and return back to its own position. In order to show robustness and effectiveness it tracks four different spatial position trajectories as given in Figure 4.7a) eight-shaped trajectory 4.7b) infinity-shaped trajectory 4.7c) circular-shaped trajectory 4.7d) square-shaped trajectory. Both the controllers are shown in real time are experimental platform deployed. We have conducted every experiment five times in the real time environment on JR2. Two error quantifiers along with two position and orientation error have been used. Figures 4.8 to 4.11 presents the time trend of the given preferred operational-space positions for the performance evaluation of eight-shaped trajectory, infinity-shaped trajectory, circular-shaped trajectory, square-shaped trajectory. For any manipulator, task is strenuous to achieve the complicated eight and infinity shaped trajectories. In case of resolved operational-space motion to the configuration-space velocity control in all four cases initial errors are higher. The error quantifiers prove that both the control schemes are performing equivalent. Figure 4.12 shows the flowchart representation of the kinematic control model in the real time environment.

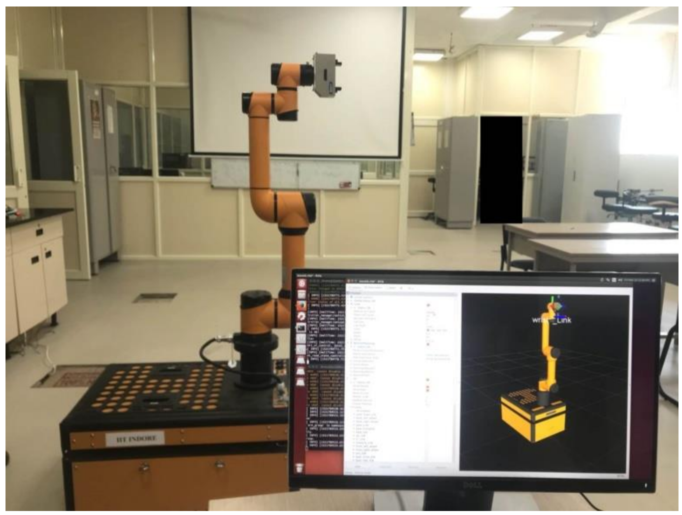

Figure 4.6 Photographic image of the JR2 vehicle-manipulator along with its kinematic control package, namely, the MoveIt software in the lab environment

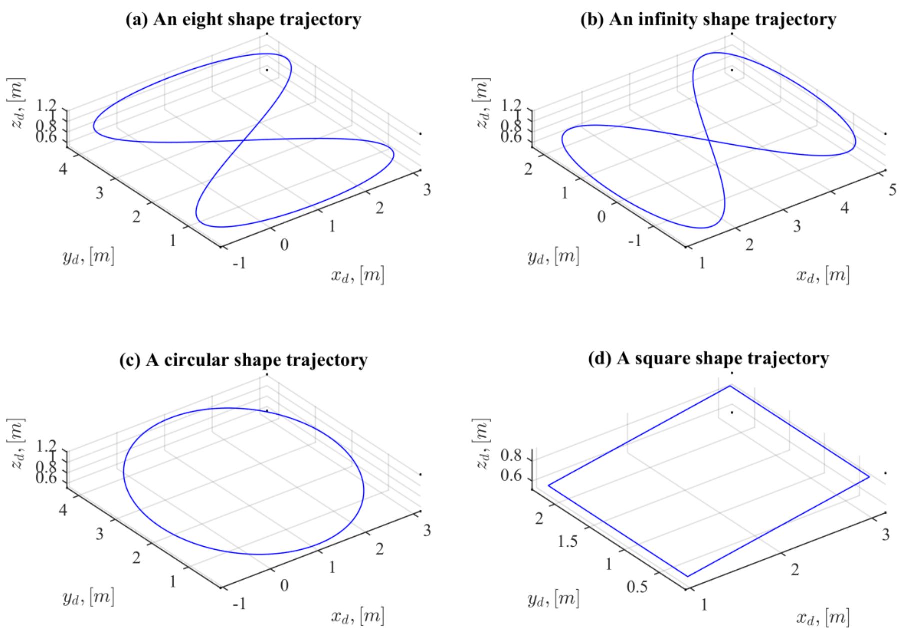

Figure 4.7 Desired complex spatial operational-space position trajectories for the performance evaluation

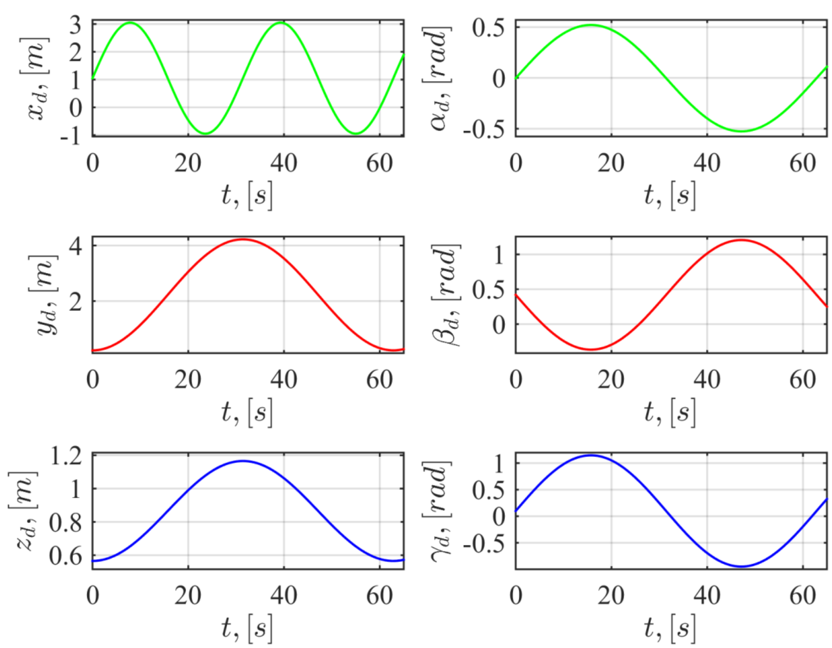

Figure 4.8 Time trend of the given preferred operational-space positions for the performance evaluation in eight-shaped trajectory

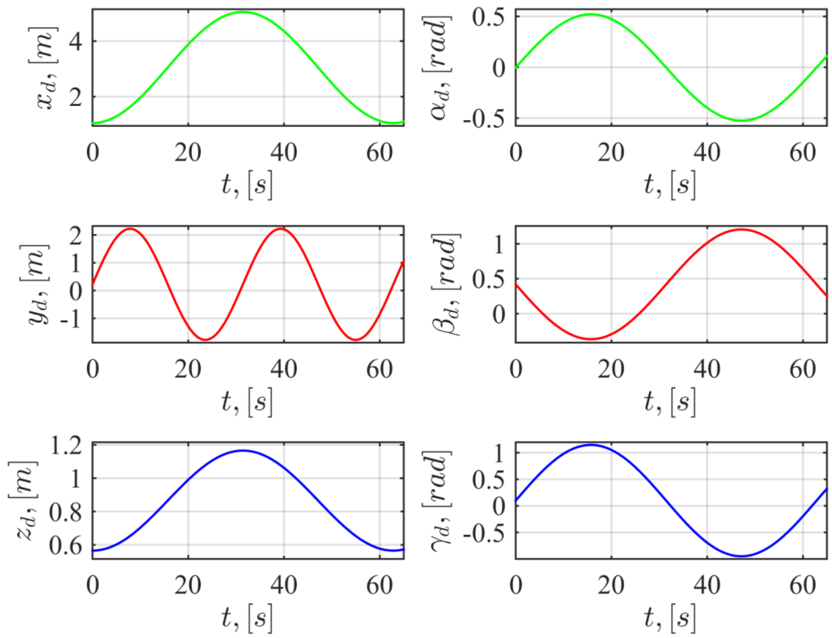

Figure 4.9 Time trend of the given preferred operational-space positions for the performance evaluation in infinity-shaped trajectory

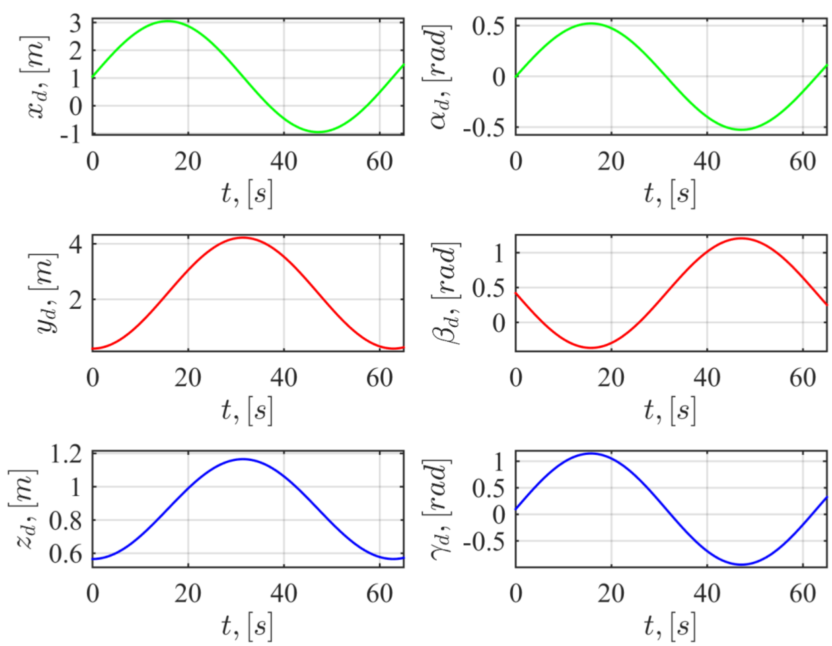

Figure 4.10 Time trend of the given preferred operational-space positions for the performance evaluation in circular-shaped trajectory

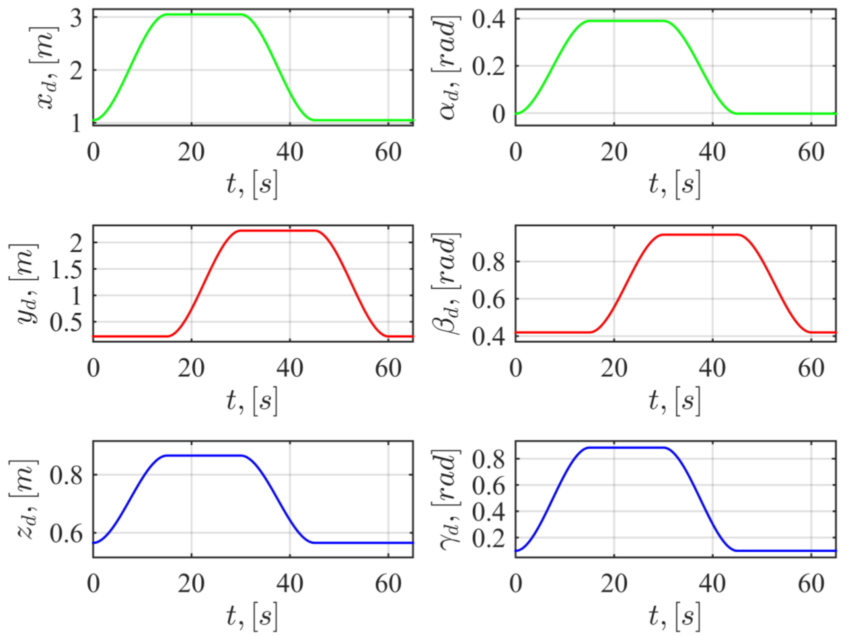

Figure 4.11 Time trend of the given preferred operational-space positions for the performance evaluation in square-shaped trajectory

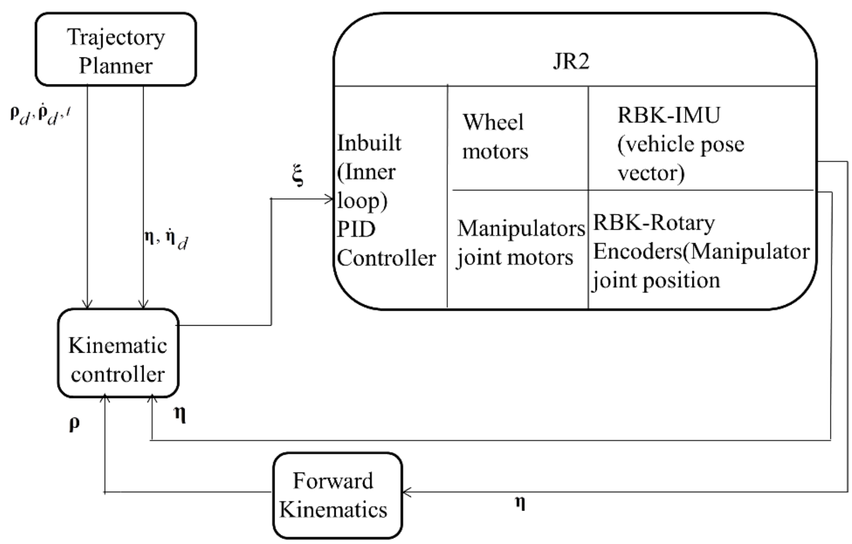

Figure 4.12 Flowchart representation of the kinematic control model in the real time environment

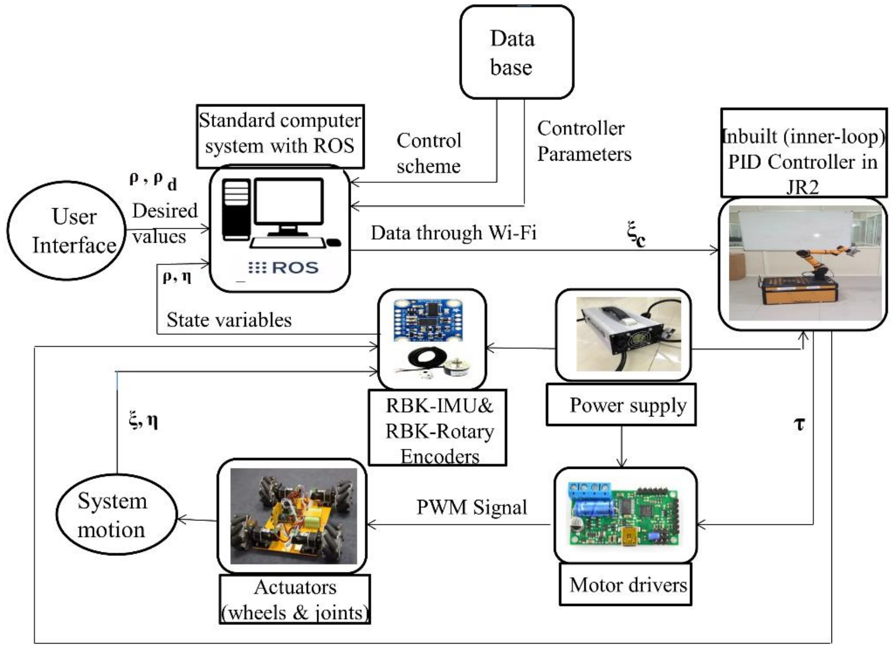

Figure 4.13 Sequence of flow between the components of the JR2 vehicle-manipulator in real-time working conditions

Figure 4.13 demonstrates sequence of flow between the system components of the JR2 vehicle-manipulator. In the above-mentioned flowchart data base containing all the desired values, controller parameters and control scheme are provided to the open-source robot operating system (ROS) computer system by the user. The entire database is transferred to the inbuilt PID control system of the JR2 vehicle-manipulator system. When power is supplied to the motor drivers pulse width modulation signals are sent to the actuator wheels and joints which thereby helps in the motion of the system. System motion values are further sent to the IMU sensor and rotary encoders for calibrating the real-time values from IMU and rotary encoders. State variable values obtained from the sensor and encoders are transferred to the ROS integrated system. The controller parameters of both schemes, namely, k and ω values are chosen as 5 and 3 in such a way that both controllers are giving almost same performance in terms of error quantifiers. For better quantification, the values of root mean square (RMS) errors and integral-time of absolute errors (ITAE) have been recorded. Both control schemes are equivalent after initial transient point. The steady state behaviour is also equivalent. These proposed controller follows all the four patterns successfully which are used in commercial sector. In this article for analysing the trajectory performance following conventional operational space backstepping control scheme is used. For measuring the controller's performance, two error quantifiers are used in this article, namely, Integral Time of Absolute error and Root Mean Square Error. The error quantifier's act plays a significant role in measuring controller's performance. Integral Time of Absolute error integrates the absolute error multiplied by the time over time. It is the square root of the average of squared errors. Equation 5.3 calculates the end-effector position and orientation error values which is used in measuring performance quantifiers. Equation 5.3 calculates root mean square error values and Integral Time of Absolute error as shown below:

$$\begin{aligned} \tilde{p} &= \sqrt{(x_{\mathrm{d}} - x)^2 + (y_{\mathrm{d}} - y)^2 + (z_{\mathrm{d}} - z)^2} \\ \tilde{o} &= \sqrt{(\alpha_{\mathrm{d}} - \alpha)^2 + (\beta_{\mathrm{d}} - \beta)^2 + (\gamma_{\mathrm{d}} - \gamma)^2} \end{aligned} \tag{4.58}$$

$$\begin{aligned} \tilde{x}_{\mathrm{rms}} &= \sqrt{\frac{\sum_{i=1}^{n} (x_{\mathrm{di}} - x_{\mathrm{i}})^2}{n}} \\ \tilde{x}_{\mathrm{itae}} &= \int t \left| x_{\mathrm{d}} - x \right| dt \end{aligned} \tag{4.59}$$

4.2.4 Robust Dual Loop Control

Double-loop controller consists of inner-loop controller and outer-loop controller. The outer-loop controller consists of the operational-space kinematics whereas inner-loop controller consists of the configurational-space system dynamics.

$$\boldsymbol{\sigma}_{con} = \hat{\mathbf{M}}(\mathbf{x}_1)\begin{pmatrix} \mathbf{J}^+\left(\mathbf{x}_1\right)\left(\ddot{\mathbf{x}}_{1d} + \mathbf{K}_1\dot{\mathbf{e}}_1\right) + \\ \dot{\mathbf{J}}^+\left(\mathbf{x}_1\right)\left(\dot{\mathbf{x}}_{1d} + \mathbf{K}_1\mathbf{e}_1\right) \\ +\mathbf{K}_2\mathbf{e}_2 + \mathbf{J}^{\mathrm{T}}\left(\mathbf{x}_1\right)\mathbf{e}_1 \end{pmatrix} + \hat{\boldsymbol{\eta}}\left(\mathbf{x}_1, \mathbf{x}_2\right) - \hat{\boldsymbol{\sigma}}_{dis} \tag{4.60}$$

where, $\dot{e}_1$, $\dot{e}_2$ and $\dot{e}_3$ are the error time derivatives. By choosing proper stabilizing function to the virtual control input and substituting virtual control in error derivatives. $\mathbf{J}^+(\mathbf{x}_1)$ is the pseudo inverse of the Jacobian matrix. K_2 is the controller gain matrix and presumed as a symmetric positive definite matrix. i.e., $K_2 = K_2^T > 0$ choose an adaptive law based on velocity feedback as follows:

$$\begin{aligned} \hat{\boldsymbol{\sigma}}_{dis} &= \mathbf{K}_3\hat{\mathbf{M}}(\mathbf{x}_1)\mathbf{x}_2 + \mathbf{x}_3 \\ \dot{\mathbf{x}}_3 &= -\mathbf{K}_3\left(\boldsymbol{\sigma}_{con} - \hat{\boldsymbol{\sigma}}\left(\mathbf{x}_1, \mathbf{x}_2\right) + \hat{\boldsymbol{\sigma}}_{dis} + \mathbf{e}_2\right) - \mathbf{K}_3\dot{\hat{\mathbf{M}}}(\mathbf{x}_1)\mathbf{x}_2 \end{aligned} \tag{4.61}$$

$$\dot{\mathbf{e}}_3 = \dot{\boldsymbol{\sigma}}_{dis} - \mathbf{K}_3\left(\mathbf{e}_3 - \mathbf{e}_2\right) \tag{4.62}$$

Since, the vehicle-manipulator moves slowly, and its disturbance vector is also slowly varying, i.e. $\dot{\xi}_{dis} \approx 0$. $\dot{e}_3$ reduces as follows:

$$\dot{\mathbf{e}}_3 = -\mathbf{K}_3\left(\mathbf{e}_3 - \mathbf{e}_2\right) \tag{4.63}$$

4.2.4.1 Stability Analysis and Disturbance Observer

Consider the system of which the governing equations are given. The system dynamic model can be rewritten as two single order sub-systems in a control-affine form which is expressed as:

$$\begin{aligned} \dot{\mathbf{x}}_1 &= \dot{\boldsymbol{\mu}} = \mathbf{J}\left(\mathbf{x}_1\right)\ \mathbf{x}_2 \\ \dot{\mathbf{x}}_2 &= \dot{\boldsymbol{\xi}} = \mathbf{M}(\mathbf{x}_1)^{-1}(\mathbf{B}\boldsymbol{\kappa} - \boldsymbol{\sigma}\left(\mathbf{x}_1, \mathbf{x}_2\right) + \boldsymbol{\sigma}_{dis}) \end{aligned} \tag{4.64}$$

Here, $\mathbf{x}_1 = \boldsymbol{\mu}$ and $\mathbf{x}_2 = \mathbf{q}$ are the state variables and they will be available as state feedback signals to the motion controller. $\mathbf{x}_1 = \begin{bmatrix} x & y & z \end{bmatrix}^{\mathrm{T}}$ and $\mathbf{x}_2 = \begin{bmatrix} u & v & r & \dot{\theta}_1 & \dot{\theta}_2 & \dot{\theta}_3 \end{bmatrix}^{\mathrm{T}}$. For the proper choice of $\mathbf{x}_2$ can stabilize the first subsystem and allow the sub-system $\boldsymbol{\mu}$ to track the given desired position trajectory, $\boldsymbol{\mu}_d$. However, $\mathbf{x}_2$ is the state vector and available as feedback to the controller and controller cannot choose any values. Therefore, the controller chooses a virtual control vector called $\mathbf{x}_2^{vc}$ and the state $\mathbf{x}_2$ should follows the given, $\mathbf{x}_2^{vc}$. This action can be controlled by the second sub-system with a proper input vector. From these actions, the closed-loop system contains three error state vectors namely,

$$\begin{aligned} \mathbf{e}_1 &= \mathbf{x}_{1d} - \mathbf{x}_1 \\ \mathbf{e}_2 &= \mathbf{x}_2^{vc} - \mathbf{x}_2 \\ \mathbf{e}_3 &= \boldsymbol{\tau}_{dis} - \hat{\boldsymbol{\tau}}_{dis} \end{aligned} \tag{4.65}$$

where, $\mathbf{x}_{1d}$ is the desired operational-space position vector $\boldsymbol{\mu}_d$. $\mathbf{x}_2^{vc}$ is the virtual control input vector or in other words virtual reference vector of velocities. $\hat{\boldsymbol{\tau}}_{dis}$ is the estimated disturbances vector .

In order to design the motion control for the mobile manipulator, consider a positive Lyapunov's candidate function as follows:

$$V\left(\mathbf{e}_1, \mathbf{e}_2, \mathbf{e}_3\right) = \frac{1}{2}\left(\mathbf{e}_1^{\mathrm{T}}\mathbf{e}_1 + \mathbf{e}_2^{\mathrm{T}}\mathbf{e}_2 + \mathbf{e}_3^{\mathrm{T}}\mathbf{K}_3^{-1}\mathbf{e}_3\right) \tag{4.66}$$

Where, K_3 is a design matrix and assumed as a symmetric positive definite matrix. On differentiating the Lyapunov function when relating to time along with state trajectories, it presents as:

$$\dot{V}\left(\mathbf{e}_1, \mathbf{e}_2, \mathbf{e}_3\right) = \mathbf{e}_1^{\mathrm{T}}\dot{\mathbf{e}}_1 + \mathbf{e}_2^{\mathrm{T}}\dot{\mathbf{e}}_2 + \mathbf{e}_3^{\mathrm{T}}\mathbf{K}_3^{-1}\dot{\mathbf{e}}_3 \tag{4.67}$$

where, $\dot{e}_1$, $\dot{e}_2$ and $\dot{e}_3$ are the error time derivatives. By choosing proper stabilizing function to the virtual control input and substituting virtual control in error derivatives. $\mathbf{J}^{+}(\mathbf{x}_1)$ is the pseudo inverse of the Jacobian matrix. Choose a control vector as presented:

$$\boldsymbol{\sigma}_{con} = \hat{\mathbf{M}}(\mathbf{x}_1)\begin{pmatrix} \mathbf{J}^{+}(\mathbf{x}_1)(\ddot{\mathbf{x}}_{1d} + \mathbf{K}_1\dot{\mathbf{e}}_1) + \\ \dot{\mathbf{J}}^{+}(\mathbf{x}_1)(\dot{\mathbf{x}}_{1d} + \mathbf{K}_1\mathbf{e}_1) \\ +\mathbf{K}_2\mathbf{e}_2 + \mathbf{J}^{\mathrm{T}}(\mathbf{x}_1)\mathbf{e}_1 \end{pmatrix} \quad (4.68)$$

$$+\hat{\boldsymbol{\eta}}(\mathbf{x}_1, \mathbf{x}_2) - \hat{\boldsymbol{\sigma}}_{dis}$$

K_2 is the controller gain matrix and presumed as a symmetric positive definite matrix. i.e., $K_2 = K_2^T > 0$ choose an adaptive law based on velocity feedback as follows:

$$\begin{aligned} \hat{\boldsymbol{\sigma}}_{dis} &= \mathbf{K}_3\hat{\mathbf{M}}(\mathbf{x}_1)\mathbf{x}_2 + \mathbf{x}_3 \\ \dot{\mathbf{x}}_3 &= -\mathbf{K}_3\left(\boldsymbol{\sigma}_{con} - \hat{\boldsymbol{\sigma}}(\mathbf{x}_1, \mathbf{x}_2) + \hat{\boldsymbol{\sigma}}_{dis} + \mathbf{e}_2\right) - \mathbf{K}_3\dot{\hat{\mathbf{M}}}(\mathbf{x}_1)\mathbf{x}_2 \end{aligned} \quad (4.69)$$

$$\dot{\mathbf{e}}_3 = \dot{\boldsymbol{\sigma}}_{dis} - \mathbf{K}_3(\mathbf{e}_3 - \mathbf{e}_2) \quad (4.70)$$

Since, the vehicle-manipulator moves slowly, and its disturbance vector is also slowly varying, i.e. $\dot{\xi}_{dis} \approx 0$. This assumption reduces as follows:

$$\dot{\mathbf{e}}_3 = -\mathbf{K}_3(\mathbf{e}_3 - \mathbf{e}_2) \quad (4.71)$$

Substituting all error derivatives, it gives,

$$\dot{V}(\mathbf{e}_1, \mathbf{e}_2, \mathbf{e}_3) = -\left(\mathbf{e}_1^{\mathrm{T}}\mathbf{K}_1\mathbf{e}_1 + \mathbf{e}_2^{\mathrm{T}}\mathbf{K}_2\mathbf{e}_2 + \mathbf{e}_3^{\mathrm{T}}\mathbf{e}_3\right) \quad (4.72)$$

The Lyapunov candidate function's time derivative is negative definite which means that chosen control design is globally asymptotically reliable and asymptotically the error converges to zero. If the disturbance vector $\dot{\xi}_{dis}$ is not slowly varying and it is bounded, the choice of K_3 can guarantees the stability of the system.

$$\dot{V}\left(\mathbf{e}_1,\mathbf{e}_2,\mathbf{e}_3\right) = -\left(\mathbf{e}_1^{\mathrm{T}}\mathbf{K}_1\mathbf{e}_1 + \mathbf{e}_2^{\mathrm{T}}\mathbf{K}_2\mathbf{e}_2 + \mathbf{e}_3^{\mathrm{T}}\mathbf{e}_3\right) + \mathbf{e}_3^{\mathrm{T}}\mathbf{K}_3^{-1}\dot{\boldsymbol{\sigma}}_{dis} \tag{4.73}$$

4.2.4.2 Description of the System and Task for Robust Dual Loop Control

In this paper to verify the recommended double-loop motion control design scheme, performance investigations for tracking the trajectory of vehicle-manipulator have been done using MATLAB/Simulink package. Figure 4.14 describes with the help of block diagram, double-loop motion control scheme. Double-loop controller consists of inner-loop controller and outer-loop controller. The outer-loop controller consists of the operational-space kinematics whereas inner-loop controller consists of the configurational-space system dynamics. Real- time vehicle-manipulator namely JR2 is considered for performing the dynamic simulations. However, the derived dynamic model is verified in the virtual robot model in Gazebo package environment and the JR2 vehicle manipulator in the virtual background is presented in Figure 4.15.

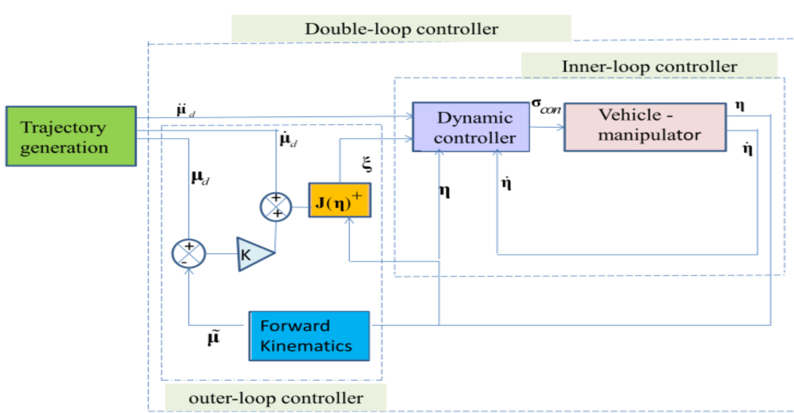

Fig. 4.14 Block diagram of the double-loop controller

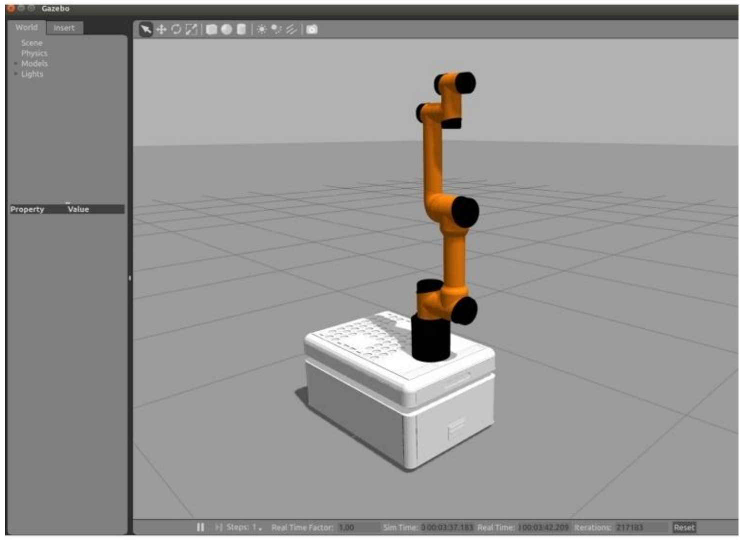

Figure 4.15 JR2 vehicle- manipulator in Gazebo Environment

The derived model is almost matching with the virtual system motion in both forward and inverse dynamic cases. For the performance evaluation manipulator has to begin from a given initial position and end to the original position. While travelling, the manipulator will track an eight-shaped spatial position trajectory. Under the existence of the internal and external disturbances, the effectiveness and feasibility is verified by the recommended motion control design. Fig.4.15 shows the photography image of JR2 vehicle-manipulator in gazebo environment. To testify the controller, the dynamic simulations are performed at uncertain conditions. Uncertain conditions comprise of process noises, sensor noises such as white Gaussian noises and external effect like unknown payload can also cause dynamic variations in the system. Fig.4.16 shows the desired eight-shaped complex trajectory. Figure 4.17 shows the time trend of the proposed spatial operational-space trajectory.

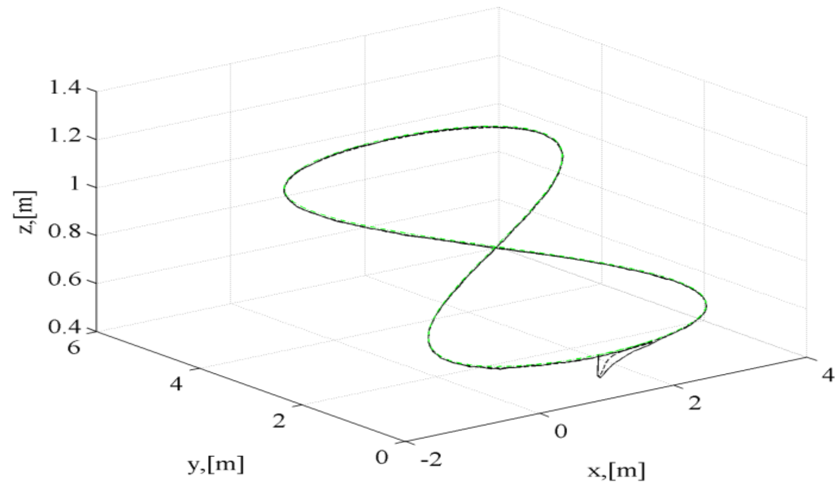

Figure 4.16 Desired Eight-shaped complex trajectory

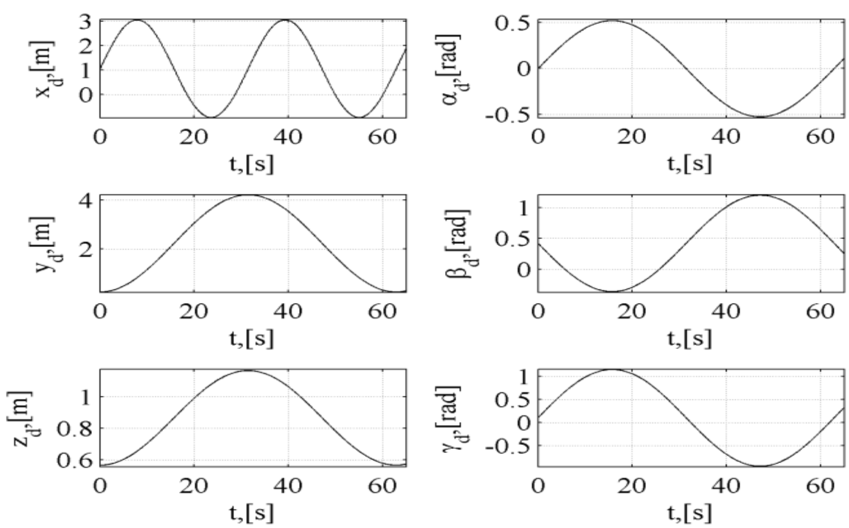

Figure 4.17 Time Trend of the proposed spatial operational-space trajectory

4.2.5 Actuator Fault Tolerant Control

In this research computed velocity control is implemented to achieve the aim to follow the desired operational space pose vector trajectory of the vehicle-manipulator with uncertainties and time varying external disturbances. The main target of the recommended controller is that the tracking errors must converge to zero and the controller should overcome and adapt itself from all the issues associated with the system that is, variations in parameters, frictional effects, external and internal disturbances, Unmodeled dynamics, etc. To perform motion control, kinematic control scheme used in this article is as follows:

$$\xi = J^{-1}[\dot{\eta}_d + K_p(\eta_d - \eta)] \quad (4.74)$$

$\dot{\eta}_d$ is the vector of desired inertial frame (earth-fixed) configuration-space velocities which is obtained from the desired operational-space velocities. $\tilde{\eta} = \eta_d - \eta$ is the vector of configuration-space pose errors. η_d is the desired configuration-space pose vector. η is the actual configuration-space pose vector. K_p is the controller gain matrix and chosen as a symmetric positive definite matrix, that is, $K_p = K_p^{\mathrm{T}} > 0$. $J^{-1} \in \Re^{3\times1}$ is the vector of inverse of Jacobian matrix. In order to correlate the generalized input velocity vector with the individual actuator inputs (rotational speeds) of the system, the input (control) vector can be rewritten as follows:

$$\boldsymbol{\xi} = Bk \quad (4.75)$$

where, B is the actuator configuration matrix and k (kappa) is the vector of actuator velocity inputs or command velocities. Figure 4.18 demonstrates the flowchart representation of the fault tolerant control scheme. Figure 4.19 describes the fault tolerant control scheme with the help of algorithmic representation. Algorithm 1explains no fault wheel configuration case where the control scheme used is computed torque control. In first step, we have to find the vector of input velocity command $(\boldsymbol{\xi})$ and in second step we will find the wheel angular velocities (k) with the help of Moore-Penrose pseudo left inverse and $(\boldsymbol{\xi})$.Algorithm demonstrates the condition when number of actuator faults are one. Here in first step, we will find the vector of input velocity command $(\boldsymbol{\xi})$ with the help of $(\boldsymbol{\eta}, \dot{\boldsymbol{\eta}})$ where $\boldsymbol{\eta} = [x \quad y \quad \varphi]^{\mathrm{T}}$ and $\dot{\boldsymbol{\eta}} = \mathbf{J}(\boldsymbol{\eta})\boldsymbol{\xi}$. In second step two methods has been used for finding the wheel angular velocities (k) namely, weighted pseudo inverse and reduced configuration matrix. In Algorithm 3, line of sight method has been used to find the input velocity command in step 1 where the number of actuator faults is two. In step 2 for finding the wheel angular velocity (kappa), Moore-Penrose right Pseudo inverse has been used. In this case diagonal wheels are faulty in nature. In Algorithm 3, side wheels' actuators are considered as faulty in nature. Front or rear wheels are considered faulty in Algorithm 5. Moore-Penrose right Pseudo inverse has been used for calculating kappa. Table 4.1 shows values of command velocities in all the three cases.

Table 4.3 Values of command velocities in all cases

Command Velocities ($\boldsymbol{\kappa}$)	Values
No Fault case	$\boldsymbol{\kappa} \in \Re^{4\times1}$
One Fault case	$\boldsymbol{\kappa} \in \Re^{3\times1}$
Two Fault case	$\boldsymbol{\kappa} \in \Re^{2\times1}$

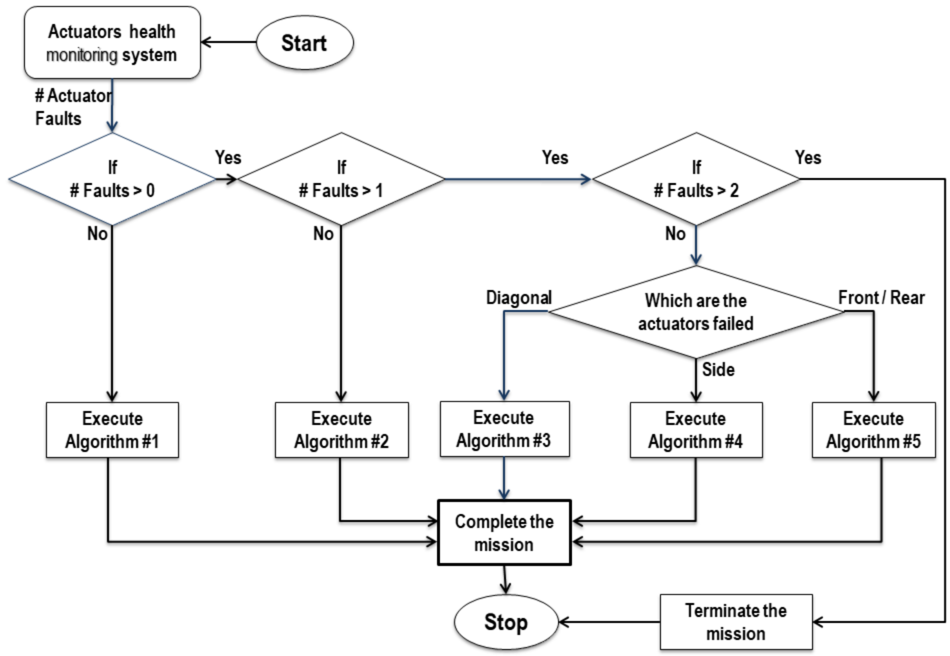

Figure.4.18 Flowchart representation of the proposed fault tolerant control scheme

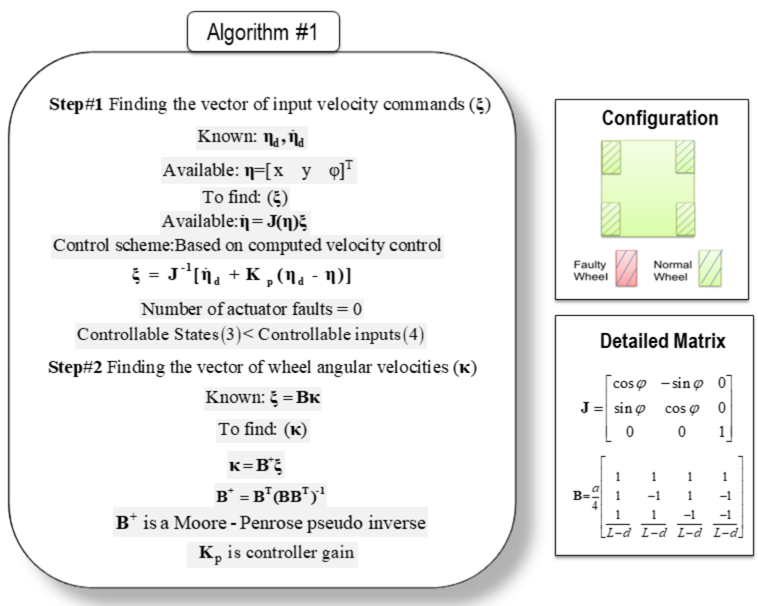

Algorithm #2

Step#1 Finding the vector of input velocity commands (ξ)

Known: $\boldsymbol{\eta}_d, \dot{\boldsymbol{\eta}}_d$

Available: $\boldsymbol{\eta}=[x \quad y \quad \varphi]^T$

To find: (ξ)

Available: $\dot{\boldsymbol{\eta}} = \mathbf{J}(\boldsymbol{\eta})\xi$

Control scheme: Based on computed velocity control

$$\xi = \mathbf{J}^{-1}[\dot{\boldsymbol{\eta}}_d + \mathbf{K}_p(\boldsymbol{\eta}_d - \boldsymbol{\eta})]$$

Number of actuator faults = 1

Controllable States(3) = Controllable inputs(3)

Step#2 Finding the vector of wheel angular velocities ($\boldsymbol{\kappa}$)

Known: $\xi = \mathbf{B}\boldsymbol{\kappa}$

To find: ($\boldsymbol{\kappa}$)

Method 1 : using Pseudo Inverse

$\mathbf{B_W} = \mathbf{BH}$

$\xi = (\mathbf{B_W})\boldsymbol{\kappa}$

$\boldsymbol{\kappa} = \mathbf{B_W^+}\xi$

Method 2 : using Reduced Configuration Matrix

$\mathbf{B_r}$ = reduced configuration matrix

$\xi = \mathbf{B_r}\boldsymbol{\kappa}$

$\boldsymbol{\kappa} = \mathbf{B_r^{-1}}\xi$

$$(\mathbf{BH})^+ = (\mathbf{BH})^T\left((\mathbf{BH})(\mathbf{BH})^T\right)^{-1}$$

$\mathbf{H}$ is a health performance matrix

$\mathbf{B_W^+}$ is a weighted pseudo inverse

$\mathbf{K_p}$ is controller gain

Configuration

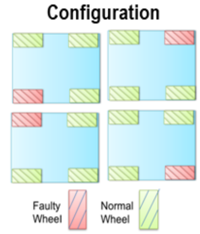

Detailed Matrix

$$\mathbf{J} = \begin{bmatrix} \cos\varphi & -\sin\varphi & 0 \\ \sin\varphi & \cos\varphi & 0 \\ 0 & 0 & 1 \end{bmatrix}$$

$$\mathbf{B} = \frac{a}{4}\begin{bmatrix} 1 & 1 & 1 & 1 \\ 1 & -1 & 1 & -1 \\ \frac{1}{L-d} & \frac{1}{L-d} & \frac{-1}{L-d} & \frac{-1}{L-d} \end{bmatrix}$$

$$\mathbf{H} = \begin{bmatrix} \lambda 1 & 0 & 0 & 0 \\ 0 & \lambda 2 & 0 & 0 \\ 0 & 0 & \lambda 3 & 0 \\ 0 & 0 & 0 & \lambda 4 \end{bmatrix}$$

Algorithm #3

Step#1 Finding the vector of input velocity commands (ξ)

Known: $\boldsymbol{\eta}_d, \dot{\boldsymbol{\eta}}_d$

Available: $\boldsymbol{\eta}=[x \quad y \quad \varphi]^T$

To find: (ξ)

Positions: $\boldsymbol{\eta}_d = x_d, y_d$ and $\varphi_d = \tan^{-1}\left(\frac{y_d}{x_d}\right)$

Available: $\dot{\boldsymbol{\eta}} = \mathbf{J}(\boldsymbol{\eta})\xi$

Control scheme: Based on computed velocity control

$$\xi = \mathbf{J}^{-1}[\dot{\boldsymbol{\eta}}_d + \mathbf{K}_p(\boldsymbol{\eta}_d - \boldsymbol{\eta})]$$

Number of actuator faults = 2

Controllable States(3) > Controllable inputs(2)

Step#2 Finding the vector of wheel angular velocities ($\boldsymbol{\kappa}$)

Known: $\xi = \mathbf{B_d}\boldsymbol{\kappa}$

To find: ($\boldsymbol{\kappa}$)

$\boldsymbol{\kappa} = \mathbf{B_d^+}\mathbf{K_p}$

$\mathbf{B_d^+} = (\mathbf{B_d^T}\mathbf{B_d})\mathbf{B_d^T}$

$\mathbf{K_p}$ is controller gain

$\mathbf{B^+}$ is a Moore-Penrose pseudo inverse

Configuration

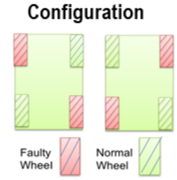

Detailed Matrix

$$\mathbf{J} = \begin{bmatrix} \cos\varphi & -\sin\varphi & 0 \\ \sin\varphi & \cos\varphi & 0 \\ 0 & 0 & 1 \end{bmatrix}$$

$$\mathbf{B_d} = \frac{a}{2}\begin{bmatrix} 1 & 1 \\ 1 & 1 \\ \frac{1}{L-d} & \frac{-1}{L-d} \end{bmatrix}$$

Algorithm #4

Step#1 Finding the vector of input velocity commands ($\boldsymbol{\xi}$)

Known: $\boldsymbol{\eta}_d, \dot{\boldsymbol{\eta}}_d$

Available: $\boldsymbol{\eta}=[x \quad y \quad \varphi]^T$

To find: ($\boldsymbol{\xi}$)

Positions: $\boldsymbol{\eta}_d = x_d, y_d$ and $\varphi_d = \tan^{-1}\left(\frac{y_d}{x_d}\right)$

Available: $\dot{\boldsymbol{\eta}} = \mathbf{J}(\boldsymbol{\eta})\boldsymbol{\xi}$

Control scheme: Based on computed velocity control

$$\boldsymbol{\xi} = \mathbf{J}^{-1}[\dot{\boldsymbol{\eta}}_d + \mathbf{K}_p(\boldsymbol{\eta}_d - \boldsymbol{\eta})]$$

Number of actuator faults = 2

Controllable States(3) > Controllable inputs(2)

Step#2 Finding the vector of wheel angular velocities ($\boldsymbol{\kappa}$)

Known: $\boldsymbol{\xi} = \mathbf{B}_s\boldsymbol{\kappa}$

To find: ($\boldsymbol{\kappa}$)

$\boldsymbol{\kappa} = \mathbf{B}_s^{+}\mathbf{K}_p$

$\mathbf{B}_s^{+} = (\mathbf{B}_s^{T}\mathbf{B})\mathbf{B}_s^{T}$

$\mathbf{B}_s^{+}$ is a Moore-Penrose pseudo inverse

$\mathbf{K}_p$ is controller gain

Configuration

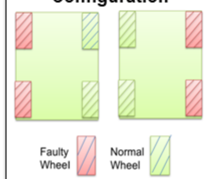

Detailed Matrix

$$\mathbf{J} = \begin{bmatrix} \cos\varphi & -\sin\varphi & 0 \\ \sin\varphi & \cos\varphi & 0 \\ 0 & 0 & 1 \end{bmatrix}$$

$$\mathbf{B}_s = \frac{a}{2}\begin{bmatrix} 1 & 1 \\ -1 & 1 \\ \frac{1}{L-d} & \frac{-1}{L-d} \end{bmatrix}$$

Algorithm #5

Step#1 Finding the vector of input velocity commands ($\boldsymbol{\xi}$)

Known: $\boldsymbol{\eta}_d, \dot{\boldsymbol{\eta}}_d$

Available: $\boldsymbol{\eta}=[x \quad y \quad \varphi]^T$

To find: ($\boldsymbol{\xi}$)

Positions: $\boldsymbol{\eta}_d = x_d, y_d$ and $\varphi_d = \tan^{-1}\left(\frac{y_d}{x_d}\right)$

Available: $\dot{\boldsymbol{\eta}} = \mathbf{J}(\boldsymbol{\eta})\boldsymbol{\xi}$

Control scheme: Based on computed velocity control

$$\boldsymbol{\xi} = \mathbf{J}^{-1}[\dot{\boldsymbol{\eta}}_d + \mathbf{K}_p(\boldsymbol{\eta}_d - \boldsymbol{\eta})]$$

Number of actuator faults = 2

Controllable States(3) > Controllable inputs(2)

Step#2 Finding the vector of wheel angular velocities ($\boldsymbol{\kappa}$)

Known: $\boldsymbol{\xi} = \mathbf{B}_F\boldsymbol{\kappa}$ or $\boldsymbol{\xi} = \mathbf{B}_R\boldsymbol{\kappa}$

To find: ($\boldsymbol{\kappa}$)

$\boldsymbol{\kappa} = \mathbf{B}_F^{+}\mathbf{K}_p$

$\mathbf{B}_F^{+} = (\mathbf{B}_F^{T}\mathbf{B})\mathbf{B}_F^{T}$

$\mathbf{B}_F^{+}$ is a Moore-Penrose pseudo inverse

$\mathbf{K}_p$ is controller gain

Configuration

Detailed Matrix

$$\mathbf{J} = \begin{bmatrix} \cos\varphi & -\sin\varphi & 0 \\ \sin\varphi & \cos\varphi & 0 \\ 0 & 0 & 1 \end{bmatrix}$$

$$\mathbf{B}_F = \frac{a}{2}\begin{bmatrix} 1 & 1 \\ 1 & -1 \\ \frac{1}{L-d} & \frac{-1}{L-d} \end{bmatrix}$$

Figure 4.19 Algorithmic representation of the proposed fault tolerant control scheme and its algorithms

4.2.5.1 Description of the System and Task for Actuator Fault Tolerant Control Scheme

The kinematic control on the mobile platform has been tested using MATLAB simulation environment in real-time without random noise No obstacle has been introduced in the simulation environment instead desired path has been given which automatically encompasses the obstacle avoidance. For the same the dimension of the platform considered is mentioned in Table 5.3.

Table 4.4 Specification of Mobile Platform

Aspect	Dimension
Length	335 mm
Width	310 mm
Diameter of Wheel	253 mm
Diameter of Roller	20 mm
Aspect Ratio(d/L)	0.9213

The time duration of the simulation is taken sufficient so that the mobile platform makes a complete circle for trajectory-tracking and in set-point control time interval the platform reaches the goal point. Line of sight method has been used for the two-fault case. Depending upon the number of actuator failure and behavior the mobile platform afterward, appropriate kinematic motion control scheme is designed and tested.

A. No-Fault Case

The objective here is to make mobile robot to follow a trajectory (circular profile), since the mobile robot is over-actuated this is simply done by using Moore-Penrose Pseudo-Inverse to get to the angular velocities of the actuators from :

$$k = B^{+} J^{\mathrm{T}}(\dot{\eta}) \tag{4.76}$$

where $B^{+} = B^{\mathrm{T}}\left(BB^{\mathrm{T}}\right)^{-1}$. The kinematic control was tested tuning the proportionality gain. The analysis results are given in Fig. 4.19 where the mobile platform and path traced have been depicted. Initial error in the graph is because the mobile robot is not positioned and oriented on the desired trajectory.

B. One-Fault Cases

Due to kinematic redundancy, Omni-directional mobile robot equipped with four mecanum wheels can still give desired performance with three functional actuators. In case one of the actuators fails and failure has been detected the following proposed method can be used. Here, the desired wheel velocity can be calculated by using:

$$k = B^{+} J^{\mathrm{T}}(\dot{\eta}) \tag{4.77}$$

where $B^{+} = B^{-1}$ since **B** is a square matrix of $B \in \Re^{3\times3}$. Kinematic control scheme with designed FTC method is used make mobile robot follow circular trajectory. There are four possible cases since either of the actuators can fail and the mobile robot would behave differently. For the one-fault case both pseudo inverse and weighted pseudo inverse has been used.

The proportionality gain for both the cases is 2 and it has been assumed that the actuator-1 fails after 20 seconds for the wheel configuration-3. Similar results can be expected in case of failure of any other actuators using the same method. Fig. 4.20 shows that effect of an actuator failure on rest of three functional actuators. For the case of pseudo inverse, there is abrupt change in the angular velocities of the three actuators, but incase of weighted pseudo inverse, the performance or health matrix distributes the load on all the remaining actuators and no such abrupt changes are experienced resulting smooth functioning of the actuators. The effect of one actuator failure is easily compensated by weighted pseudo inverse than simple pseudo inverse.

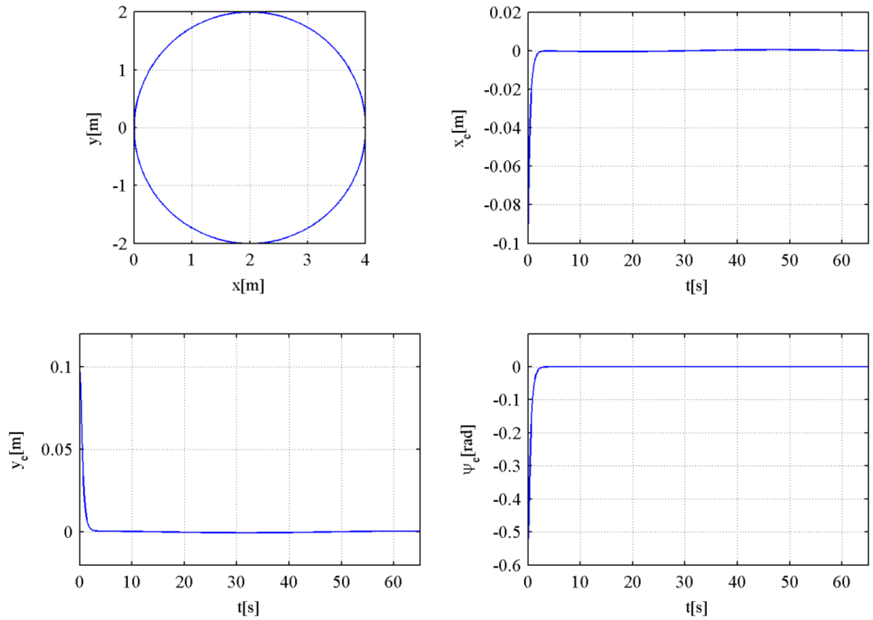

Figure 4.20 Path traced by the mobile robot and error incurred in no-fault case.

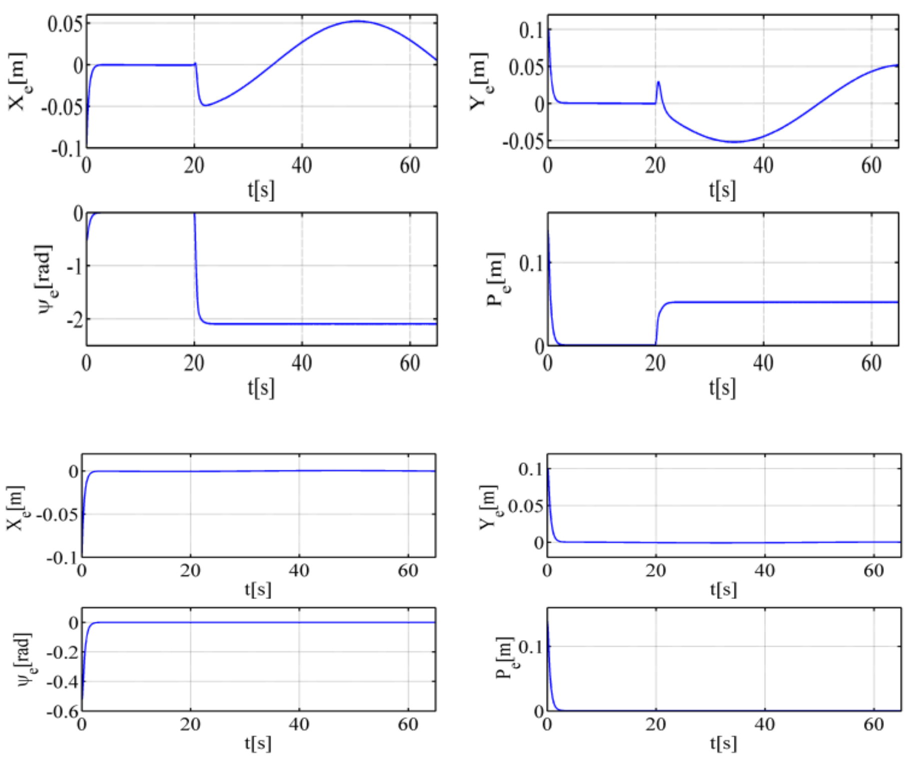

Figure 4.21 Error incurred with weighted pseudo inverse in one fault.

C. Two-Fault Cases

In case of two-faults, the system becomes under-actuated and it is not feasible to obtain both position and orientation of the platform in two-dimensional space simultaneously and therefore line-of-sight method has been used here along with kinematic control scheme. For the rectangular matrix Moore-Penrose Pseudo inverse has been use where actuator matrix will have the elements corresponding to the actuators which are functional. Appropriate state transformations are introduced to convert the kinematics of the mobile robot into a differential drive model. Depending upon which two actuators have failed the platform is going to behave differently. Moreover, the wheel configurations and the aspect ratio also plays an important role. All the six possible combinations of the two actuators failure have been considered for four different wheel configurations.

***C (i)* SET-POINT CONTROL**

Initially the analysis was done for set-point control scheme to check whether the platform reaches the desired set-point. The initial position of the mobile robot was $(0,0)$ and the desired point was $(10,10)$ for all the cases of different wheel configurations and the desired wheel velocity was calculated using:

$$k = B^{+} J^{\mathrm{T}}(\dot{\eta}) \tag{4.78}$$

where, $B \in \Re^{3\times 2}$ and $B^{+} = \left(B^{\mathrm{T}}B\right)^{-1} B^{\mathrm{T}}$. The proportionality gain is 2 for all the cases. It was observed in most of the cases that error tends to converge to zero.

C(ii). TRAJECTORY TRACKING CONTROL

After testing for set-point control scheme, this was further extended to trajectory tracking

where circular profile is considered, and line-of-sight method has been used with the kinematic control scheme. The desired path was given as of circle and the desired velocity was obtained as the derivative of the path and the resulting the wheel velocity of the wheel was obtained from

$$k = B^{+} J^{\mathrm{T}} (\dot{\eta}) \tag{4.79}$$

where $B \in \Re^{3\times 2}$ and $B^{+} = \left(B^{\mathrm{T}} B\right)^{-1} B^{\mathrm{T}}$. The proportionality gain is tuned as earlier cases and Moore-Penrose Pseudo inverse has been used. All the cases were analysed with the same control scheme.

In this chapter, robust motion control schemes have been introduced and their stability has also been proved. Further system description along with the task has been explained. Next chapter discusses the results of the motion control schemes studied in the thesis work.

Chapter 5

Results and Discussions

5.1 Simulation Results and Discussion for Operational-space End Effector position tracking control

The results of the task space motion control performance are discussed, and these can be used as a reference to gauge the performance of the manipulator and the control scheme in practical circumstances as the considerations done while performing these simulations are quite elaborate and they emulate the actual manipulator to a satisfactory extent. Considerations such as disturbances, parameter uncertainties and sensor noises (white Gaussian noises) have all been incorporated in the numerical model ensuring the usage of the proposed controller in an actual prototype without compromising either performance or effectiveness. The task space position trajectories are presented in Figure 5.1 and from this it observed that the proposed task space nonlinear PID control along with uncertainty estimator performs quite satisfactorily. Further, the time trajectories of the tracking error norm (Euclidean norm) are presented in Figure 5.2 and this confirms the proposed scheme performance. The controller parameters are as follows: $\mathbf{K}_O = 20, \mathbf{K}_C = 20, \gamma = 1.2, \mathbf{\Gamma} = 3$.

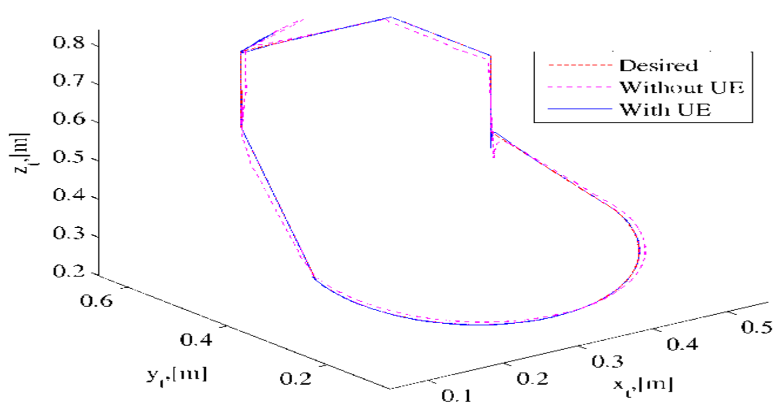

Figure 5.1 End effector (task space) 3D spatial trajectories for with and without estimator schemes

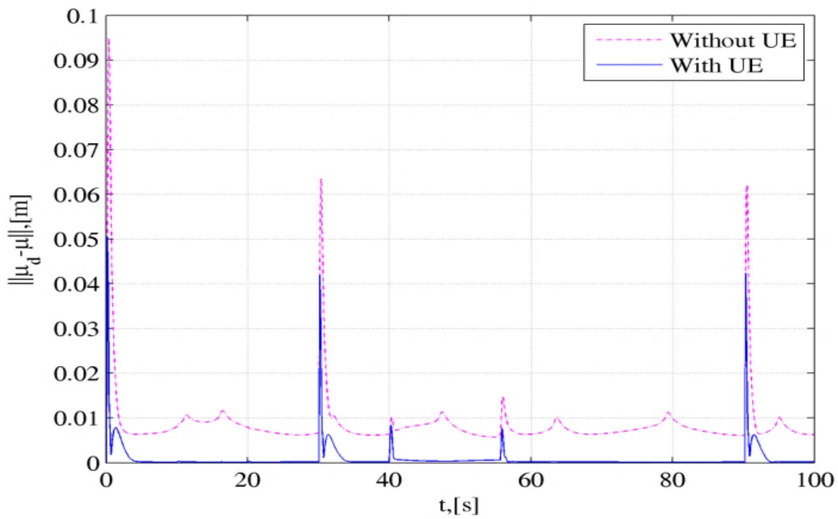

Figure 5.2 Time histories of the norm of the tracking position errors for with and without estimator schemes

In addition, the controller parameter sensitivity and its robustness are verified by conducting simulations for spatial circular task space trajectory tracking. There are four controller parameters namely observer gain $\mathbf{K}_O$, controller gain $\mathbf{K}_C$ and two positive constants ($\boldsymbol{\Gamma}, \gamma$) and, four different uncertainty parameters are considered for the analysis.The vector of desired task space motion trajectory is given as follows:

$$\boldsymbol{\mu} = \begin{bmatrix} 0.6 + 0.3\sin\omega t \\ 0.3 - 0.3\cos\omega t \\ 0.95 + 0.3\sin\omega t \end{bmatrix} \text{in m} \tag{5.1}$$

where ω is the trajectory frequency, which varied and performed simulations. The payload is varied from 0 kg (no load) to 2.5 kg (maximum payload). The system uncertainty also varied from -30 % to 30% and verified the robustness. To understand the system robustness, an external disturbance vector apart from system uncertainty is included and given as follows:

$$\boldsymbol{\delta}_{dis} = \begin{bmatrix} 5\cos\omega_d t \\ 5\sin\omega_d t \\ 5\cos\omega_d t \end{bmatrix} \text{in N} \tag{5.2}$$

where ω_d is the external disturbance frequency, which varied from 0 to 2 rad/s and performed simulations for understanding the controller performance for fast varying disturbances.

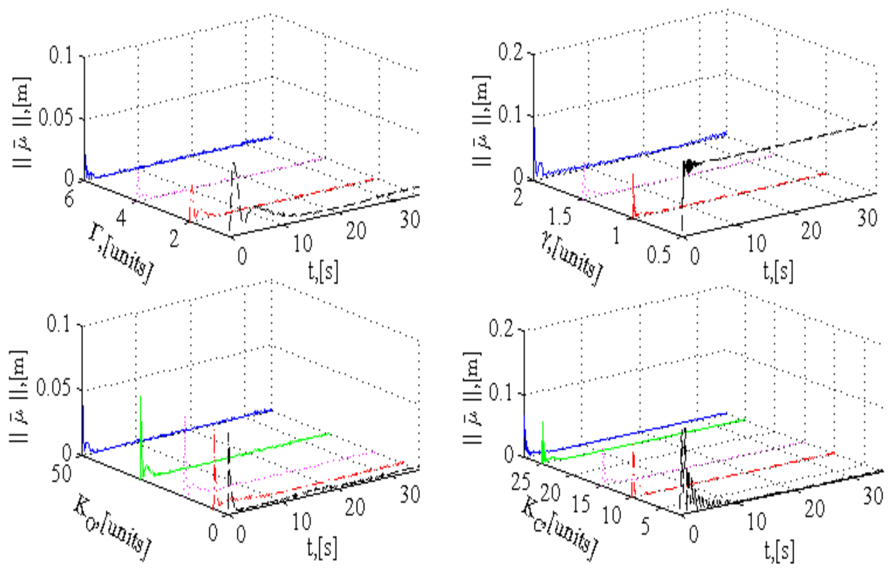

Figure 5.3 Time histories of the norm of tracking errors for controller parameters' variations

Time histories of the norm of tracking errors for the controller parameter variations are presented in Figure 5.3. The constant $\boldsymbol{\Gamma}$ variation from 2 to 6 shows the parameter sis sensitive in terms of controller performance, however lower than 2 and higher than 6 provide system unstable and for value 3, the controller provides better results. Similarly, γ values from 0.7 to 1.6 provide better results. Controller gain value is good from 10 to 20 in terms of minimum tracking errors. However, observer gain variations could not change the performance in significant way; probably it reduces the rise time of the system but come with more control activity.

Time histories of the norm of tracking errors for disturbance variations are presented in Figure 5.4. From the results, it is observed that the proposed controller is robust for the payload variations and parameter uncertainty, however for the motion trajectory velocity variations and fast varying disturbances the controller provides more tracking error compared to slow speed and slowly varying disturbances. In overall, even in these cases the tracking errors are well below the permissible limits. Consequently, it is apparent from the above discussion that the proposed controller provides robust and efficient control performance while tracing a complex pre-defined path in the task space. The proposed control scheme can be easily extended to three-dimensional task space position and orientation tracking problem of a mobile manipulator (with a wrist and a tool).

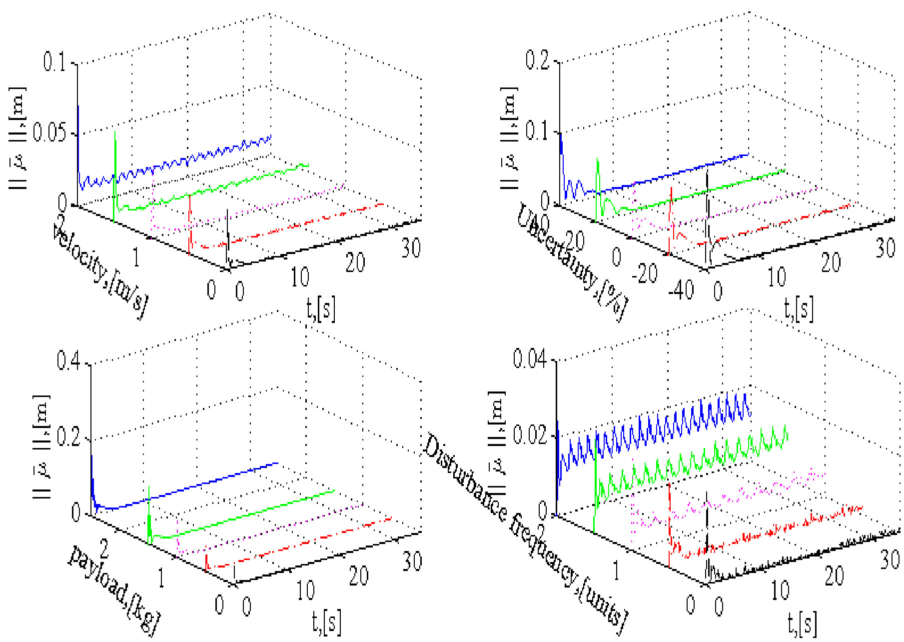

Figure 5.4 Time histories of the norm of tracking errors for disturbance variations

5.2 Simulation Results and Discussion for Operational-space End Effector Position and Orientation Trajectory Tracking Control

The numerical simulation outcomes are attained based on the improved backstepping controller for a given spatial trajectory tracking and shown in Figure. 5.5-5.7. The main aim is to gauge the effectiveness and feasibility of the designed control technique the simulations are performed in the uncertain conditions. The uncertain conditions consist of ambiguities such as noises which are inserted in the simulation to dissect the behaviour of the proposed scheme for the dynamic variations of the system. In the same way, the effect of external disturbances is believed as simple variations in payload (i.e., payload is changeable all through the preferred trajectory).

To have better comparison, the controller is tuned by genetic algorithm software in such a way that both controllers give an acceptable control performance under an ideal condition. There are two different working situations are taken into consideration for the numerical simulation analysis: an ideal working situation (it means that there are no external disturbances and uncertainties, no friction on road and joints) and working in uncertain situation. The ideal working situation is deliberated to illustrate that the conventional and the proposed performances in terms of gains and constants of the controller are approximately identical in terms of tracking feature and quantifiers. Figure 5.5 shows the time trend of the norm of operational-space position tracking errors at an ideal condition where both the controllers provide almost same results. $\tilde{\boldsymbol{\mu}} = \boldsymbol{\mu}_d - \boldsymbol{\mu}$ is the operational-space pose errors vector which is defined as the difference between desired operational-space pose errors $\boldsymbol{\mu}_d$ and actual operational space pose errors $\boldsymbol{\mu}$. In fact, the tuning has been done in such a way that the conventional control is doing well at the ideal conditions. From the results, it can be noticed that the proffered controller is initially has more tracking errors than the conventional control scheme. This is due to the inclusion of adaptive law depends on the disturbance observer. The disturbance observer is started with zero initial values of the arbitrary vector and there is 10% of system parameter uncertainties have considered for the ideal conditions.

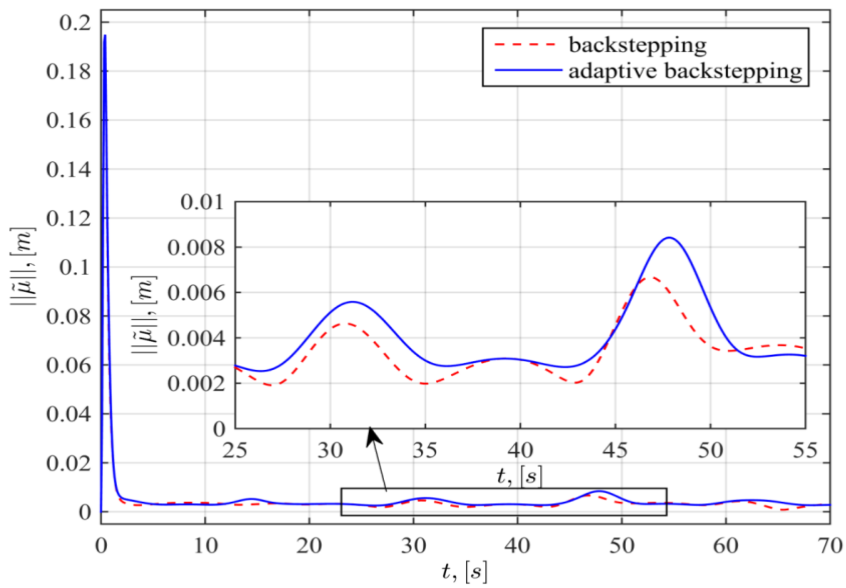

Figure 5.5 Operational-space position tracking errors at an ideal condition

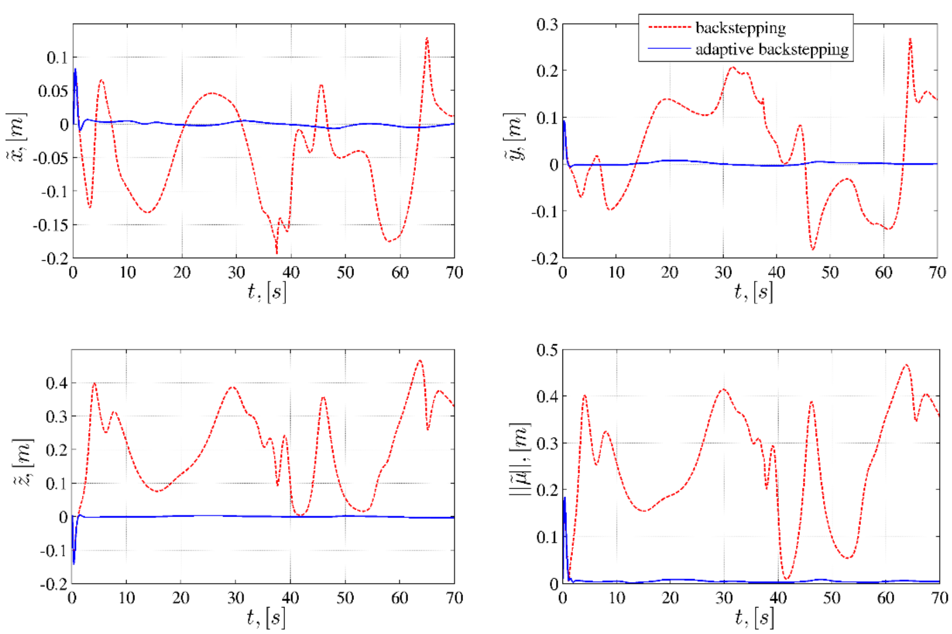

Figure 5.6 Operational-space position tracking errors at an uncertain condition

In Figure 5.6, it depicts the time histories of the norm of the operational-space position tracking errors at an uncertain situation showing x, y, z pose vectors. Both controllers are trying to follow the same classical test profile, however, the proposed controller over performs the conventional controller. The values of Euclidean norm (L_2 norm) of errors are presented to quantify the controller tracking performance. The comparative motion trajectories of the mobile manipulator during the complex operational-space position trajectory tracking are described in Figure 5.7.

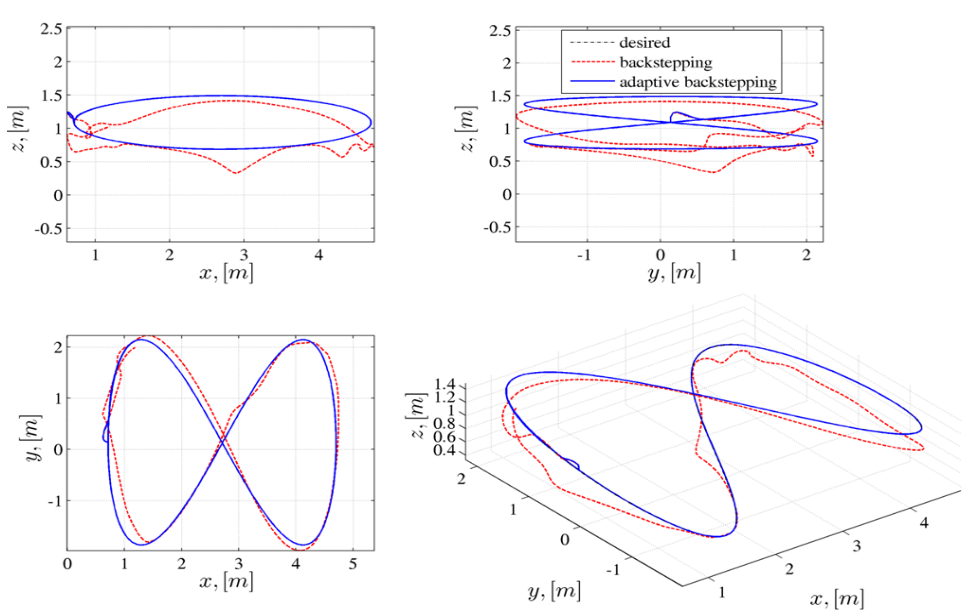

Figure 5.7 Comparative motion trajectories of the mobile manipulator during complex operational-space position trajectory tracking

Table 5.1 Controller parameters

Controller Parameters	Values
$\mathbf{K}_1$	$3\,\mathbf{I}_{3\times3}$
$\mathbf{K}_2$	$3\,\mathbf{I}_{3\times3}$
$\mathbf{K}_3$	$3\,\mathbf{I}_{3\times3}$
Uncertainty (%)	10

The controller parameters of the motion controller system used for the simulation are given in Table 5.1. By conducting simulations for spatial operational-space trajectory in the presence of the system dynamic variations the controller parameter robustness is successfully verified. There are four different working parameters are used to demonstrate the system dynamic changes namely percentage of system uncertainties, payload, disturbance frequency and forward velocity of the system.

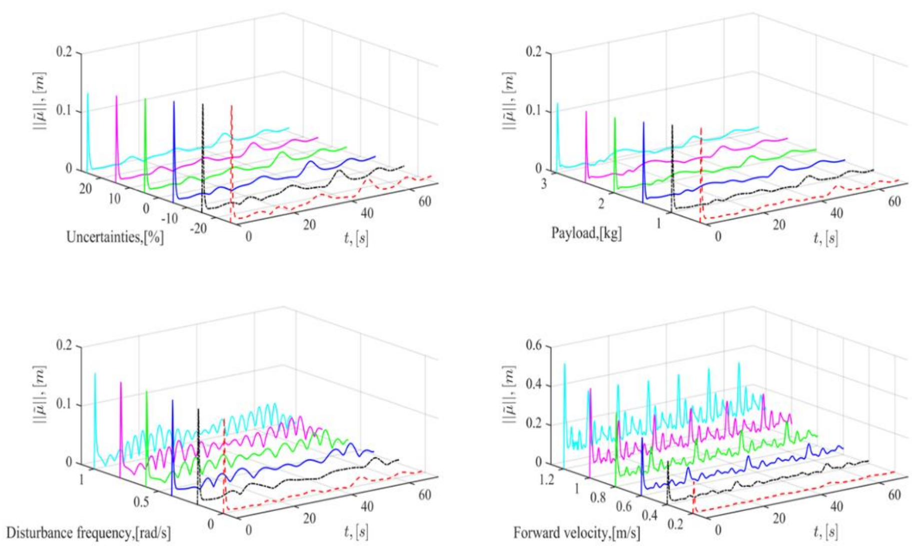

Figure 5.8 Time trend of the norm of operational-space position tracking errors under system dynamic variations (controller robustness results)

Figure 5.8 shows the variation in the norm of tracking errors for system dynamic changes. The uncertainty in the system is varied from -20% to 20%, from no load i.e. 0 kg to 3 kg maximum payload the unknown payload is varied. An external disturbance velocity is introduced in the controller apart from the uncertainty which varies from 0 to 1 rad/s and simulations has been performed for gauging the efficacy of the controller for fast fluctuating disturbances as well.

It has been noted that when frequency and velocity of the system increase, the amplitude of the disturbances are also increase which gives the variation in the tracking errors norm. However, for the variations in payload and system uncertainties are not influencing the proposed controller much. In other words, the recommended controller is robust enough to the system dynamic variations as long the disturbances are bounded or slowly varying. According to the numerical simulation results, under the variations caused by payload and uncertainties occurred due to parameters with slow changing external disturbances acting on the mobile manipulator, it has been observed that the suggested control scheme is robust in nature.

5.2.1 Real-Time Experiments and Discussions

In real-time experiments, an in-house fabricated mobile manipulator is considered for the performance analysis. The fabricated mobile manipulator subsists of 3 dof mobile base with four mecanum wheels attached with a 3 dof serial manipulator arm with rotary axes. In this in-house fabricated prototype, an Arduino mega as a low-cost microcontroller, two dual dc motor drivers 20A and high torque encoder geared dc motor 12V, 600rpm are used.

Table 5.2 Technical Parameters of the In-house Fabricated Mobile Manipulator

Parameters of Fabricated prototype	**Values**
Size of the mobile base	600mmX350mmX130mm
Maximum speed of the mobile base	1.03m/s
Number of wheels	3
Number of manipulator axes	3
Work envelope of the manipulator	$0.629m^3$
Horizontal distance between the vehicle frame to the manipulator base (L_v)	0.19m
Vertical distance between the vehicle frame to the manipulator base (d_1)	0.16m
Vehicle frame from the ground	0.136m

(height) (d_v)	
Joint distance of the manipulator's second frame (d_2)	0
Joint distance of the manipulator's fourth frame (d_3)	0.09m
Length of the manipulator second link (L_2)	0.105m

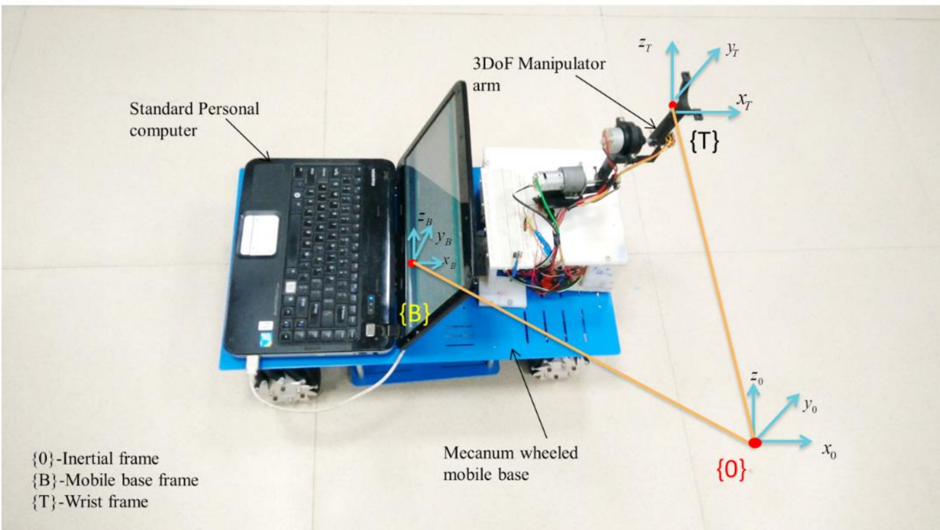

Figure 5.9 In-house fabricated prototype attached with the standard personal computer

Figure 5.9 shows in-house fabricated prototype attached with 2GB ram standard personal computer with Intel 2.2 GHz processor along with 32bit operating system. In the real-time prototype {O} is the inertial frame, the mobile base frame is denoted by {B} and {T} is the wrist or tool frame. Fabricated prototype is also following the desired complex spatial operational-space position trajectory for the performance evaluation. Table 5.2 shows the simulation parameters used for performance evaluation of the fabricated mobile manipulator. Figure 5.10 presents time histories of the norm of operational-space position tracking errors during real-time tracking experiments on a fabricated prototype. It has been observed that adaptive backstepping shows better result than conventional backstepping in real-time prototype in the dynamic unknown environment.

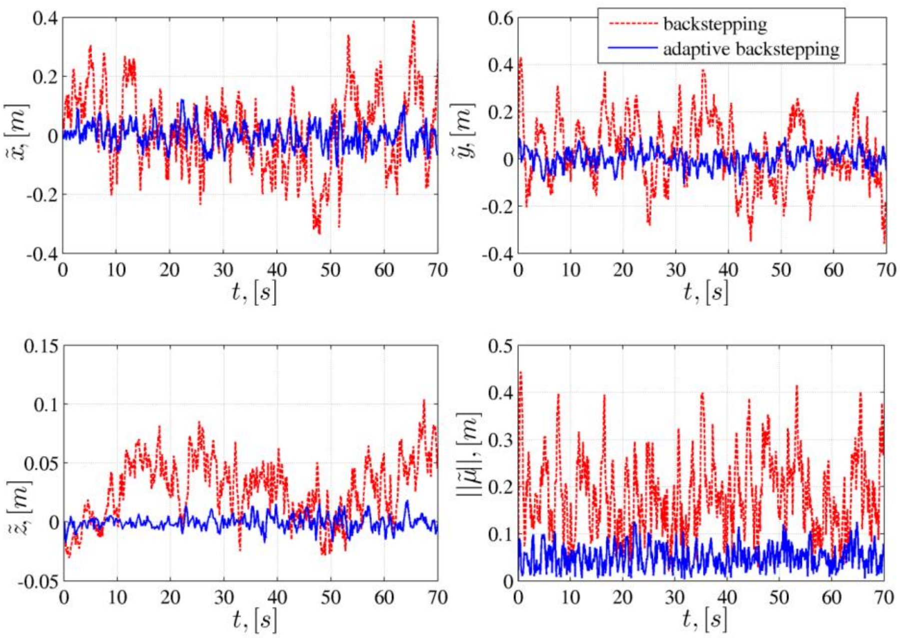

Figure 5.10 Operational-space position tracking errors during real-time tracking experiments on a fabricated prototype

Table 5.3 Comparison of controller performances during operational-space position tracking at ideal and uncertain conditions

Condition	Scheme	Integral of Time Absolute Error (ITAE) in units		
		in x position	**in y position**	**in z position**
Ideal (Simulations on JR2)	Conventional Backstepping	3.388	5.088	0.285
	Adaptive Backstepping	6.077	5.598	1.111
Uncertain (Simulations on JR2)	Conventional Backstepping	175.973	263.363	533.306
	Adaptive Backstepping	6.352	5.997	3.977
Real-time Experiments (on a fabricated prototype)	Conventional Backstepping	279.138	272.087	87.853
	Adaptive Backstepping	76.023	77.656	8.375

The performance comparison of conventional and adaptive backstepping controllers between ideal and uncertain conditions are tabulated in terms of one of the popular error quantifiers namely integral of time absolute error (ITAE). Table 5.3 discusses the comparison of the controller performances in two different operating conditions i.e. in the ideal and uncertain conditions during operational-space tracking control.

5.3 Simulation Results and Discussion for Resolved Motion Control

Resolved motion scheme is as effective as conventional kinematic control based on operational space along with generalized inverse of Jacobian matrix. The norm of pose error in square shaped profile is almost same as in conventional control. The variable Λ, is playing a significant role in the proposed controller scheme. In the proposed scheme the minimum safe distance is always considered based on the dexterous workspace which means the manipulation quality always high. In that sense proffered scheme is simple and better, these qualities allow the motion control on a low-cost microcontroller. The controller parameter sensitivity analysis has been successfully performed for the spatial operational space trajectory in the presence of system dynamic variations. To have a reasonable comparison, all the controller gain matrices are tuned in such a way that controller provides better control performance. This control scheme is more suitable because of considering the dexterous workspace of the manipulator arm as the operational region but if opting for operational-space control, it can have collision between the vehicle and the manipulator due to the generalized inverse. The vehicle-manipulator's kinematically redundancy is effectively utilized in this scheme because vehicle base is kept at some distance from the target and allow the manipulator to perform its manipulation. Further, it does not require any soft or hard limit switches for the manipulator joints to avoid the collisions between the vehicle and the manipulator.

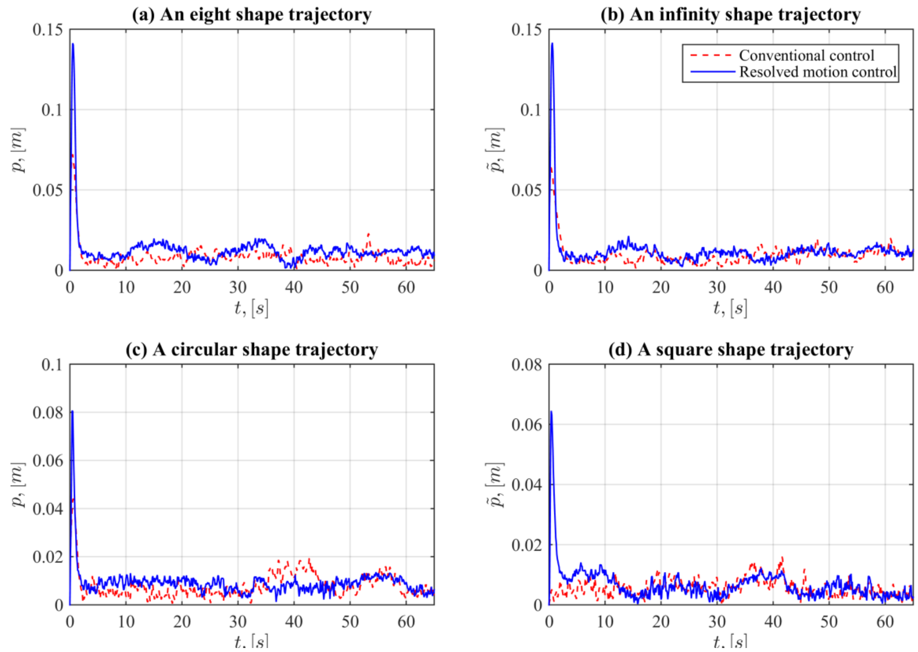

Figure 5.11 Time trend of the norm of operational-space position tracking errors

Table 5.4 describes the comparison of controller performances through quantifiers between the conventional operational- space kinematic control scheme and the proposed resolved motion kinematic control scheme in configuration-space. In the table, the operational space pose tracking errors for four desired complex trajectories are calculated and compared between the conventional operational-space kinematic control scheme and the proposed kinematic control scheme. The proposed new kinematic control scheme is successful in tracking the operational space position and performance. Further, based on experiments, it assured its closed-loop stability as well. Figure 5.11 presents time trend of the norm of operational-space position tracking errors. Figure 5.12 depicts the desired operational-space positions trajectories along with time trend of the end-effector orientations. Figure 5.13 depicts time trend of the norm of operational-space position tracking errors under system dynamic variations (controller sensitivity results).

TABLE 5.4 Comparison of Controller Performance Quantifiers Between Conventional Operational-Space Kinematic Control Scheme and Resolved Motion Kinematic Control Scheme in Configuration-Space

Parameter or performance quantifier	Conventional operational-space kinematic control scheme				Resolved motion kinematic control scheme in configuration-space			
	Eight shape	Infinity shape	Circular shape	Square shape	Eight shape	Infinity shape	Circular shape	Square shape
$\tilde{x}_{rms}$ in mm	9.8	7.6	7.6	3.1	15.1	9.1	7.2	3.9
$\tilde{y}_{rms}$ in mm	5.3	8.9	3.2	3.3	7.1	13.2	3.8	3.7
$\tilde{z}_{rms}$ in mm	3.5	3.1	3.6	3.3	7.3	7.5	7.1	7.3
$\tilde{\alpha}_{rms}$ in rad	0.030	0.029	0.030	0.013	0.008	0.009	0.008	0.006
$\tilde{\beta}_{rms}$ in rad	0.025	0.023	0.025	0.011	0.013	0.015	0.015	0.012
$\tilde{\gamma}_{rms}$ in rad	0.015	0.018	0.015	0.012	0.006	0.005	0.006	0.003
$\tilde{x}_{itae}$ in units	9.51	11.93	9.31	6.76	17.23	8.33	8.53	3.33
$\tilde{y}_{itae}$ in units	9.39	10.91	8.00	5.29	7.76	15.32	8.15	6.52
$\tilde{z}_{itae}$ in units	5.27	6.31	8.82	5.36	10.31	10.27	9.87	5.20
$\tilde{\alpha}_{itae}$ in units	58.93	53.76	60.76	17.53	13.65	13.92	13.05	8.29
$\tilde{\beta}_{itae}$ in units	26.85	25.82	27.29	12.22	23.20	23.03	22.85	11.63
$\tilde{\gamma}_{itae}$ in units	32.83	37.06	31.62	16.78	11.18	10.50	10.21	7.67

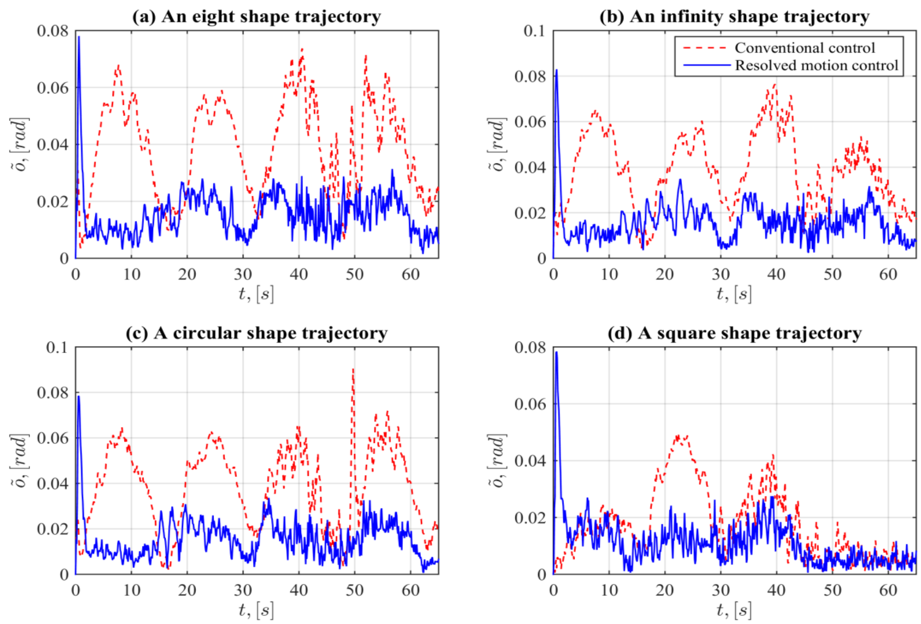

Figure 5.12 Time trend of the norm of operational-space orientation tracking errors

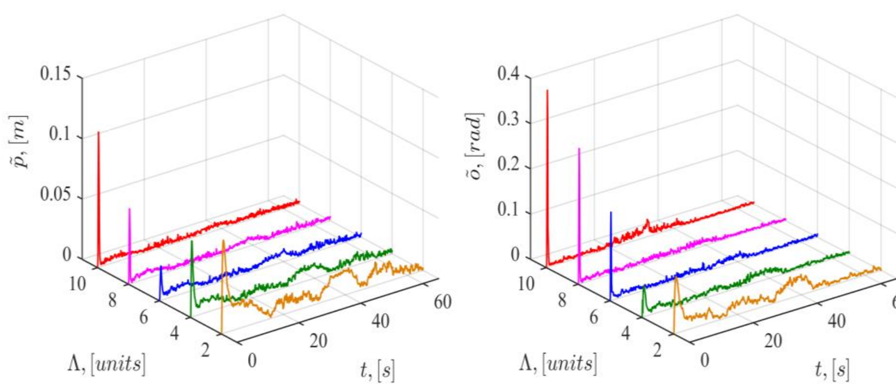

Figure 5.13 Time trend of the norm of operational-space position and orientation tracking errors for the variations of the controller parameters.

In Figure 5.11, the time trend of end-effector pose tracking errors is presented for the variations of the controller gain matrix values (here it is a scalar value); the scalar value is varied from 2 to 10 units. Both the controllers are working within the design limits (in the real-time it is considered as the norm of error should not exceed 0.15 m in position and

0.1 rad in orientation). Controller gain sensitivity has been observed in terms of the end effector pose errors and it was found that the increase in controller gain ($\mathbf{\Lambda}$) values giving faster convergence and value of steady state errors are decreasing. However, the actuator inputs (wheel speeds and joint velocities) are getting higher at the initial phase due to the faster convergence, therefore, it is considered the particular value based on the trade-off between both values of tracking errors, convergence rate and actuator inputs. The proposed controller has large error at initial stages due to the resolved motion in its task space; however, the conventional control scheme the errors are smaller at the initial stages as compared to the proposed scheme. Overall, the mean values of ITAE are as equal to the operational-space control scheme. Further, in order to validate its robustness for the controller parameter variations, the sensitivity analysis has been done. Cubic polynomial profile has been considered for performing sensitivity analysis. The values of Λ, have been varied, the error quantifiers in terms of position and orientation errors are almost same at the steady states but the response time is varied, in fact, faster response obtained in the higher regions of gain values. However, in terms of the position error values, it is least when controller gain is 5 to 7 units and the orientation error values; it is least between 3 to 5 units.

5.4 Simulation Results and Discussion for Robust Dual Loop Control

The computer based dynamic simulation results are obtained based on the proposed double-loop controller as shown from Figure 5.14 to Figure 5.16. To validate the controller, the dynamic simulations are performed at uncertain conditions. Uncertain conditions comprise of process noises, sensor noises such as white Gaussian noises and external effect like unknown payload can also cause dynamic variations in the system.

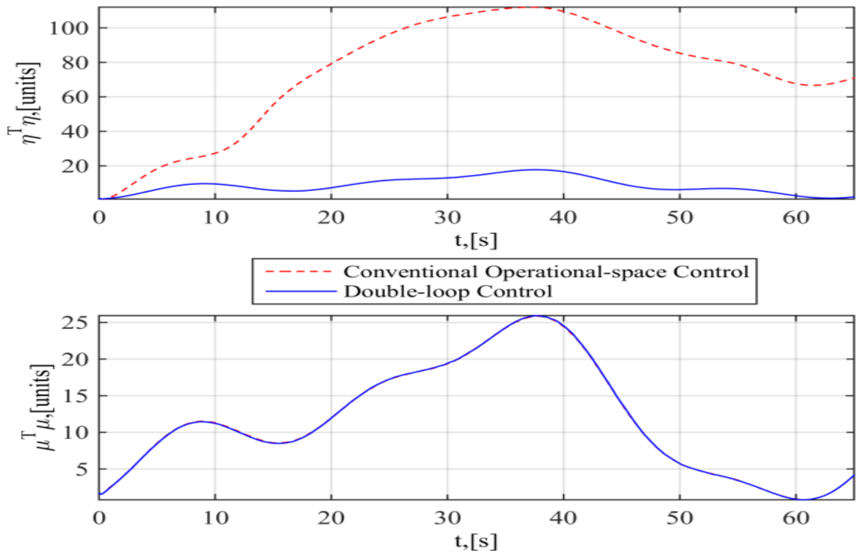

Figure 5.14 Time trend of configurational-space and operational-space trajectories.

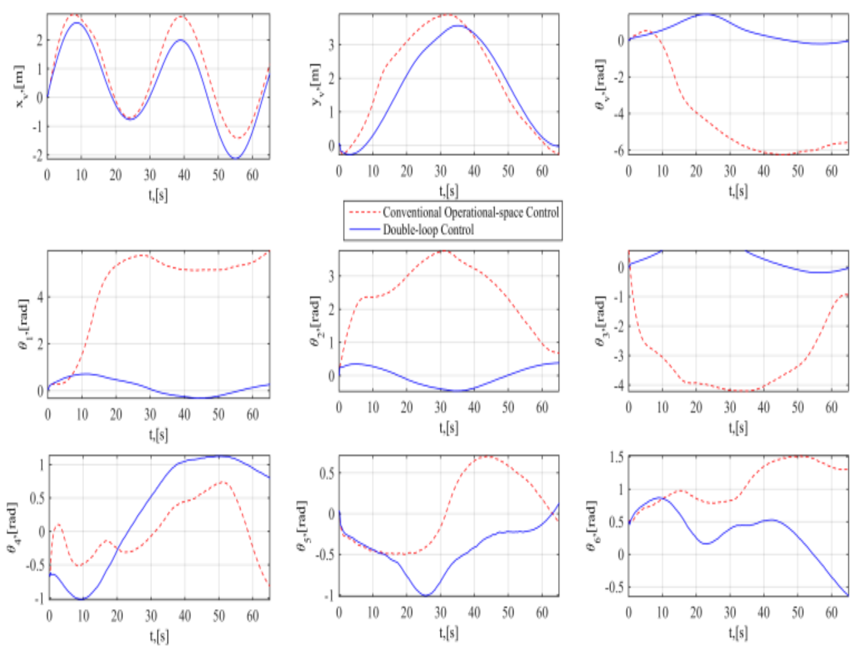

Figure 5.15 Time trend of joint angles in the operational-space trajectory

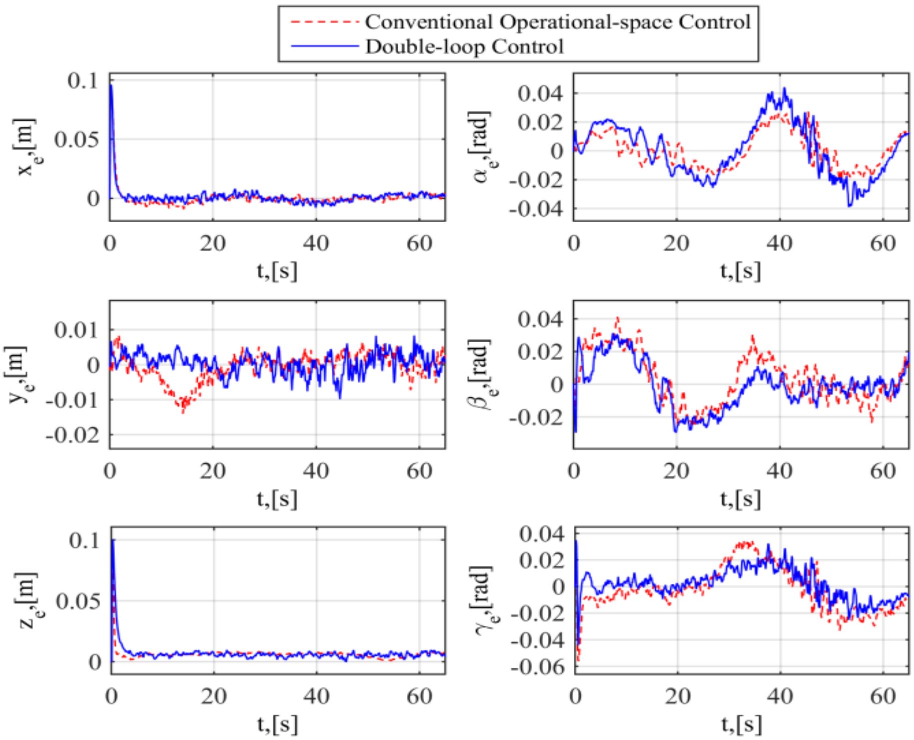

Figure 5.16 Error norm of the operational space trajectory

5.5 Simulation Results and Discussion for Actuator Fault Tolerant Control Scheme

Depending upon the number of actuator failure and behavior the mobile platform afterward, appropriate kinematic motion control scheme is designed and tested.

1.1 No-Fault Case

The objective here is to make mobile robot to follow a trajectory (circular profile), since the mobile robot is over-actuated this is simply done by using Moore-Penrose Pseudo-Inverse to get to the angular velocities of the actuators from equation mentioned below:

$$k = B^{+} J^{T} (\dot{\eta}) \tag{5.3}$$

where $B^{+} = B^{\mathrm{T}}\left(BB^{\mathrm{T}}\right)^{-1}$. The kinematic control was tested tuning the proportionality gain.

1.2 One-Fault Cases

Due to kinematic redundancy, Omni-directional mobile robot equipped with four mecanum wheels can still give desired performance with three functional

actuators. In case one of the actuators fails and failure has been detected the following proposed method can be used. Here, the desired wheel velocity can be calculated by using:

$$k = B^{+} J^{\mathrm{T}}(\dot{\eta}) \tag{5.4}$$

where $B^{+} = B^{-1}$ since **B** is a square matrix of $B \in \Re^{3\times 3}$. Kinematic control scheme with designed FTC method is used make mobile robot follow circular trajectory. There are four possible cases since either of the actuators can fail and the mobile robot would behave differently. For the one-fault case both pseudo inverse and weighted pseudo inverse has been used. The proportionality gain for both the cases is 2 and it has been assumed that the actuator-1 fails after 20 seconds for the wheel configuration-3. Similar results can be expected in case of failure of any other actuators using the same method.

The table 5.5 clearly shows that error in position is only about 0.8% when weighted pseudo inverse is used which is easily tolerable, however error is a bit more in case of pseudo inverse. For the case of pseudo inverse, there is abrupt change in the angular velocities of the three actuators, but incase of weighted pseudo inverse, the performance or health matrix distributes the load on all the remaining actuators and no such abrupt changes are experienced resulting smooth functioning of the actuators. The effect of one actuator failure is easily compensated by weighted pseudo inverse than simple pseudo inverse.

Table 5.5 Corresponding root mean square (RMS) errors of the vehicle positions

	RMS position error(m)							
Parameters	Actuator-1 failure		Actuator-2failure		Actuator-3 failure		Actuator-4 failure	
	x_e	y_e	x_e	y_e	x_e	y_e	x_e	y_e
With fault with pseudo inverse	0.027	0.033	0.111	0.013	0.011	0.135	0.030	0.031
With fault with weighted pseudo inverse	0.006	0.008	0.006	0.008	0.006	0.008	0.006	0.008

1.3 Two-Fault Cases

In case of two-faults, the system becomes under-actuated and it is not feasible to obtain both position and orientation of the platform in two-dimensional space simultaneously and therefore line-of-sight method has been used here along with kinematic control scheme. For the rectangular matrix Moore-Penrose Pseudo inverse has been use where actuator matrix will have the elements corresponding to the actuators which are functional. Appropriate state transformations are introduced to convert the kinematics of the mobile robot into a differential drive model. Depending upon which two actuators have failed the platform behaves differently. Moreover, the wheel configurations and the aspect ratio (Table I) also plays an important role. All the six possible combinations of the two actuators failure has been considered for four different wheel configurations.

5.5.1 SET-POINT CONTROL

Initially the analysis was done for set-point control scheme to check whether the platform reaches the desired set-point. The initial position of the mobile robot was $(0,0)$ and the desired point was $(10,10)$ for all the cases of different wheel configurations and the desired wheel velocity was calculated using:

$$k = B^{+} J^{\mathrm{T}} (\dot{\eta}) \tag{5.5}$$

where, $B \in \Re^{3\times 2}$ and $B^{+} = \left(B^{\mathrm{T}} B\right)^{-1} B^{\mathrm{T}}$. The proportionality gain is 2 for all the cases. It was observed in most of the cases that error tends to converge to zero. The results have been shown in Figure 5.17. Likewise, the RMS error has been tabulated below in Table 5.6.

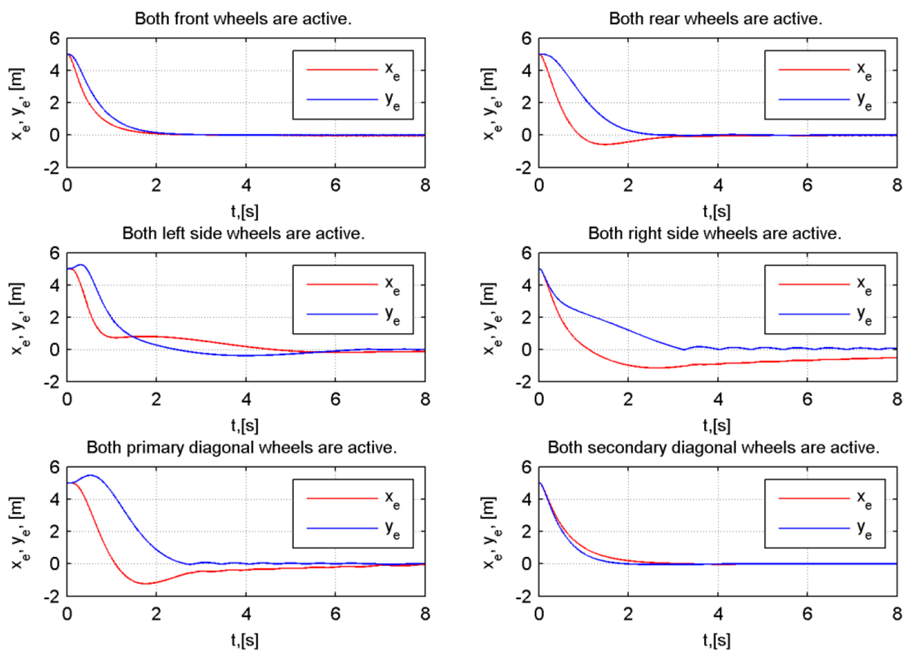

(a)Wheel-configuration 1

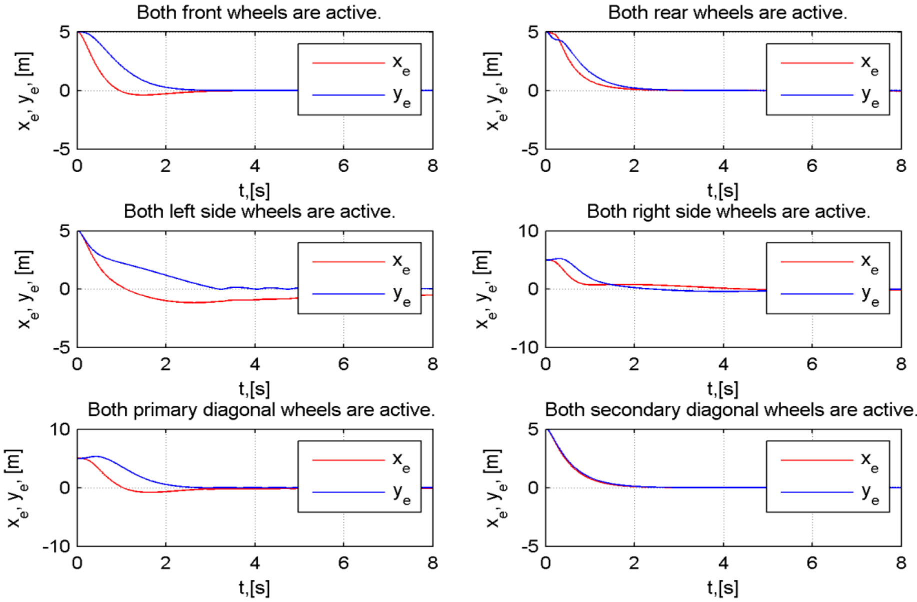

(b)Wheel-configuration 2

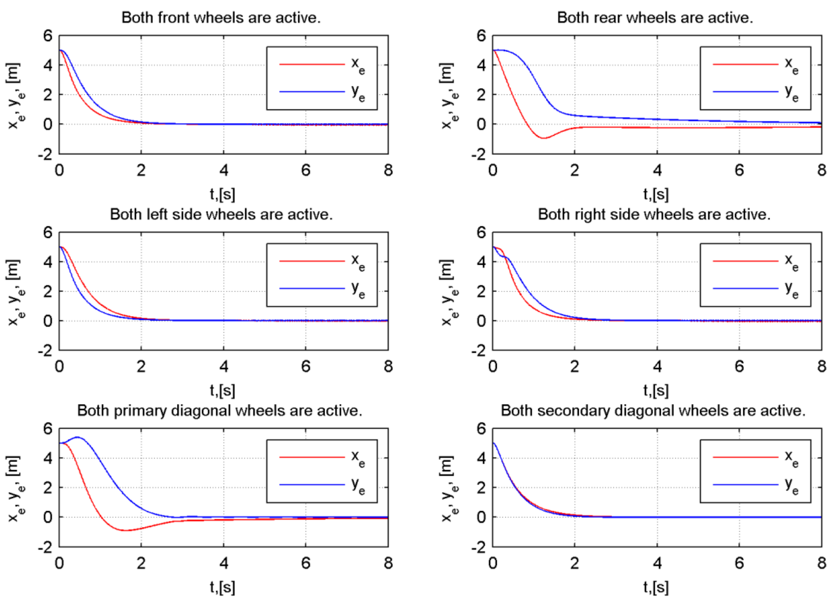

(c) Wheel-configuration 3

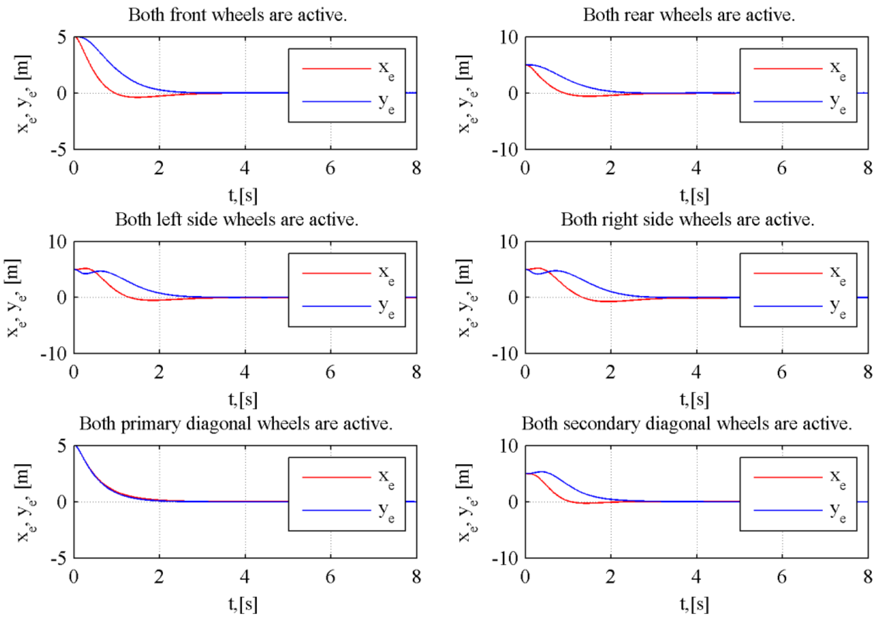

(d)Wheel-configuration 3

Figure 5.17 Errors during set-point control

TABLE 5.6 RMS values of the error for different cases of four-wheel configuration

(a)Wheel-configuration 1

Cases	RMS error(m)	
	X_{e_RMS}	Y_{e_RMS}
Both front wheels are active	0.980	1.192
Both rear wheels are active	0.967	1.521
Both left side wheels are active	1.187	1.578
Both right side wheels are active	1.227	1.362
Both primary diagonal wheels are active	1.357	2.065
Both secondary diagonal wheels are active	1.071	1.003

(b)Wheel-configuration 2

Cases	RMS error(m)	
	X_{e_RMS}	Y_{e_RMS}
Both front wheels are active	0.951	1.362
Both rear wheels are active	1.183	1.308
Both left side wheels are active	1.227	1.362
Both right side wheels are active	1.187	1.578
Both primary diagonal wheels are active	1.233	1.871
Both secondary diagonal wheels are active	1.019	1.050

(c)Wheel-configuration 3

Cases	RMS error(m)	
	X_{e_RMS}	Y_{e_RMS}
Both front wheels are active	0.980	1.192
Both rear wheels are active	1.012	1.731
Both left side wheels are active	1.192	0.979
Both right side wheels are active	1.183	1.308
Both primary diagonal wheels are active	1.237	1.921
Both secondary diagonal wheels are active	1.032	1.026

(d)Wheel-configuration 3

Cases	RMS error(m)	
	X_{e_RMS}	Y_{e_RMS}
Both front wheels are active	0.951	1.362
Both rear wheels are active	0.967	1.521
Both left side wheels are active	1.362	1.779
Both right side wheels are active	1.530	1.882
Both primary diagonal wheels are active	1.032	1.026
Both secondary diagonal wheels are active	1.237	1.921

The RMS error (Table 5.6) seems to be significant since it has been desired to obtain both position and orientation with under actuated system, but the proposed FTC techniques proved to be effective in achieving goal position within the tolerance limit of 5%-7% in almost all the cases from Figure 5.17. There is difference in variation of RMS error for different cases because the combination of two-faulty actuators significantly affects the orientation and thereby the computed wheel velocity.

5.5.2 TRAJECTORY TRACKING CONTROL

After testing for set-point control scheme, this was further extended to trajectory tracking where circular profile is considered and line-of-sight method has been used with the kinematic control scheme. The desired path was given as of circle and the desired velocity was obtained as the derivative of the path and the resulting the wheel velocity of the wheel was obtained from equation which can be expressed as:

$$k = B^{+} J^{\mathrm{T}} (\dot{\eta}) \tag{5.6}$$

where $B \in \Re^{3\times 2}$ and $B^{+} = \left(B^{\mathrm{T}} B\right)^{-1} B^{\mathrm{T}}$. The proportionality gain is tuned as earlier cases and Moore-Penrose Pseudo inverse has been used. All the cases were analysed with the same control scheme. The analysis results are given in Figure 5.18. Similarly, the corresponding RMS error values have been tabulated in Table 5.7.

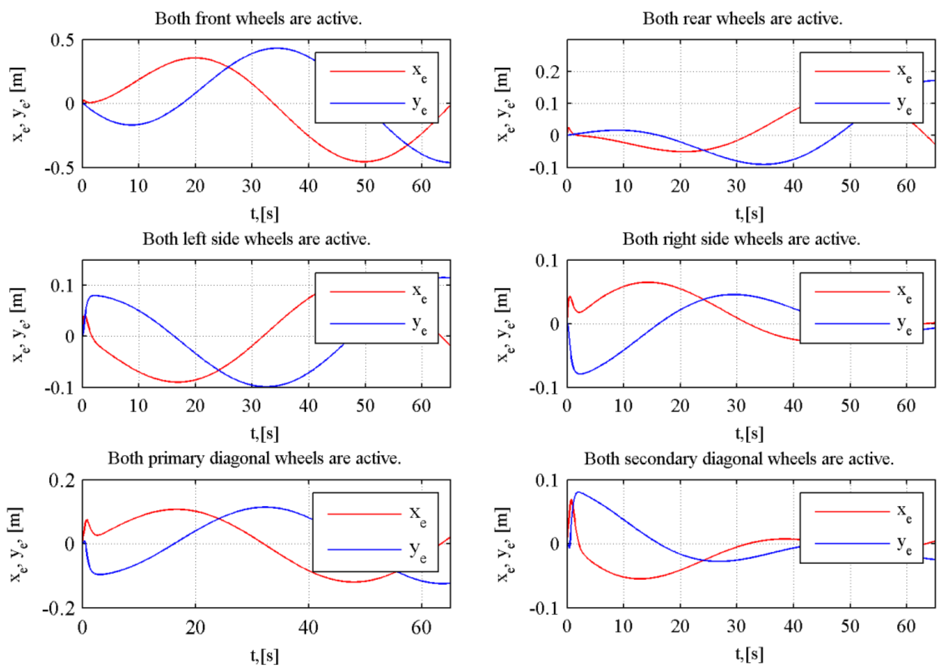

(a)Wheel-configuration 1

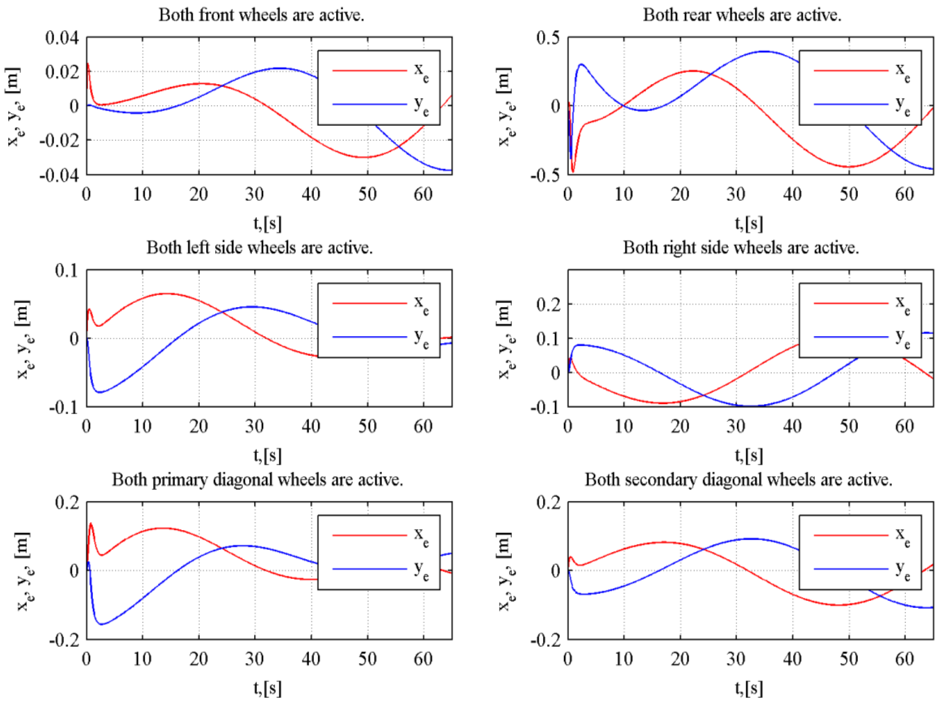

(b)Wheel-configuration 2

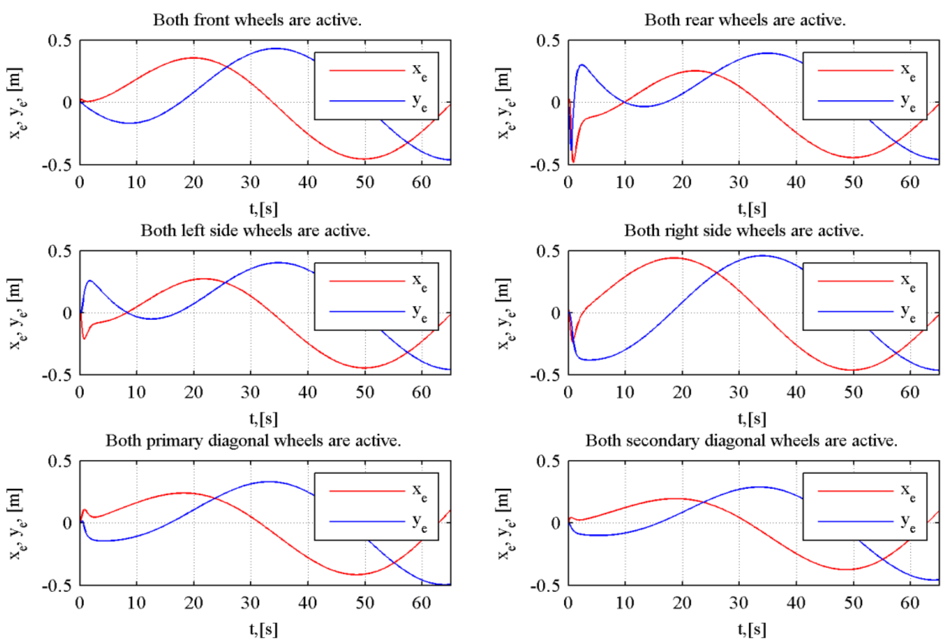

(c)Wheel-configuration 3

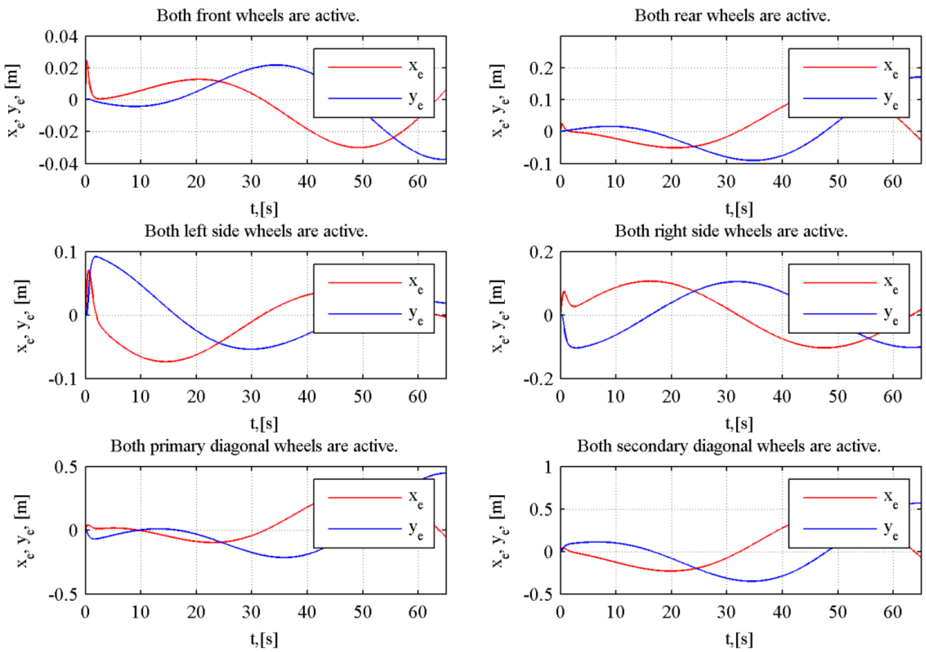

(d)Wheel-configuration 3

Figure 5.18 Error while tracking circular profile

TABLE 5.7.RMS Error value during trajectory tracking control

(a)Wheel-configuration 1

Cases	RMS error(m) X_{e_RMS}	Y_{e_RMS}
Both front wheels are active	0.280	0.271
Both rear wheels are active	0.067	0.075
Both left side wheels are active	0.068	0.071
Both right side wheels are active	0.033	0.033
Both primary diagonal wheels are active	0.079	0.080
Both secondary diagonal wheels are active	0.027	0.028

(b) Wheel-configuration 2

Cases	RMS error(m) X_{e_RMS}	Y_{e_RMS}
Both front wheels are active	0.015	0.017
Both rear wheels are active	0.252	0.257
Both left side wheels are active	0.033	0.033
Both right side wheels are active	0.068	0.071
Both primary diagonal wheels are active	0.062	0.061
Both secondary diagonal wheels are active	0.063	0.065

(c)Wheel-configuration 3

Cases	RMS error(m)	
	X_{e_RMS}	Y_{e_RMS}
Both front wheels are active	0.280	0.271
Both rear wheels are active	0.252	0.257
Both left side wheels are active	0.251	0.256
Both right side wheels are active	0.313	0.313
Both primary diagonal wheels are active	0.233	0.251
Both secondary diagonal wheels are active	0.205	0.223

(d)Wheel-configuration 4

Cases	RMS error(m)	
	X_{e_RMS}	Y_{e_RMS}
Both front wheels are active	0.015	0.017
Both rear wheels are active	0.067	0.075
Both left side wheels are active	0.030	0.030
Both right side wheels are active	0.073	0.073
Both primary diagonal wheels are active	0.166	0.185
Both secondary diagonal wheels are active	0.250	0.267

Since the system is under-actuated, we only bother about position error not orientation as both of these cannot be achieved simultaneously. The position errors are very small in majority of cases and are even in few centimetres while it is significant in some cases extending to few decimetres. The tolerance limit varies between 5% to about 30%. The proposed FTC is quite effective for majority of cases of different wheel configurations. For some cases the FTC is unable to minimize the error to the desired tolerance limit because of the wheel configuration where the resultant of two active wheel velocity and roller velocity is unable to give the desired velocity. This can be simply understood as the resultant of two vectors in a plane cannot produce a vector of desired magnitude in desired direction. The RMS error is quite less i.e. in second decimal point in majority of the cases showing the effectiveness of the applied FTC method. The four-mecanum mobile robot can follow the desired path within the tolerance limit with two faults. This can be further extended by modifying the desired path to any complex path and the path can be such that obstacle avoidance can be incorporated and the outcomes are expected to be nearly same. During the analysis it has also been observed that the angular velocities of the wheels are much larger in case of faults. There is much load on functional actuators since number to actuators to bear the load decreases also, friction has not been considered, in practical the friction has impact and to overcome that the actuators need to apply more torque. Commercially, mecanum wheel with roller mounted at 35^0 inclined to the axis of wheel are available. For some special cases, the roller may be inclined other angle, like $\alpha = 30^\circ$, $\alpha = -30^\circ$, $\alpha = 60^\circ$, $\alpha = -60^\circ$ etc. For these cases, the kinematic modelling shall be adopted as per [32]. Moreover, the complexities will increase since for roller angle other than 45° the net resultant of the roller velocity should not be zero and the control of the mobile robot will be much complex. Analysis for those roller angles has been left of further research. Likewise, aspect ratio also has major impact on the performance of the mobile robot when the diagonal actuator fails. Above all the analysis has been done on aspect ratio on about 1 as shown in Table I. We further analysed the case when diagonal actuators fail for wheel configuration-3. The result of analysis has been depicted in Figure 5.19. The graph indicates that when the aspect ratio is less than one the instead of circle the mobile robot moves on a spiral that will converge at the centre of the circle while for aspect ratio greater than one, the mobile robot will move on the spiral that is diverging away from the centre of circle. For aspect ratio one, few terms in $\mathbf{B}$ matrix will be undefined and there for the FTC method proposed will not work. Kinematic control scheme with proposed FTC is found quite effective for the four-mecanum wheeled drive mobile robots for both set-point control and trajectory-tracking control. Here, proportionality gained has been tuned accordingly to minimize the error.

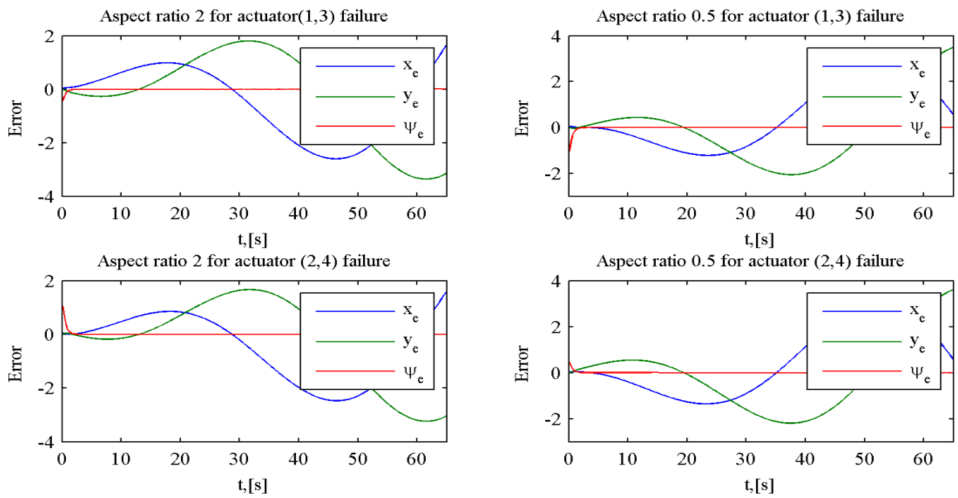

Figure 5.19 Error incurred for different aspect ratio on diagonal actuator failure

For inverse kinematics pseudo inverse is found less effective than weighted pseudo inverse, error is relatively smaller using weighted pseudo inverse than pseudo inverse. Likewise, the modification of four-mecanum wheeled mobile platform to differential drive system for two fault cases is effective compared to modification of the platform to unicycle model.

Chapter 6

Conclusions & Future Scope

6.1 Conclusions

In this thesis, an improved robust nonlinear PID control method is proposed and successfully extended for a complex predefined task space motion control . The validity and feasibility of the proposed method has been confirmed by comprising its performance with LPID and CTC methods. Under ideal working condition (i.e. $f\ dis$ = 0), the control performance given by all the controllers are almost same and acceptable. However, under practical working scenario (i.e. uncertain working conditions), the LPID and CTC methods produces significant steady state error in spatial trajectory tracking control. In the proposed control approach, the control performance of LPID is enhanced by nonlinear PID (NPID) and this has been verified through numerical simulations. Nevertheless, the effects of lumped disturbance are not completely compensated. The improved robustness is achieved by integrating an effective and efficient disturbance estimator with the proposed NPID controller. This combination reduces the steady state error to almost zero even under uncertain working conditions and has been confirmed through numerical simulations. In addition to this, proposed control method shows robust performance under variations in the controller parameters as well as variations in the different disturbances like payload, parameter uncertainty, frequency of time varying disturbance etc. In overall, the proposed method offers some superior advantages like simplicity in design, simple and efficient design approach for disturbance estimator which would solve the problem of real-time implementation of the control algorithm.

A comparative analysis of conventional and robust nonlinear adaptive backstepping control method for the desired operational-space motion control of a simple spatial 6 dof wheel-based vehicle-manipulator system has been performed and analysed. The proposed controllers ‘viability is investigated under ideal and uncertain operating conditions. The control performance of the two motion control schemes is almost same and acceptable. The main intention in this motion control system is to track the operational-space position and performance of the kinematic redundant mobile manipulator so that the tracking error congregates to zero. Global asymptotic stability and asymptotic tracking performance has been proved by the resultant proposed control law. The tracking performance shown under parametric uncertainty, nonlinear variations and uncertain friction property are stable. Comparison of controller performances has done with integral time of absolute errors at ideal and uncertain conditions also have been calculated in the XYZ positions. The results indisputably are a sign of the reduction in error accumulation. Hence the prospective controller’s potency is demonstrated and established using simulations in Gazebo software for the mobile manipulator and investigations of the motion behaviour. Real-time experimental results for operational-space position and orientation trajectory tracking also prove that the adaptive backstepping control scheme gives better results and follows the desired predefined complex spatial trajectory.

New resolved motion kinematic control scheme is proposed and compared with the conventional operational-space kinematic control scheme. The control scheme is demonstrated experimentally; it is effective and can be extended up to the dynamic motion control scheme as well. Further the motion control scheme simplifies the computability. Since the motion control scheme is effective so no need to use any advanced complex schemes like reinforcement learning, visual servoing and other complex resolution algorithms. The proposed end-effector motion trajectory is tracked with the help of resolved configuration-space motion without using the Jacobian matrix inverse. So, the system becomes stable and tracking errors are also converging to zero. In the absence of Jacobian matrix inverse, the proposed control scheme shows better results and almost closes to the conventional operational-space controller's performance. The proposed scheme can be applied to any similar robotic system and is giving a generalised frame work for controlling mobile robotic systems.

An inverse dynamic of the ground-based vehicle-manipulator system is proposed by virtue of a double-loop motion control scheme in addition with a nonlinear disturbance observer. The proposed motion control scheme achieves asymptotic stability for the slowly varying unknown external disturbances and system dynamic changes by means of the feedback of the positions, velocities of the mobile robot and the manipulator joints. The control rule is capitulated agreeable tracking assets regardless of the system/parameter uncertainties, disturbing and actuator dynamic effects. The end-effector tracking pose errors increase specifically in z-axis position (heave) and y-axis rotation (pitch) when the system dynamic changes in terms of modelling errors and the unknown external effects are introduced. Nevertheless, these error values are procured to be in acceptable design limits as the requirement for low energy operation of the overall system is concerned. Further, these errors can be decreased if higher values of gains are used at the expenditure of a higher sampling rate of the controller and lower response time of the actuator.

In fault tolerant scheme a thorough analysis about the behaviour of four-mecanum wheeled drive mobile robot for one-fault and two-fault conditions with FTC has been presented. The analysis presented is for both set-point control and trajectory-tracking control with proportional controller been used with kinematic control scheme. The idea behind this analysis is to showcase the behaviour of the mobile robot when FTC is used with the identified faults. Since understanding the nature of fault and the behaviour of mobile robot with it can greatly assist in implementing the FTC to obtain the desired performance from the mobile robot.

Moreover, the analysis presented is for the entire possible wheel configuration and all the possible case for two actuators failure which can be used even for designing mecanum wheeled based mobile robots. It has been considered that the fault has already been detected .

Current research directions are towards minimizing the error occurred during set-point control and trajectory-tracking control to obtain the desired performance within further minimum tolerance limit of the mecanum wheel drive mobile robot even on the occurrence of one-fault or two-fault within the limited workspace or occluded area.

In order to obtain the effectiveness, results are compared with traditional controllers (for benchmarking) and with advanced controllers. From the comparative results, it shows the significant reduction in error accumulation, control activity and substantial enhancement in the responsiveness of the controller in the uncertain environment and disturbances. The overall experimental results revealed that the suggested controllers are effective in trajectory tracking performance.

6.2 Scope of Future Works

An improved robust nonlinear PID control method suffer from one limitation that the control design is restricted to slow varying lumped disturbances only. However, under fast varying disturbances, the task space tracking errors can be minimized arbitrarily by appropriate choice of design parameters (K *c* and *K o)* and the uniform ultimate boundedness is guaranteed. As a future work, the proposed control design can be extended for fast varying lumped disturbances.

All the proposed controller schemes can be tested with different type of real-time mobile manipulators on real working conditions along with applications. There are various applications such as warehouse automation, library automation, etc.

REFERENCES

1. Angeles J. (2003) Fundamentals of Robotic Mechanical Systems. New York. Springer-Verlag New York Inc., pp13-129
2. Behm A. (2013) Highlights der Hannover Messe 2013, Image extracted from online video: 3:15
3. Bouton, N., Mezouar, Y., & Sabourin, L. (2015) Autonomous Collaborative Mobile Manipulators: State of the Art. TrC-IFToMM Symposium on Theory of Machines and Mechanisms, Izmir, Turkey, June
4. Padois V., Fourquet J. Y., Chiron, P., Renaud, M. (2006) On contact transition for nonholonomic mobile manipulators. In Experimental Robotics IX. Springer, pp 207–216
5. Sugawara T., Tomokuni N., Lee J. H., Tomizawa T., Ohara K., Kim B. K., Ohba, K (2007) Development of ubiquitous mobile manipulator system with RT-middleware. (ICCAS), International Conference on Control, Automation and Systems, IEEE, pp 2373–2376
6. www.neobotix-robots.com/mobile-manipulator-mm-500.html
7. www.robotnik.eu/manipulators
8. Frejek M. C., Nokleby S. B. (2009) Simplified tele-operation of mobile-manipulator systems using knowledge of their singular configurations. In International Design Engineering Technical Conferences and Computers and Information in Engineering Conference, ASME, pp 311–318
9. López-Franco C., Hernández-Barragán. J, Y., Alanis A., Arana-Daniel N., López-Franco M. (2018) Inverse kinematics of mobile manipulators based on differential evolution. International Journal of Advanced Robotic Systems 15 (1), pp1-22

10. Seraji H. (1998) A Unified Approach to Motion Control of Mobile Manipulators. The International Journal of Robotics Research 17(2), pp 107 – 118
11. www.robotpark.com/All-Types-Of-Robots
12. Papadopoulos E., Poulakakis J. (2000) Planning and Model-Based Control for Mobile Manipulators. Proceedings IROS 2000 Conference on Intelligent Robots and Systems, Takamatsu, Japan
13. Pedersen M R., Nalpantidis L., Andersen R S., Schou C., Bøgh S., Krüger V., Madsen O. (2016) Robot skills for manufacturing: From concept to Industrial deployment. Robotics and Computer-Integrated Manufacturing 37, pp 282-291
14. Singh Y., Mohan S. (2015), Inverse dynamics and robust sliding mode control of a planar parallel (2-PRP and 1-PPR) robot augmented with a nonlinear disturbance observer, Mechanism and Machine Theory,92, pp. 29-50
15. Ellekilde L., Christensen H I. (2009) Control of mobile manipulator using the dynamical systems approach. 2009 IEEE International Conference on Robotics and Automation Kobe, Japan 12-17, May 2009
16. Radzak M S A., Ali M A H., Sha'amri S., Azwan A R. (2018) An overview on real-time control schemes for wheeled mobile robot. IOP Conf. Series: Materials Science and Engineering 332
17. Li L., W.A. Gruver., Qixian Zhang., Zongxu Yang. (2001) Kinematic control of redundant robots and the motion optimizability measure IEEE Transactions on Systems, Man, and Cybernetics, Part B (Cybernetics), 31(1), pp 155 – 160
18. Mashali M., Alqasemi R., Dubey R. (2016) Mobile manipulator dual-trajectory tracking using control variables introduced to end-effector task vector. 2016 World Automation Congress (WAC) 31 July-3 Aug. 2016, Rio Grande, Puerto Rico

19. Bayle B., Fourquet J. Y., Renaud M. (2003) Manipulability of Wheeled Mobile Manipulators: Application to Motion Generation. The International Journal of Robotics Research, 22(7-8), pp. 565 - 581

20. Luca A. De., Oriolo G., Giordano P. R. (2006) Kinematic modeling and redundancy resolution for nonholonomic mobile manipulators (ICRA 2006) Proceedings 2006 IEEE International Conference on Robotics and Automation, pp. 1867-1873, 2006

21. H Seraji. (1998) A unified approach to motion control of mobile manipulators. The International Journal of Robotics Research,17(2), pp. 107-118

22. Yamamoto Y., Yun X. (1992) Coordinating locomotion and manipulation of a mobile manipulator. Proceedings of the 31st IEEE Conference on Decision and Control, 3, pp. 2633-2638

23. Normey-Rico J. E., Alcalá I., Gómez-Ortega J., Camacho E. F. (2001) Mobile robot path tracking using a robust PID controller Control Engineering Practice, 9(11), pp 1209-1213

24. Kawabe T., Tagami T. (1997) A real coded genetic algorithm for matrix inequality design approach of robust PID controller with two degrees of freedom Proceedings of 12th IEEE International Symposium on Intelligent Control 16-18 July 1997, Istanbul, Turkey

25. Ahmet S. Yigit. (1993) On the Stability of PD Control for a Two-Link Rigid-Flexible Manipulator J. Dyn. Sys., Meas., Control 116(2), 208-215

26. Ouyang R., Zhang W.J., Wu F.X. (2002) Nonlinear PD control for trajectory tracking with consideration of the design for control methodology, Proceedings 2002 IEEE International Conference on Robotics and Automation,11-15 May 2002, Washington, DC, USA

27. Utkin V. I. (1992) Sliding Modes in Control and Optimizations. New York: Springer-Verlag.
28. Slotine J. J., Sastry S. S. (1983) Tracking control of nonlinear system using sliding surface with application to robot manipulators," Int. J. Control, 38 (2), pp 365–392
29. Chwa D. K. (2003) Sliding-mode tracking control of nonholonomic wheeled mobile robots in polar coordinates," IEEE Trans. Control Syst. Technol.,12(3), pp. 637–633
30. Xu D., Zhao D., Yi J., Tan X. (2009) Trajectory Tracking Control of Omnidirectional Wheeled Mobile Manipulators: Robust Neural Network-Based Sliding Mode Approach IEEE Transactions. On Systems, Man, And Cybernetics—Part B: Cybernetics, 39(3), June 2009
31. Ge W., Ye D., Jiang W., Sun X. (2008) Sliding mode control for trajectory tracking on mobile manipulators. APCCAS 2008 2008 IEEE Asia Pacific Conference on Circuits and Systems. 30 Nov.-3 Dec. 2008 Macao, China
32. Boukattaya M., Damak T., Jallouli M. (2017) Robust Adaptive Sliding Mode Control for Mobile Manipulators, Robotics & Automation Engineering Journal, Short Communication, 1 (1)
33. Yang J.M., Kim J. H. (1999) Sliding Mode Control for Trajectory Tracking of Nonholonomic Wheeled Mobile Robots. IEEE Transactions On Robotics And Automation, 15(3), pp 578 - 587
34. Slotine J. J., Sastry S. S. (1983) Tracking control of nonlinear system using sliding surface with application to robot manipulators, Int. J. Control, 38(2), pp. 365-392
35. Chwa D. K. (2003) Sliding-mode tracking control of nonholonomic wheeled mobile robots in polar coordinates IEEE Trans. Control Syst. Technol., 12(3), pp. 637-633
36. Krstic M., Kanellakopoulos I., Kokotovic P.V. (1995) Nonlinear and Adaptive Control Design. New York: Wiley.

37. Londhe P.S., Mohan S., Patre B.M., Waghmare L.M. (2017) Task space control of an autonomous underwater vehicle manipulator system by robust single-input fuzzy logic control scheme. IEEE J Oceanic Eng., 32(1), pp13–28

38. Wang F., Zou Q., Zong Q. (2017) Robust Adaptive Backstepping Control for an Uncertain Nonlinear System with Input Constraint based on Lyapunov Redesign. International J Control Autom & Systems. 15, pp 212-225

39. Anwar A., Shao X., Hu Q., Moldabayeva A., Li B. (2016) Adaptive Backstepping Control of Uncertain Nonlinear Systems with Input Backlash. IEEE Chinese Guidance, Navigation and Control Conference (CGNCC), Nanjing, 2016. pp. 1237-1232

40. Zouari F., Saad K. B., Benrejeb M. (2013) Robust Adaptive Control for a Class of Nonlinear Systems Using the Backstepping Method. International J of Advanced Robotic Systems. 10(3), pp. 1-12

41. Bouadi H., Mora-Camino F. (2011) Adaptive Backstepping for Trajectory Tracking of Nonlinearly Parameterized Class of Nonlinear Systems.12th IEEE International Symposium on Computational Intelligence and Informatics Budapest, Hungary, pp. 213-217

42. Tong S., Li Y., Li Y., Liu Y. (2011) Observer-Based Adaptive Fuzzy Backstepping Control for a Class of Stochastic Nonlinear Strict-Feedback Systems. IEEE Transactions on Systems, Man, and Cybernetics—Part B: Cybernetics. 31(6), pp. 1693-1703.

43. Rong M., Xian W. Q., Sheng J. C. (2010) Robust adaptive backstepping control for a class of uncertain nonlinear systems based on disturbance observers. Science China Information Sciences, Springer., 53 (6), pp 1201-1215

44. Huang H.C., Tsai C.C. (2008) Adaptive Robust Control of an Omnidirectional Mobile Platform for Autonomous Service Robots

in Polar Coordinates. J of Intelligent Robotic Systems. 51, pp. 339-360.

45. Zhou J, Wen C., Zhang Y. (2003) Adaptive backstepping control of a class of uncertain nonlinear systems with unknown backlash-like hysteresis. IEEE Transactions on Automatic Control, 39(10), pp. 1751-1759
46. Ge SS, Wang J. 2003 Robust Adaptive Tracking for Time-Varying Uncertain Nonlinear Systems with Unknown Control Coefficients. IEEE Transactions on Automatic Control ,38(8), pp. 1363-1369
47. Papadopoulos E., Poulakakis J. (2000) Planning and model-based control for mobile manipulators. 2000 IEEE/RSJ International conference on intelligent robots and systems (IROS 2000), 3, pp. 1810-1815.
48. Wilson D.G., Robinett R.D. (2001) Robust Adaptive Backstepping Control for a Non-Holonomic Mobile Robot. IEEE International Conference on Systems Man and Cybernetics ,5, pp. 3231-3233.
49. Jiang Z.P., Hill D. (1999) A Robust Adaptive Backstepping Scheme for Nonlinear Systems with Unmodeled Dynamics. IEEE Transactions on Automatic Control, 33(9), pp. 1705-1711.
50. Jiang Z.P., Praly L. (1998) Design of Robust Adaptive Controllers for Nonlinear Systems with Dynamic Uncertainties. Automatica Elsevier, 33(7), pp. 825-830
51. Peng J., Wang J.Y.Y. (2013) Robust adaptive tracking control for nonholonomic mobile manipulator with uncertainties. ISA Transactions, 53, pp. 1035–1033
52. Yip P.P., Hedrick J.K. (1998) Adaptive dynamic surface control: a simplified algorithm for adaptive backstepping control of nonlinear systems. International J of Control. 71 (5), pp. 959-979
53. Yamamoto Y., Yun X. (1996) Effect of the dynamic interaction on coordinated control of mobile manipulators. IEEE Trans Rob Autom. 12(5), pp. 816–23

54. Singh Y., Mohan, S. (2015) Inverse dynamics and robust sliding mode control of a planar parallel (2-PRP and 1-PPR) robot augmented with a nonlinear disturbance observer. Mech. and Mach. Theory, 92, pp. 29-50
55. Galicki M. (2015) An adaptive non-linear constraint control of mobile manipulators. Mech. and Mach. Theory88, pp. 63–85
56. Pyrkin A. A., Bobtsov A. A., Kolyubin S.A., Faronov M.V., Borisov O.I., Gromov V.S., Vlasov S.M., Nikolaev N. (2015) A Simple Robust and Adaptive Tracking Control for Mobile Robots, IFAC-Papers Online, 38(11), pp.133-139
57. Nikdela N., Badamchizadeha M.A., Azimiradb V., Nazari M. A. (2017) Adaptive backstepping control for an n-degree of freedom robotic manipulator based on combined state augmentation. Robotics and Computer-Integrated Manufacturing.,33, pp.129-133
58. Chen N., Song F., Li G., Sun X., Ai C. (2013) An adaptive sliding mode backstepping control for the mobile manipulator with nonholonomic constraints. Communications in Nonlinear Science and Numerical Simulation, 18(10), pp. 2885-2899
59. Wu X., Wang Y., Dang X. (2013) Robust adaptive sliding-mode control of condenser-cleaning mobile manipulator using fuzzy wavelet neural network. Fuzzy Sets and Systems, 233, pp. 62–82
60. Synodinos A.I., Moulianitis V.C., Aspragathos N. (2015) A fuzzy approximation to dexterity measures of mobile manipulators, Advanced Robotics, 29(12), pp. 753-769
61. Mai T., Mao J. (2013) Adaptive motion/force control strategy for non-holonomic mobile manipulator robot using recurrent fuzzy wavelet neural networks. Engineering Applications of Artificial Intelligence 33, pp.137–153
62. Li Z., Yang C., Luo J., Wang Z., Ming A. (2013) Robust motion/force control of nonholonomic mobile manipulators using hybrid joints. Advanced Robotics, 21(11) pp. 1231-1252

63. Mishra S., Londhe P S., Mohan S., Vishvakarma S. K., Patre B. M. (2018) Robust task-space motion control of a mobile manipulator using a nonlinear control with an uncertainty estimator. Computers & Electrical Engineering, 67,pp. 729-730
64. Barbalata C., Dunniganb M. W., Petillot Y. Position/force operational space control for underwater manipulation. Robotics and Autonomous Systems, 100, pp. 150-159
65. Faria C., Ferreira F., Erlhagen W., Monteiro S., Bicho E. (2018) Position-based kinematics for 7-dof serial manipulators with global configuration control, joint limit and singularity avoidance Mech. and Mach. Theory, 121, pp. 317-333
66. Busson D., Bearee R., Olabi A. (2017) Task-oriented rigidity optimization for 7 dof redundant manipulators. IFAC-Papers OnLine, 50(1), pp. 13588-13593
67. Vigoriti F., Ruggiero F., Lippiello V., Villani L. (2018) Control of redundant robot arms with null-space compliance and singularity-free orientation representation. Robotics and Autonomous Systems, 100, pp. 186-193
68. Quiroz-Omana J.J., Adorno B.V. (2018) Whole-Body Kinematic Control of Nonholonomic Mobile Manipulators Using Linear Programming. J Intell Robot Syst, 91, pp. 263–278
69. Ancona R. (2017) Redundancy modelling and resolution for robotic mobile manipulators: a general approach. Advanced Robotics, 31(13), pp. 706-715
70. Silva F.F.A., Adorno B.V. (2018) Whole-body Control of a Mobile Manipulator Using Feedback Linearization and Dual Quaternion Algebra. J Intell Robot Syst., 91, pp. 239–262
71. Galicki M. (2012) Two-stage constrained control of mobile manipulators. Mechanism and Machine Theory. 53, pp. 18–30
72. Yamazaki K., Tomono M., Tsubouchi T. (2012) Pose Planning for a Mobile Manipulator Based on Joint Motions for Posture

Adjustment to End-Effector Error, Advanced Robotics, 22(3), pp. 311-331

73. Galicki M. (2016) Real-time constrained trajectory generation of mobile manipulators. Robotics and Autonomous Systems, 78, pp. 39–62
74. Seraji H. (1998) A Unified Approach to Motion Control of Mobile Manipulators. The International Journal of Robotics Research ,7(2) pp. 107 – 118
75. Roa M.A., Berenson D., Huang W. (2015) Mobile Manipulation: Toward Smart Manufacturing. IEEE Robotics & Automation Magazine, DOI10.1109/MRA.2015.2386583
76. Shi H. (2011) A novel scheme for the design of backstepping control for a class of nonlinear systems. Applied Mathematical Modelling, 35(3), pp. 1893-1903
77. Galicki M. (2007) Generalized Kinematic Control of Redundant Manipulators in Robot Motion and Control, Krzysztof R. Kozlowski, 1st ed., Springer-Verlag London, pp. 219-226
78. Yao X. Y., Ding H. F., Ge M. F. (2018) Task-space tracking control of multi-robot systems with disturbances and uncertainties rejection capability. Nonlinear Dynamics, 92(3), pp.1639–1663
79. Hong S., Lee W.S., Kang Y.S., Park Y.W. (2013) Kinematic control algorithms and robust controller design for rescue robot, 13th International Conference on Control Automation and Systems (ICCAS) Seoul, South Korea, Oct. 22-25, 2013, pp. 637-632
80. Li L., Gruver W. A., Zhang Q., Yang Z. (2001) Kinematic Control of Redundant Robots and the Motion Optimizability Measure. IEEE Transactions on Systems, Man, and Cybernetics-Part B: Cybernetics,31(1), pp. 155-160
81. Koga M., Kosuge K., Furuta K., Nosaki K. (1992) Coordinated Motion Control of Robot Arms Based on the Virtual Internal

Model," IEEE Transactions on Robotics and Automation, 8(1), pp. 77-85

82. Ahmad S., Luo S. (1989) Coordinated Motion Control of Multiple Robotic Devices for Welding and Redundancy Coordination through Constrained Optimization in Cartesian Space, IEEE Transactions on Robotics and Automation, 5(3), pp. 309-317
83. Walker M.W., Kim D., Dionise J. (1989) Adaptive Coordinated Motion Control of Two Manipulator Arms. Proc. IEEE International Conference on Robotics and Automation, Scottsdale, Arizoqa, 1989, pp. 1083-1090
84. Zhou S., Pradeep Y. C., Zhu M., Semprun K.A., P Chen. (2017) Motion Control of a Nonholonomic Mobile Manipulator in Task Space, Asian Journal of Control, 20(5), pp. 1–10
85. Chiaverini S. (1997) Singularity-Robust Task-Priority Redundancy Resolution for Real-Time Kinematic Control of Robot Manipulators, IEEE Transactions on Robotics and Automation, 13(3), pp. 398-310
86. Raja R., Dasgupta B., Dutta A. (2015) Motion Planning and Redundancy Resolution of a Rover Manipulator. IEEE International WIE Conference on Electrical and Computer Engineering, Dec. 19-20, pp. 90-93
87. Yang C., Paul G., Ward P., Liu D.(2016) A path planning approach via task-objective pose selection with application to an inchworm-inspired climbing robot", IEEE International Conference on Advanced Intelligent Mechatronics (AIM), Alberta, Canada, July 12-15, 2016, pp. 301-306
88. Nandi S., Singh T. (2018) Chance Constraint based Design of Open-Loop Controllers for Linear Uncertain Systems. IEEE/ASME Transactions on Mechatronics, DOI10.1109/TMECH.2018.2830107, pp. 1-1

89. Caccavale F., Chiaverini S., Siciliano B. (1997) Second-order kinematic control of robot manipulators with Jacobian damped least-squares inverse: theory and experiments, IEEE/ASME Transactions on Mechatronics, 2(3), pp. 188 – 193
90. Chiaverini S., Oriolo G., Walker I.D. (2008) Kinematically Redundant Manipulators, Springer Handbook of Robotics, Springer Verlag, pp. 235–268
91. Tsai M.C., Yang F.Y., Chen C.L. (2013) A Double-loop Control Structure for Tracking Control and Disturbance Attenuation, Proceedings of the 19th World Congress. The International Federation of Automatic Control Cape Town, South Africa, August 23-29
92. Mohan S., Mohanta J.K. (2018) Dual Integral Sliding Mode Control Loop for Mechanical Error Correction in Trajectory-Tracking of a Planar 3-PRP Parallel Manipulator, Journal of Intelligent Robotic Systems, 89(3–3), pp. 371–385
93. Agarwal A., Nasa C., Bandyopadhyay S. (2011) Dual-loop Control for Backlash Correction in Trajectory-tracking of a Planar 3-RRR Manipulator, Proceedings of 15th National Conference on Machines and Mechanisms NacoMM 2011, (189), pp.1-8 Chennai
94. DeSantis R.M., (2000) PID Dual Loop Control for Industrial Processes, IFAC Proceedings Volumes, Elsevier, 33(3), pp. 397-302
95. Zhang Y., Jiang J. Bibliographical review on reconfigurable fault-tolerant control systems. IFAC Proc. Vol., 2003, 36(5), pp. 257–268
96. Zhou D. H., Frank., P. M. Fault diagnostics and fault tolerant control. Aerosp. Electron. Syst. IEEE Trans., 33(2), pp. 320–327
97. Blanke M., Staroswiecki M., Wu, N. E. (2001) Concepts and methods in fault-tolerant control. In Proc. 2001 Am. Control Conf. (Cat. No.01CH37138), 3, pp. 2606–2620

98. Vlantis P., Bechlioulis C. P., Karras G., Fourlas G., Kyriakopoulos K. J. (2016) Fault tolerant control for omni-directional mobile platforms with 4 mecanum wheels. In Proc. - IEEE Int. Conf. Robot. Autom., pp. 2395–2300
99. Jiang J., Yu X. (2012) Fault-tolerant control systems: A comparative study between active and passive approaches, Annual Reviews in Control.
100. Yin S., Luo H., Ding S. X. (2013) Real-time implementation of fault- tolerant control systems with performance optimization IEEE Trans. Ind. Electron., 61(5), pp. 2302–2311
101. Blyth. W. A., Barr D. R. W., Baena F. R. Y. (2016) A reduced actuation mecanum wheel platform for pipe inspection. IEEE/ASME Int. Conf. Adv. Intell. Mechatronics, AIM, pp. 319–323
102. Song B., Zhang Y., Cheng J., Wang J. (2010) Path Following Control of a Mobile Robot via Line-of-Sight Method. Second Int. Conf. Intell. Human-Machine Syst. Cybern. 10.1109/IHMSC.2010.135
103. Yamamoto Y., Yun X. (1996) Effect of the dynamic interaction on coordinated control of mobile manipulators. IEEE Trans Rob Autom 12(5) pp. 816–23
104. Bloch A., Reyhanoglu M., McClamroch N. Control and stabilization of nonholonomic dynamic systems. IEEE Trans Autom Control ,37(11), pp.1736–57
105. Galicki M. (2010) Task space control of mobile manipulators. Robotica, 29(02), pp. 221–32
106. Padois V., Fourquet J-Y., Chiron P. (2007) Kinematic and dynamic model-based control of wheeled mobile manipulators: a unified framework for reactive approaches. Robotica , 25(02)
107. Galicki M. (2011) Collision-free control of mobile manipulators in a task space. Mech Syst Signal Process, 25(7), pp. 2766–83

108. Tchon K, Jakubiak J. (2003) Endogenous configuration space approach to mobile manipulators: a derivation and performance assessment of Jacobian inverse kinematics algorithms. Int J Control 76(13), pp.1387–319

109. Galicki M. (2005) Control-based solution to inverse kinematics for mobile manipulators using penalty functions. J Intell Rob Syst, 32(3), pp.213–38

110. Bouteraa Y., Abdallah IB., Ghommam J. (2017) Task-space region-reaching control for medical robot manipulator. Comput Electr Eng. DOI: 10.1016/j. compeleceng.2017.02.003

111. Galicki M. (2015) An adaptive non-linear constraint control of mobile manipulators. Mech. and Mach. Theory, 88, pp.63–85

112. F. Caccavale, S. Chiaverini, B. Siciliano. (1997) Second-order kinematic control of robot manipulators with Jacobian damped least-squares inverse: theory and experiments. IEEE/ASME Transactions on Mechatronics 2 (3), pp. 188 – 193

113. From P.J., Gravdahl J.T., Pettersen K.Y. (2013) Vehicle Manipulator Systems: Modeling for Simulation, Analysis, and Control Springer London Heidelberg New York.

114. Li Z., Ge S.S. (2013) Fundamentals in Modeling and Control of Mobile Manipulators, CRC Press, 39

115. White G.D., Bhatt R.M., Tang C. P., Krovi V.N. (2009) Experimental evaluation of dynamic redundancy resolution in a nonholonomic wheeled mobile manipulator. IEEE/ASME Transactions on Mechatronics, 13(3), pp. 339-357

116. Nakanishi J., Cory R., Mistry M., Peters J., Schaal S. (2005) Comparative experiments on task space control with redundancy resolution. Proc on 2005 IEEE/RSJ International Conference on Intelligent Robots and Systems, Edmonton, CA, pp. 3901–3908

117. Buss S. R. (2003) Introduction to inverse kinematics with Jacobian transpose pseudoinverse and damped least squares methods. IEEE Journal of Robotics and Automation, 17, pp. 1-19
118. Boukattaya M., Jallouli M., Damak T. (2012) On trajectory tracking control for nonholonomic mobile manipulators with dynamic uncertainties and external torque disturbances, Robotics and Autonomous systems, 60(12), pp. 1630-163
119. Papadopoulos E., Poulakakis J. (2000) Planning and model-based control for mobile manipulators. In Proc. IEEE/RSJ International Conference on Intelligent Robots and Systems 2000, Takamatsu, Japan, 31 Oct.- 5 November, 3, pp. 1810-1815
120. Nakanishi J., Cory R., MistryM., Peters J., Schaal S. Operational space control: a theoretical and empirical comparison, 27(6), pp. 737-757
121. Sutton R. S., Barto A. G. (1998) Reinforcement learning: An introduction. MIT press, 2nd ed., Cambridge, Massachusetts London, England, ch.1, pp.1-11
122. Denavit J., Hartenberg R. S. (1995) A Kinematic Notation for Lower-Pair Mechanisms Based on Matrices," Journal of Applied Mechanics, pp. 215—221
123. www.aubo-robotics.com
124. Craig J. J. (1986) Introduction to robotics: mechanics and control. Boston, MA,USA: Addison Wesley